Boron-Bridged Ferrocenophanes: Strained Monomers for Metallopolymers

A Thesis Submitted to the
College of Graduate and Postdoctoral Studies
in Partial Fulfillment of the Requirements
for the Degree of Doctor of Philosophy
in the Department of Chemistry
University of Saskatchewan
Saskatoon

By

Hridaynath Bhattacharjee

PERMISSION TO USE

In presenting this dissertation in partial fulfillment of the requirements for a Postgraduate degree from the University of Saskatchewan, I agree that the Libraries of this University may make it freely available for inspection. I further agree that permission for copying of this dissertation in any manner, in whole or in part, for scholarly purposes may be granted by Professor Jens Müller who supervised my dissertation work or, in their absence, by the Head of the Department or the Dean of the College in which my thesis work was done. It is understood that any copying or publication or use of this dissertation or parts thereof for financial gain shall not be allowed without my written permission. It is also understood that due recognition shall be given to me and to the University of Saskatchewan in any scholarly use which may be made of any material in my dissertation.

Requests for permission to copy or to make other uses of materials in this dissertation in whole or part should be addressed to:

Head of the Chemistry Department
165-110 Science Place
University of Saskatchewan
Saskatoon, Saskatchewan S7N 5C9
Canada

OR

Dean
College of Graduate and Postdoctoral Studies
University of Saskatchewan
116 Thorvaldson Building, 110 Science Place
Saskatoon, Saskatchewan S7N 5C9
Canada

ABSTRACT

Incorporating metals in synthetic polymers can impose a diverse range of different new and valuable properties. Organometallic polymers containing three-coordinate boron have the potential for intriguing electronic and optical properties associated with the electron deficient nature of the boron centers. Boron-containing conjugated polymers can potentially be obtained via ring-opening polymerization (ROP) of strained boron-bridged [*n*]ferrocenophanes ([*n*]FCPs). The first three boron-bridged [1]FCPs (**21a-c**) were reported almost two decades ago. Unfortunately, thermal ROP of those highly strained monomers resulted only in some insoluble materials which brought the chemistry to a dormancy. This chemistry, which is described in this thesis, was revitalized by developing flexible approaches to synthesize new boron-bridged [1]FCPs (**27a-c^{R1R2}**). The strategy of adding alkyl groups on the Cp rings was adopted to provide steric protection to the bridging moiety as well as to increase the solubility of the monomers and the resulting polymers. Detailed studies were performed by fine tuning of the bulk of alkyl groups (CHR^1R^2) on Cp rings as well as the reaction conditions in order to understand the mechanism of the formation of strained [1]FCPs (**27a-c^{R1R2}**). Moreover, thermal ROP of these boron-bridged [1]FCPs gave soluble metallopolymers with moderate molecular weights ($M_w \approx 10$ kDa).

Synthesis and complete characterization of the first examples of azabora[2]ferrocenophanes (**30a-c**) with unsaturated BN moieties at the bridging position are also described in this thesis. Albeit large tilt angles ($\alpha \approx 24°$) these species showed thermal stability even up to 300 °C and did not ring open under such conditions. However, DFT studies revealed that these [2]FCPs (**30a-c**) are equally strained as the well-known $SiMe_2$-bridged [1]FCP.

Even though electronic stabilization from an amino substituent at the boron atom seemed essential to prepare isolable boron-bridged [*n*]FCPs, such stabilization resulted in decreased

electrophilicity of the boron center and caused a lack of polymerizability of the monomers. To address this issue, the first examples of sterically protected bora[1]ferrocenophanes (**27d-f**$^{\mathbf{MeMe}}$) as highly reactive strained ferrocenophanes were synthesized. Species **27d**$^{\mathbf{MeMe}}$ and **27e**$^{\mathbf{MeMe}}$ showed exceptional bathochromic shifts in UV-Vis spectroscopy. Optimized geometry of **27e**$^{\mathbf{MeMe}}$ at the B3PW91/6-311+G(d,p) level of theory revealed this species to be the new record holder with respect to Cp ring tilting ($\alpha \approx 34°$). Moreover, thermal ROP of **27d**$^{\mathbf{MeMe}}$ resulted in poly(ferrocenylborane) which showed a helical secondary structure in solution.

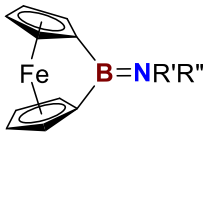

	NR'R"
21a	$N(SiMe_3)_2$
21b	$N(tBu)SiMe_3$
21c	$NiPr_2$

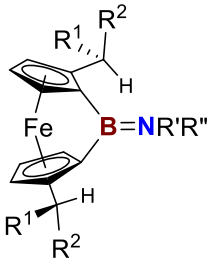

	NR'R"
27a$^{\mathbf{R1R2}}$	NEt_2
27b$^{\mathbf{R1R2}}$	$NiPr_2$
27c$^{\mathbf{R1R2}}$	$N(tBu)SiMe_3$

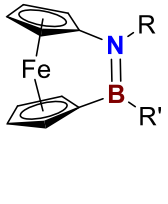

	R	R'
30a	$SiMe_3$	$NiPr_2$
30b	CH_2tBu	$NiPr_2$
30c	CH_2tBu	Tsi

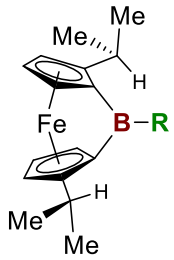

	R
27d$^{\mathbf{MeMe}}$	Mes
27e$^{\mathbf{MeMe}}$	Tip
27f$^{\mathbf{MeMe}}$	Tsi

ACKNOWLEDGEMENTS

I am grateful to my supervisor Prof. Jens Müller for his support, guidance, and encouragement during my studies as a Ph.D. student.

I would like to thank the University of Saskatchewan and Department of Chemistry for providing me with the opportunity to study here, the members of my advisory committee for their support, and the staff at the Saskatchewan Structural Science Centre and the Department of Chemistry. In particular, I am grateful to Dr. Jianfeng Zhu (NMR and XRD), Dr. Keith C. Brown (NMR), Ken Thoms (MS and CHN), and Dr. Valerie MacKenzie (DSC) for their support and help in measurements.

I would like to acknowledge all present and past members of the Müller group for their help and support. In particular, I would like to acknowledge Jonathon D. Martell, Dr. Phan Thuy My Cao, Dr. Subhayan Dey, and Dr. Saeid Sadeh for their support and inspiration.

I would like to express my gratitude to Dr. Pia Wennek for her immense support and encouragement during my studies. I am thankful to Eshita Das for her unfailing love and understanding over the last few years of ups and downs. Last but not the least, I am extremely grateful to my parents Ram Chandra and Rai Kishori Bhattacharjee and sister Shrabani Bhattacharjee for their unconditional love and support throughout my life.

TABLE OF CONTENTS

LIST OF FIGURES

LIST OF SCHEMES

LIST OF CHARTS

LIST OF TABLES

LIST OF ABBREVIATIONS

Ar′	2-[(dimethylamino)methyl]phenyl
CBS	Corey-Bakshi-Shibata
CD	circular dichroism
Cp	cyclopentadienyl
DFT	density functional theory
DSC	differential scanning calorimetry
fc	$Fe(H_4C_5)_2$
FCP	ferrocenophane
GPC	gel permeation chromatography
Mamx	2,4-di-*tert*-butyl-6-[(dimethylamino)methyl]phenyl
Me_2Ntsi	[(dimethylamino)dimethylsilyl]bis(trimethylsilyl)methyl
Mes	2,4,6-trimethylphenyl
PFS	poly(ferrocenylsilane)
pmdeta	*N*,*N*,*N*′,*N*′,*N*″-pentamethyldiethylenetriamine
PS	poly(styrene)
Pytsi	[dimethyl(2-pyridyl)silyl]bis(trimethylsilyl)methyl
ROP	ring-opening polymerization
Tip	2,4,6-tri(isopropyl)phenyl
tmeda	*N*,*N*,*N*′,*N*′-tetramethylethylenediamine
Tsi	tris(trimethylsilyl)methyl

1 Introduction

Polymers are ubiquitous in modern daily life in both natural and synthetic forms. Many of the natural polymers exhibit certain properties due to the presence of metals in their molecular structure. In recent years, scientists showed major interest in making metal-containing synthetic polymers in anticipation of intriguing chemical and physical properties. Metal-containing polymers (or metallopolymers) are indeed unique due to the combination of organic and inorganic components in one macromolecular system.[1] Metallopolymers can possess diverse properties such as electronic, catalytic due to the wide range of oxidation states, coordination numbers, and geometries that transition metals can adopt.[2] One of the effective ways to obtain metallopolymers is the ring-opening polymerization (ROP) of strained [*n*]metallocyclophanes, which are defined as a broad class of sandwich compounds where two metal-coordinated mancude-ring systems[a] are linked by *n* bridging atoms (Chart 1-1). The largest subclass of such sandwich compounds is formed when the rings are cyclopentadienyl (Cp) ligands and known as [*n*]metallocenophanes (**A**; Chart 1-1). The most studied [*n*]metallocenophanes are ferrocenophanes (FCPs) where two Cp rings are π-bound to the transition metal iron in a η^5-fashion. For the sake of scope of this thesis, only [*n*]FCPs will be discussed in detail; interested readers are encouraged to refer to published reviews for comprehensive discussions on metallocyclophanes.[3]

Chart 1-1. Different Types of Metallocyclophanes

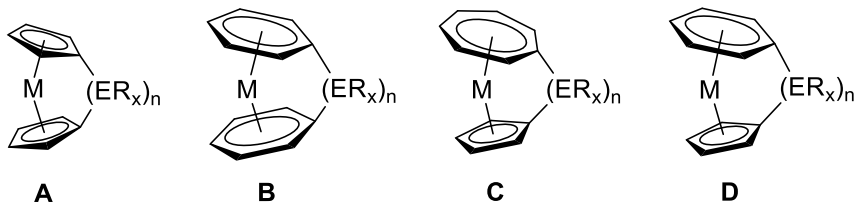

[a] According to IUPAC Gold book (http://goldbook.iupac.org/), mancude-ring systems are defined as "rings having (formally) the maximum number of noncumulative double bonds".

1.1 Ferrocenophanes

Shortly after the landmark discovery of ferrocene,[4] the first strained sandwich compound was reported in the form of the carba[3]ferrocenophane **E** (Chart 1-2) by Rinehart et al. in 1957.[5] Although within a few years the same research group reported the synthesis of the first [2]FCP **F**,[6] it took almost two decades for the first strained [1]FCPs to be reported in the literature [$\mathbf{G^{Ph}}$ and $\mathbf{G^{fc}}$ (fc = $Fe(C_5H_4)_2$; Chart 1-2].[7] However, a tremendous research effort started in this field after Manners et al. showed the use of [1]FCPs, sila[1]ferrocenophanes in particular, as monomers in ROP for the synthesis of high-molecular-weight metallopolymers (Scheme 1-1).[8]

Chart 1-2. First Examples of [*n*]FCPs

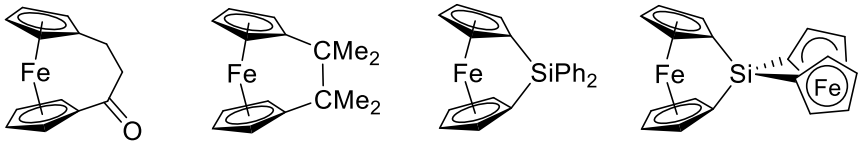

E **F** $\mathbf{G^{Ph}}$ $\mathbf{G^{fc}}$

Various ROP methodologies, viz. thermal, transition-metal-catalyzed, photolytic, and anionic ROP, have been developed for the preparation of ferrocene-based metallopolymers.[9] Poly(ferrocenylsilane)s (PFSs) are the most well-developed poly(ferrocene)s and have become a large class of metal-containing organosilicon polymers.[1j]

Scheme 1-1. Thermal ROP of Sila[1]ferrocenophanes

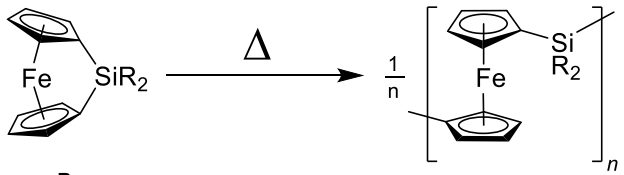

$\mathbf{G^{R}}$ **PFS**

After the first report of preparation of PFS via thermal ROP of sila[1]ferrcenophanes in 1992, many PFS homopolymers have been developed with different substituents on bridging silicon atoms.[1b,1j] Crystallinity as well as solubility of PFS homopolymers depend largely on these

substituents and such physical properties give rise to interesting applicability. For instance, PFSs symmetrically substituted at silicon with small alkyl groups (R = Me, Et, *n*Pr in Scheme 1-1) are crystalline in nature and allow access to controlled polymer architecture;[10] on the contrary, amorphous PFS materials are formed when unsymmetrical or longer alkyl substituents (such as *n*-hexyl) on silicon are used. Along with high refractive index[11] and charge transport properties,[12] PFS homopolymers are also known for their use as redox-active gels. One of the most intriguing outcomes is the discovery of photonic-ink (P-ink) where electroactive inverse polymer gel opals based on PFS were published in 2009 by research groups of Ozin and Manners.[13] Such materials are prepared by infiltrating well-defined poly(ferrocenylmethylvinylsilane) or poly(ferrocenyldivinylsilane) in silica spheres stacked on glass. Optical diffraction through this nanoporous lattice gives the reflected light a certain colour, which is dictated by the lattice spacing of the photonic crystal. Application of an oxidative potential causes influx of ions and solvent molecules resulting the infiltrated polymers to swell, whereas a reductive potential does the reverse. As a result, the lattice spacing changes and consequently affords the film to change colour across the spectral range only at low drive voltages (Figure 1-1).

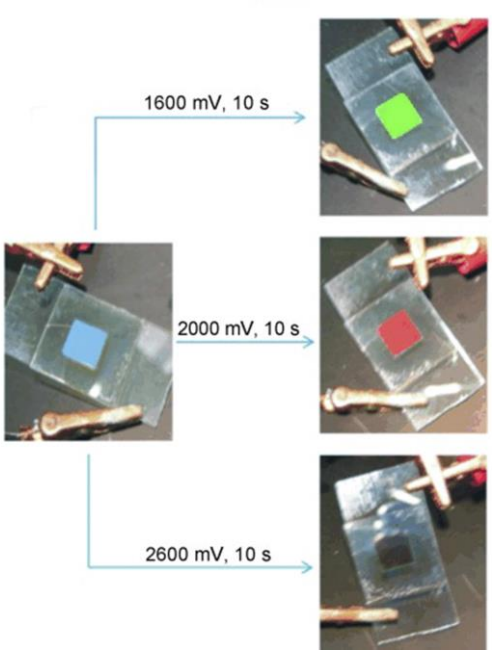

Figure 1-1. Proof of full colour tuning by photographs of the first electroactive inverse polymer-gel opal. Adapted with permission from ref. 13. Copyright © 2009 John Wiley & Sons Inc.

On the other hand, PFS-containing block copolymers are synthesized mainly via living anionic ROP routes. The ability of such block copolymers to phase separate into a number of different morphologies has resulted in their wide applications in nanolithography and nanotemplating. A landmark discovery in this field is the use of crystalline PFSs with Me_2Si- or Et_2Si-bridging moeities as core-forming blocks, causing block copolymers to form various micellar morphologies (e.g., cylinders, platelets, fibres) in block-selective solvents.[14] These crystalline cores are living at the micelle termini and able to grow longer by the addition of further block copolymers.[15] Longer micelles can be sonicated to small seed micelles, which in turn can be used to grow micelles of uniform lengths; overall this is a new bottom-up process to produce nanomaterials with controlled architectures (Figure 1-2).[16] This process is analogous to living covalent polymerisation and was termed as "crystallisation-driven self-assembly" (CDSA). Detailed discussion on this now well-established field is beyond the scope of this thesis, thus interested readers are refered to review some selected articles.[1j,16b,17]

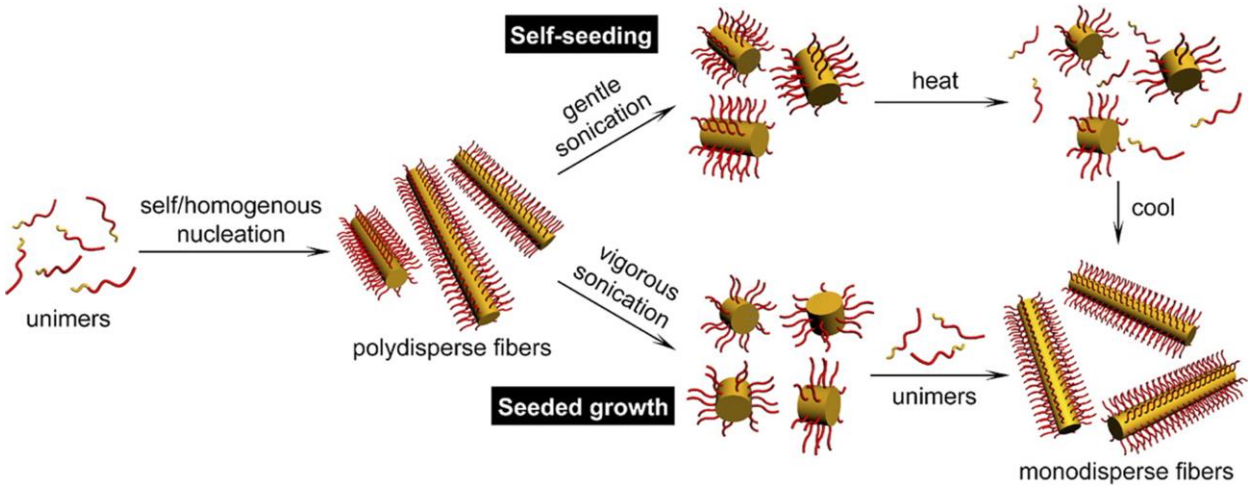

Figure 1-2. Schematic for the preparation of monodisperse cylindrical micelles by (top) self-seeding and (bottom) seeded growth methods. Reproduced with permission from ref. 16b. Copyright © 2015 American Chemical Society.

Compared to sila[1]ferrocenophanes, other strained [*n*]FCPs are far less developed maybe due to the difficulty of their synthesis or their lack of polymerizibility. Even though there are many [*n*]FCPs with different bridging elements reported in the literature,[3d,3i,18] only germanium-[19] and phosphorus-bridged [1]FCPs[20] and carbon-bridged [2]FCPs[21] could be polymerized with control over molecular weight and molecular-weight distribution. In general, major difficulties experienced in this field are as follows: (a) many strained monomers developed are encumbered with bulky bridging moeities which prevents their polymerizibility, and (b) even when the monomers could be converted into polymers, they were often poorly soluble in common organic solvents. In order to address such difficulties and further advance the chemistry, improved monomers are needed. Before going into details of the scope of such developments, the synthesis and structures of monomers (i.e., [*n*]FCPs) will be discussed.

1.1.1 Synthetic Routes

Amongst various synthetic routes for strained FCPs, the most well-known approach is the salt-metathesis method (Scheme 1-2a).[18a] It represents the reaction of dilithioferrocene with element

dihalides equipped with appropriate ligands. The key step of this reaction is dilithiation of ferrocene, which is accomplished by using *n*BuLi and an amine base such as *N*,*N*,*N*′,*N*′-tetramethylethylenediamine (tmeda) or *N*,*N*,*N*′,*N*′,*N*″-pentamethyldiethylenetriamine (pmdeta).[22] Most of the known [*n*]FCPs are synthesized using this route.

Scheme 1-2. Common Synthetic Routes to [*n*]FCPs

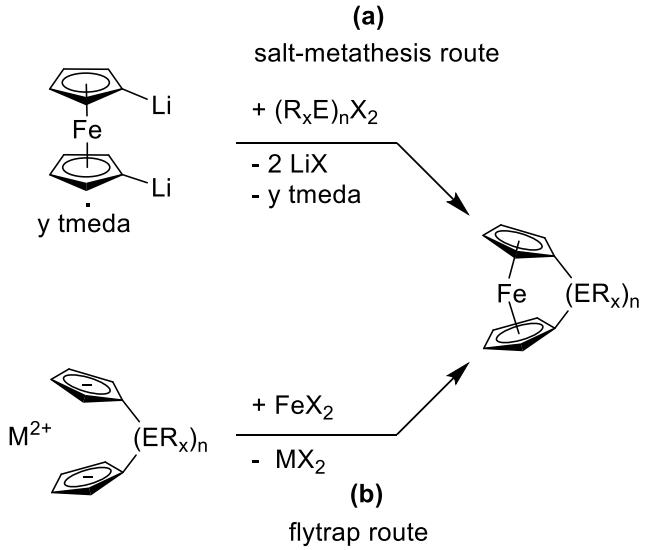

On the other hand, the flytrap route is less used and encompasses the reaction between a dianionic linker (known as "flytrap") and an iron(II) dihalide (Scheme 1-2b). This method is often used to prepare [*n*]FCPs with $n \geq 2$, for instance, compound **F** (Chart 1-2).

1.1.2 Geometrical Parameters

In ferrocene as the parent compound, the two Cp rings are parallel to each other. Introduction of a short *ansa*[*n*] bridge (n = 1, 2) results in a ring-tilted structure. The distortion in [*n*]FCPs is described by a series of geometric parameters, viz., α (angle between the least-squares planes of Cp rings), β (180° − ($Cp^{centroid}$–C^{ipso}–E)), δ ($Cp^{centroid}$–Fe–$Cp^{centroid}$), and θ (C^{ipso}–E–C^{ipso}) (Figure 1-3).

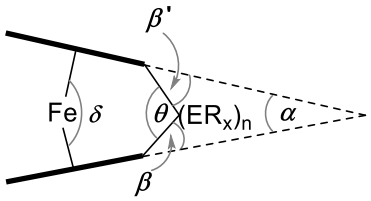

Figure 1-3. Common geometric parameters to characterize distortions in [*n*]FCPs.

The tilt angle α of [*n*]FCPs decreases with the increase of the number of bridging elements of the same kind; for example, the tilt angle α of trithia[3]ferrocenophane **J** (Chart 1-3) is 4.5°,[23] whereas that of the thia[1]ferrocenophane **I** is 31.0°.[24] The angle α is inversely proportional to the size of bridging elements; the smaller the bridging-element, the larger the angle is. The size of elements decreases along a row of the periodic table, therefore, α increases in the same direction; for instance, from silicon ($\alpha \approx 21°$ for $\mathbf{G^{Me}}$; Chart 1-3)[25] to phosphorus ($\alpha \approx 27°$ for **H**)[26] to sulfur ($\alpha \approx 31°$ for **I**)[24].

Chart 1-3. Examples of Known [1]FCPs

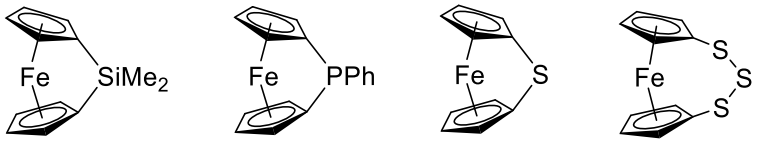

$\mathbf{G^{Me}}$ **H** **I** **J**

Similarly, α decreases in going down a group in the periodic table; for example, α of silicon-bridged [1]FCP ($\alpha \approx 21°$)[25] is higher than that of germanium-bridged [1]FCP ($\alpha \approx 19°$),[27] which is higher than that of tin-bridged [1]FCP ($\alpha \approx 14°$).[28] The degree of tilting affects the energy of molecular-orbitals, which is reflected by a change of colours in metallocyclophanes bridged by increasingly smaller elements. For instance, a gradual change in colour is observed in FCPs bridged by the third period elements from red (λ_{max}: 478 nm for $\mathbf{G^{Me}}$) to intense red (λ_{max}: 498 nm for **H**) to deep purple (λ_{max}: 504 nm for **I**). This red shift, caused by the progressive increase of tilting, can be rationalized by the gradual decrease of the HOMO-LUMO energy gap.[24]

Overall, strained [1]FCPs are the desired starting compounds in order to be able to perform controlled ROPs to access metallopolymers. Amongst a plethora of known [1]FCPs, only group-13-element bridged [1]FCPs will be discussed in details in the following section, as they are most relevant for the thesis at hand.

1.2 Group-13-Element Bridged [1]Ferrocenophanes

The first group-13-bridged [1]FCPs were reported in 1997 by the research groups of Braunschweig and Manners in the form of bora[1]ferrocenophanes.[29] In a follow-up article, published by the same research groups in 2000, it was revealed that such [1]FCPs, despite of possessing α angle as high as 32.4°, are not good candidates for the synthesis of metallopolymers.[30] Thermal ROP of those compounds only resulted in materials, which were insoluble in common organic solvents. Recently, in Müller's group, we reinvigorated this dormant chemistry by using different synthetic strategies, which will be discussed in this thesis. Some key parts of these strategies were born out of the chemistry of the heavier group-13-element bridged ferrocenophanes, which was developed in Müller's group over the last decade or so. By focusing on heavier group-13-element bridged ferrocenophanes, it was found that sterics play a major role for the outcome of the salt-metathesis reaction.[18c] The development that led to this discovery is described in the following paragraphs.

Chart 1-4. Intramolecularly Coordinating, Bulky, *trisyl*-Type Ligands[b]

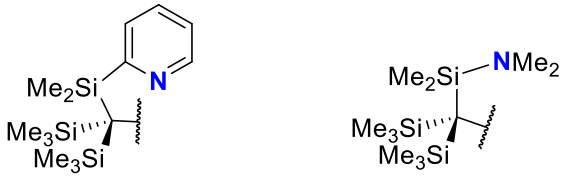

Pytsi **Me_2Ntsi**

[b] The bulky ligand *trisyl* or tris(trimethylsilyl)methyl is often symbolized by "Tsi" in chemical formulas. Therefore, its derivatives are named as Pytsi and Me_2Ntsi based on the donor moiety.

Sterically demanding ligands, like bulky *trisyl*-type ligands shown in Chart 1-4, attached to group-13 elements were used in the synthesis of desired strained [1]FCPs (Scheme 1-3). Such ligands were chosen due to their combined intramolecular donor ability with steric bulkiness and can be derived from the well-known *trisyl* ligand ($C(SiMe_3)_3$).[31] The first alumina- and galla[1]ferrocenophanes were isolated in 2005 (**1** and **2**; Scheme 1-3a) using $PytsiECl_2$ (E = Al, Ga) in the salt-metathesis reactions.[32] Structural data of compounds **1** and **2** showed tilt angles α of 14.9(3) and 15.4(2)°, respectively, much lower compared to the bora[1]ferrocenophanes. Low to moderate yields of 31 and 59%, respectively, were obtained along with formation of a significant amount of ferrocene in each case. It was speculated that acidic protons of the pyridyl moiety of the Pytsi ligand were the reason for the expectedly large amounts of ferrocene. This hypothesis led to the use of the Me_2Ntsi ligand which resulted in isolation of the new aluminum- and gallium-bridged [1]FCPs (**3** and **4**; Scheme 1-3b) in significantly higher yields of 97 and 68%, respectively.[33]

Scheme 1-3. Synthesis of the First Aluminum- and Gallium-Bridged [1]FCPs

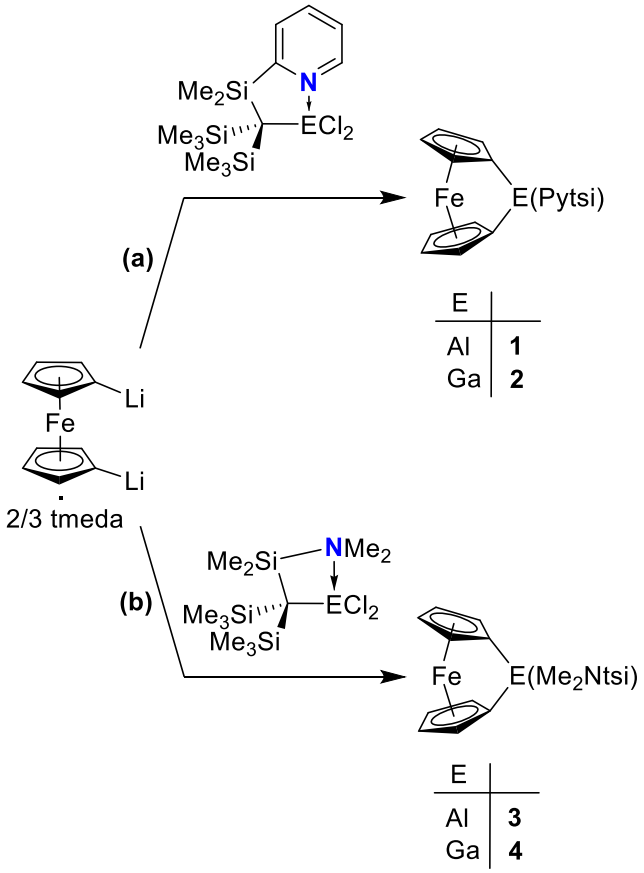

All four compounds (**1**–**4**) were tested for their proclivity towards various ROP methodologies. Unfortunately, only species **2** showed polymerizability in presence of 2 mol% [Pd(dba)$_2$] (dba = dibenzylideneacetone) in toluene or thf at room temperature or 40 °C.[34] Gel permeation chromatography (GPC) revealed the polymer to be of moderate molecular weight [M_w = 21.1 kDa, relative to polystyrene (PS)] and broad molecular weight distribution ($Đ$ = 3.0). All other ROP attempts were either very slow or did not even proceed.[34] It was then speculated that the bulkiness of the *trisyl*-type ligands blocks the initiation or the chain growth.

1.2.1 Fine-Tuning of Sterics

A logical approach of incorporating less bulky ligands (Ar′ or *p*-*t*BuAr′; Chart 1-5) was then pursued. Such one-armed phenyl ligands, however, resulted in unstrained [1.1]FCPs instead of targeted [1]FCPs (Scheme 1-4).[35]

Chart 1-5. Intramolecularly Coordinating Phenyl Type Ligands

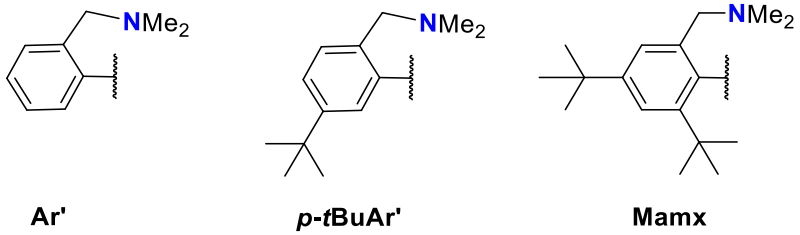

Comparison between the crystallographic data of [1]FCPs and [1.1]FCPs led to the conclusion that the steric repulsion between α-H atoms of the ferrocene moieties and the attached ligands at the group-13-bridging element plays a key role in the outcome of such salt-metathesis reactions.[36] When the steric repulsions are small or even absent, a [1.1]FCP is formed as the thermodynamically preferred species (**5** and **6**; Scheme 1-4). On the other hand, when the steric bulk is increased, [1]FCPs are formed exclusively as [1.1]FCPs simply do not offer enough space for the bridging moieties to fit in (Scheme 1-3).

Scheme 1-4. Synthesis of Aluminum- and Gallium-Bridged [1.1]FCPs

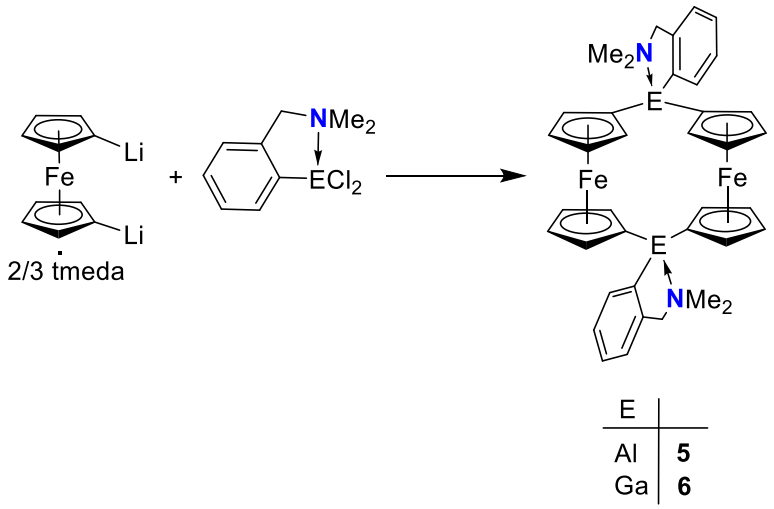

These outcome of the salt-metathesis reactions and inspection of structural data revealed that the space restrictions for the bridging unit ER gradually decreases from [1]FCPs to poly(ferrocene)s (PF) to [1.1]FCPs (Figure 1-4).[18c] It is due to parallel alignment of both ferrocenediyl moieties in a [1.1]FCP, ligands (R; Figure 1-4) are forced to be oriented in such a way that the steric repulsion between them and the ferrocenediyl moieties are maximized. However, such interactions are much less pronounced in a [1]FCP because the relative orientation of the ER group is twisted by an angle ca. 90° compared to that in [1.1]FCPs. It can be assumed that the relative orientation of the bridging ER unit as well as the steric interactions in poly(ferrocene)s are somewhere in between that of [1]FCPs and [1.1]FCPs. Therefore, the fine tuning of steric bulkiness of the ligands remained of vital importance so that [1]FCPs can be formed which are still reactive enough to undergo polymerization.

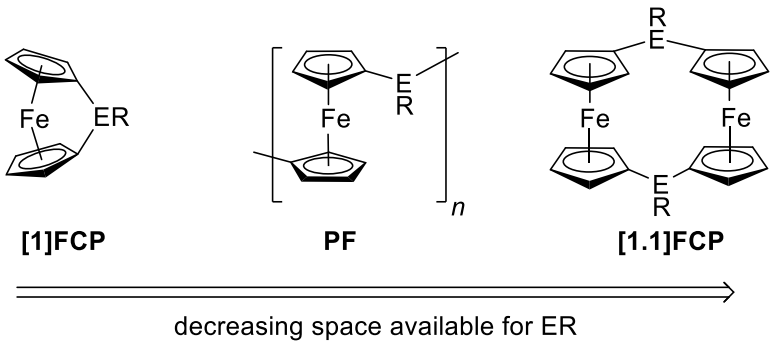

Figure 1-4. Space restrictions in [1]FCPs, poly(ferrocene)s, and [1.1]FCPs. Reproduced with permission from ref. 18c. Copyright © 2015 Elsevier B. V.

Careful review of structural data of the Ar′Ga-bridged [1.1]FCP **6** reveals the H atoms that exhibit the shortest intramolecular H···H distances as indicated by solid black spheres in Figure 1-5.[37] It seems apparent that replacing those H atoms by bulky alkyl groups would possibly block the formation of such [1.1]FCP. For example, a bulky alkyl group adjacent to gallium on the phenyl ring would be a viable possibility.

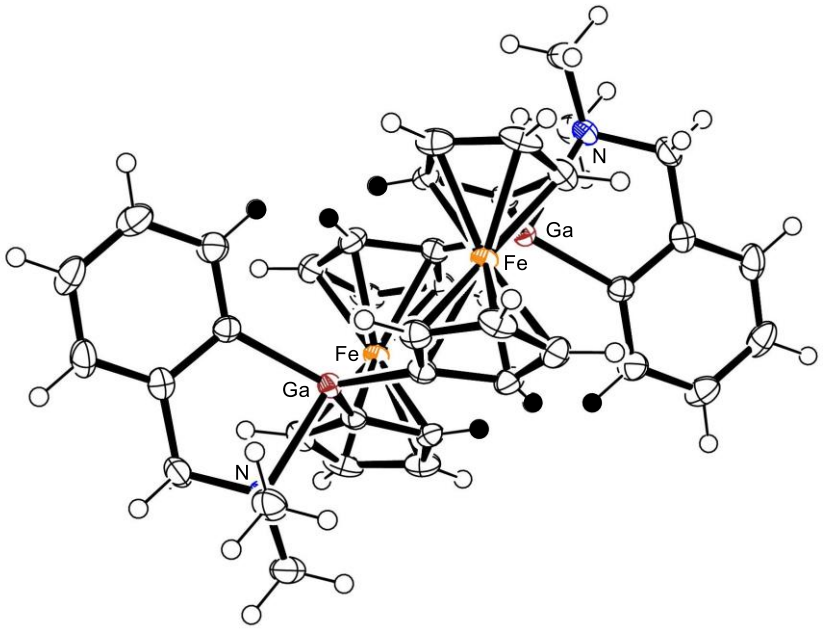

Figure 1-5. Illustration of the shortest H···H distances in the [1.1]FCP **6** (see also Scheme 1-4). Adapted with permission from ref. 37. Copyright © 2013 John Wiley & Sons Inc.

Thus, the known Mamx ligand[c] (Chart 1-5 and Scheme 1-5), with *t*Bu groups in *ortho* and *para* positions with respect to the group-13 element, was chosen for further salt-metathesis reactions. As shown in Scheme 1-5, aluminum or gallium dichlorides (Mamx)ECl_2 can be conveniently be synthesized from 3,5-di-*tert*-butyltoluene.[38]

Scheme 1-5. Synthesis of the Mamx Ligand and Its Element Dihalide Compounds

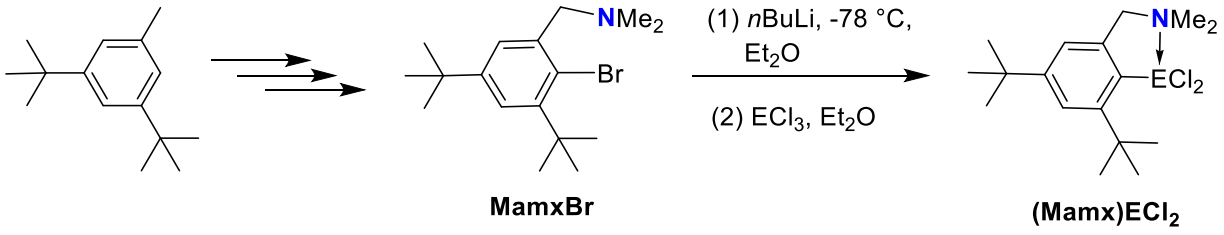

[c] Mamx stands for **m**ethyl**a**mino**m**ethyl-*m*-**x**ylyl (see ref. 38a).

It is noteworthy that the *para*-*t*Bu group does not interact sterically with the Cp moieties but only is needed to facilitate the preparation of the ligand. This tactics of increasing the bulkiness of the one-armed phenyl group by introducing *t*Bu groups in *ortho* positions (Mamx ligand) resulted in strained [1]FCPs **7** and **8** (Scheme 1-6).[38c] Interestingly, these monomers turned out to be highly reactive and polymerized when left stirring in the reaction mixture. GPC analysis of the poly(ferrocenylgallane) $\mathbf{8_n}$ suggested M_w of 48 kDa with a dispersity $Đ$ = 3.3. The Mamx ligand provides significant stability towards the group-13 element, which is enough for the polymers to be handled under ambient conditions, but not enough for the monomers to be isolated. As isolation of clean monomers is of utmost importance to have control over polymerizations, the chemistry described above led into a dead end and was not further pursued.

Scheme 1-6. Salt-Metathesis Reactions with $(Mamx)ECl_2$

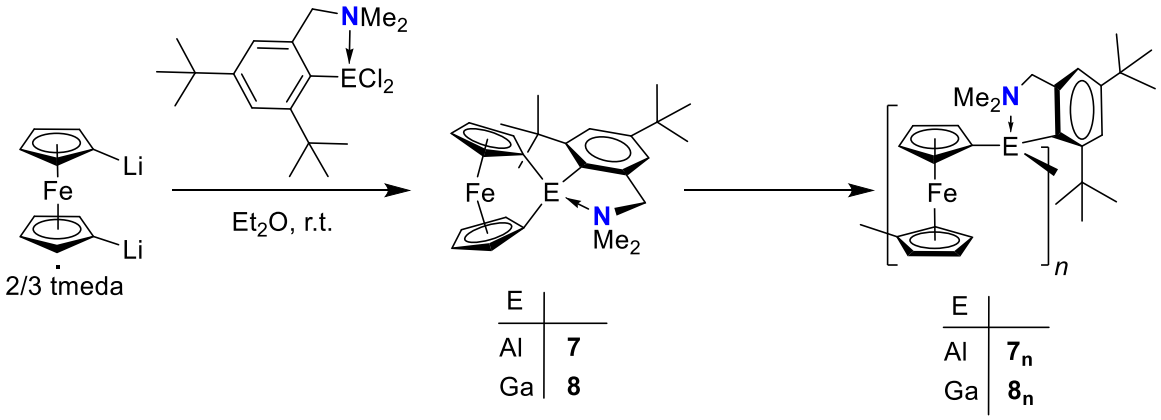

1.2.2 Introduction of Sterics from the Cp Moiety

Based on the same concept that led to the results with the Mamx ligand, a second path to control the outcome of metathesis reactions by using sterics has been recently developed in Müller's laboratory. Instead of tailoring the bulkiness of the ligand attached to the bridging element, the bulkiness of the sandwich unit has been changed. As discussed before, the molecular structure of [1.1]FCP **6** (Figure 1-5) suggests that introducing alkyl groups in the α-positions of the Cp rings

should block the formation of undesired [1.1]FCPs. Such modifications can be pursued by derivatization of dilithioferrocene such as, preparation of α-substituted 1,1′-dilithioferrocene derivatives. Despite of rarity of synthetic methodologies of such species, Müller's group recently introduced alkyl groups in the α-positions of the sandwich unit by using known chemistry (Scheme 1-7).[39]

Scheme 1-7. Preparation of Enantiopure C_2 Symmetric α-Substituted Dibromoferrocene Derivatives

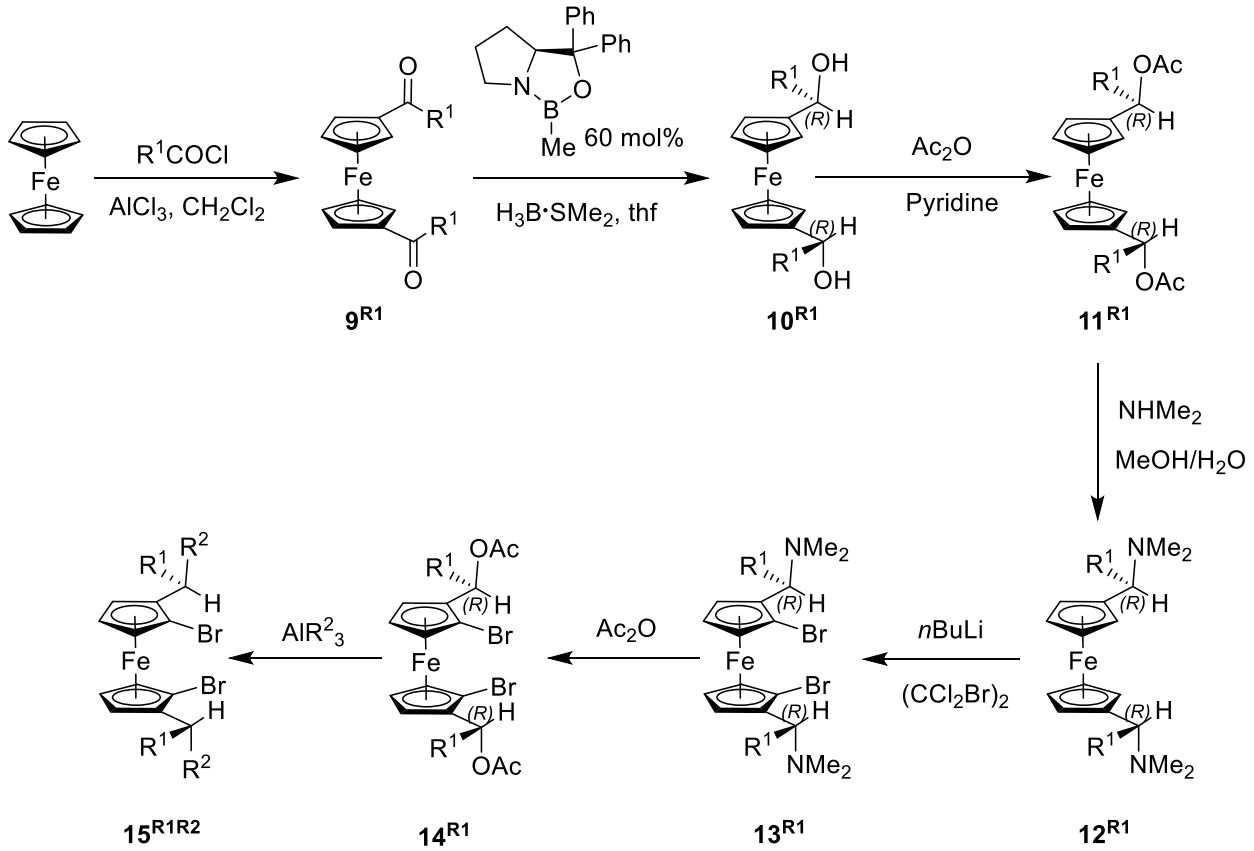

As shown in Scheme 1-7, compound **9^{R1}** was reduced enantioselectively using a Corey-Bakshi-Shibata (CBS) reduction.[40] After that, known "Ugi amine" chemistry[41] was applied to prepare the "double Ugi amine" **12^{R1}** as an enatiomerically pure C_2 symmetric ferrocene derivative. As shown by Ugi et al.,[41] the C*H(Me)NMe_2 groups on Cp moieties, like those in compound **12^{R1}**, serve as excellent directing groups for diastereoselective α lithiation. Instead of

the dilithio derivative, the dibromide **13**$^{\mathbf{R1}}$ was isolated. Followed by additional two steps, this route gives rise to enantiomerically pure C_2 symmetric ferrocene dibromide of type **15**$^{\mathbf{R1R2}}$ (Scheme 1-7). The versatility of this methodology is noteworthy as it allows the introduction of R^1 and R^2 groups separately: R^1 is incorporated in the first step whereas R^2 is introduced in the last step. Moreover, by varying both R^1 and R^2 a set of new dibromoferrocene derivatives can be obtained. The first of their kind synthesized in Müller's group is compound **15**$^{\mathbf{MeMe}}$ (R^1 = R^2 = Me). This species can readily be lithiated applying a method developed by Bailey et al.[42] and a quantitative Li/Br exchange is accomplished by using *n*BuLi in a hexanes/thf mixture (9/1) at 0 °C (Scheme 1-8). Unlike Li_2fc·tmeda, this new lithiation method provides a homogeneous solution of the dilithioferrocene derivative and, thus, has two-fold advantage as following: (a) control over the stoichiometry and (b) control over the concentration of the dilithioferrocene reagent.

Scheme 1-8. Synthesis of Galla[1]ferrocenophane **17**

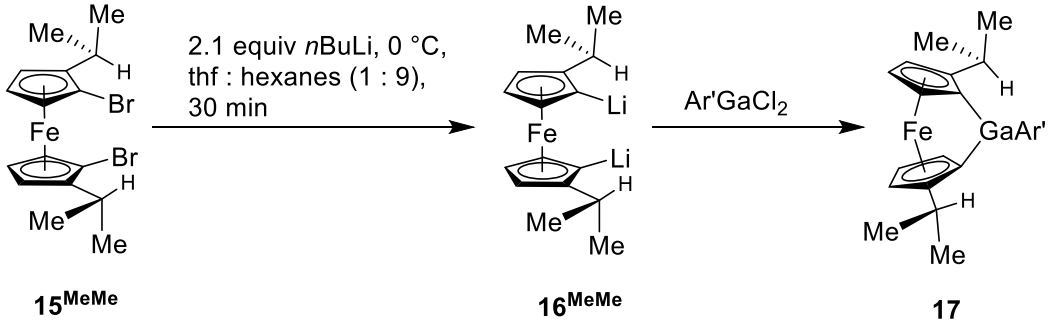

This dilithio reagent was then *in situ* reacted with Ar′$GaCl_2$ and gave rise to a clean conversion towards the targeted gallium-bridged [1]FCP **17** which was isolated in a yield of 59% (Scheme 1-8).[37] This outcome, however, is in contrast to the result obtained from the respective salt-metathesis reaction with Li_2fc·tmeda where unwanted [1.1]FCP **6** (see Scheme 1-4) instead of a targeted [1]FCP was formed. Structural data obtained from single crystals of **17** provided tilt angles α for the two independent molecules, 16.26(9) and 16.45(10)°, which match reasonably

well with previously reported galla[1]ferrocenophanes [15.4(2)° and (15.83(19)° for **2** and **4**; Scheme 1-3).[32b,33] Moreover, a differential scanning calorimetry (DSC) thermogram of this new gallium-bridged [1]FCP **17** showed an exothermic peak at 201 °C that is indicative of ROP.

Scheme 1-9. Synthesis of Inda[1]ferrocenophanes

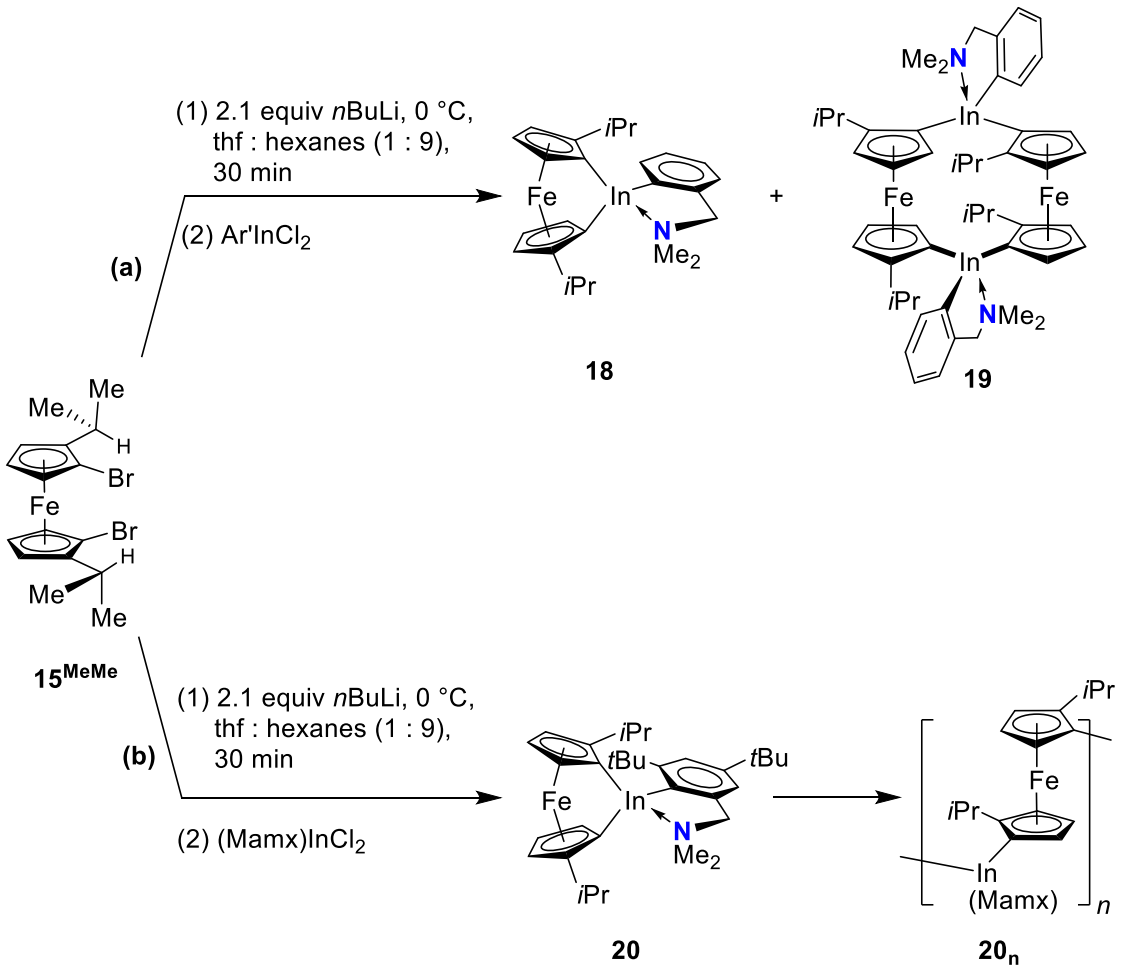

When the alkylated ferrocene dibromide **15^{MeMe}** was lithiated and reacted *in situ* with Ar′$InCl_2$ a mixture of the corresponding [1]FCP **18** and [1.1]FCP **19** were formed (Scheme 1-9a).[43] However, the [1]FCP **18** could not be isolated, and the logical approach to replace Ar′ with bulkier Mamx ligand was adopted, which resulted in a cleaner conversion to the targeted

inda[1]ferrocenophane **20**. Repeated attempts to isolate the strained compound were unsuccessful and resulted in the formation of poly(ferrocenylindigane) $\mathbf{20_n}$ in the reaction mixture.[43]

1.2.3 Reported Boron-Bridged [1]Ferrocenophanes

Metallopolymers containing the group-13-element boron are particularly interesting due to their electronic and optical properties associated with the electron deficient nature of the three-coordinate boron atom.[44] One can envision ROP of boron-bridged [*n*]FCPs as a potential method to synthesize boron-containing metallopolymers. Keeping that in mind, as mentioned earlier, the first boron-bridged [1]FCPs were already synthesized almost two decades ago (**21a–c**; Scheme 1-10).[29-30]

All three bora[1]ferrocenophanes were prepared via the salt-metathesis reaction between Li_2fc·tmeda and amino(dichloro)boranes equipped with sterically demanding substituents on the amino moiety. These new strained compounds drew special interest within scientific communities not only because they are the first and only examples of [1]FCPs with a second period element in the bridging position, but also because the molecular structure of the $(Me_3Si)_2$NB-bridged species **21a** revealed a new record for the tilt angle α. Compound **21a** with a tilt angle of 32.4(2)° took over the record holder of that time, thia[1]ferrocenophane **I** (Chart 1-3) with α = 31.05(10)°.[24] Till date, compound **21a** still has the highest α angle of all ferrocenophanes reported.

Scheme 1-10. The First Examples of Bora[1]ferrocenophanes

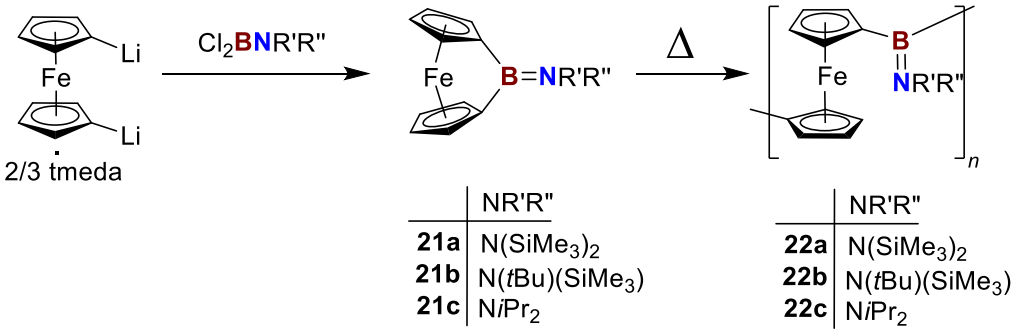

	NR'R"
21a	$N(SiMe_3)_2$
21b	$N(tBu)(SiMe_3)$
21c	$NiPr_2$

	NR'R"
22a	$N(SiMe_3)_2$
22b	$N(tBu)(SiMe_3)$
22c	$NiPr_2$

This tilt angle α is often of interest due to its correlation with the intrinsic strain of these monomers, which is released as heat (ΔH_{ROP}) during the ring-opening process.[45] For this reason, bora[1]ferrocenophanes, with the highest α angles, were anticipated to serve as excellent monomers for ROP. However, the thermal ROP of the known boron-bridged [1]FCPs at 180–200 °C afforded materials that were mainly insoluble in organic solvents; soluble fractions of **22c** were proved to be a mixture of low-molecular-weight polymers with small quantities of cyclic oligomers (n = 2, 3). It was concluded that higher molecular weight analogues of **22c** might be accessible if bora[1]ferrocenophanes with smaller substituents on boron can be prepared.[30] However, efforts to synthesize boron-bridged [1]FCPs using less sterically protected amino(dichloro)boranes [viz. Me_2NBCl_2, $Me(Ph)NBCl_2$, nBu(Me)$NBCl_2$] led to the products that were insoluble in common organic solvents.[30] Presumably, using these boranes led directly to the formation of oligomers through polycondensation without the formation of [1]FCPs as intermediates. Unfortunately, after these initial results, no further report on bora[1]ferrocenophanes was communicated.

1.3 Research Objectives

Poly(ferrocenylborane)s with three-coordinate boron moieties are of principal interest due the fact that such boron spacers can offer accessible p orbitals, which can participate in extended conjugation with Cp π-system of the polymer chain. Such conjugative interactions can lead to intriguing electronic properties in the polymer. However, not many ferrocene-based boron-containing polymers were reported since the ROP of the first bora[1]ferrocenophanes were communicated in 2000 (discussed above),[30] although there has been a significant improvement in the field of organoborane polymers.[44b,44c,44e,46] Many boron-bridged [n]FCPs ($n \geq 2$) were prepared

by the research groups of Braunschweig and Wrackmeyer, but none of them was used in the synthesis of poly(ferrocenylborane)s.[3d,3e] It was not until 2006 when a new synthetic strategy was adopted by the research groups of Jäkle and Wagner where $fc(BBr_2)_2$ (**23**; Scheme 1-11) was applied for a polycondensation to obtain poly(ferrocenylborane)s with BBr spacers (**24**; Scheme 1-11).[44a,44d] Post-polymerization modifications of these materials gave the corresponding BMes and $B[O(CH_2)_4Br]$ polymers, **25** and **26** respectively. However, such method only gave polymers of M_w up to ca. 7 kDa.

Scheme 1-11. Preparation of Poly(ferrocenylborane)s via Condensation

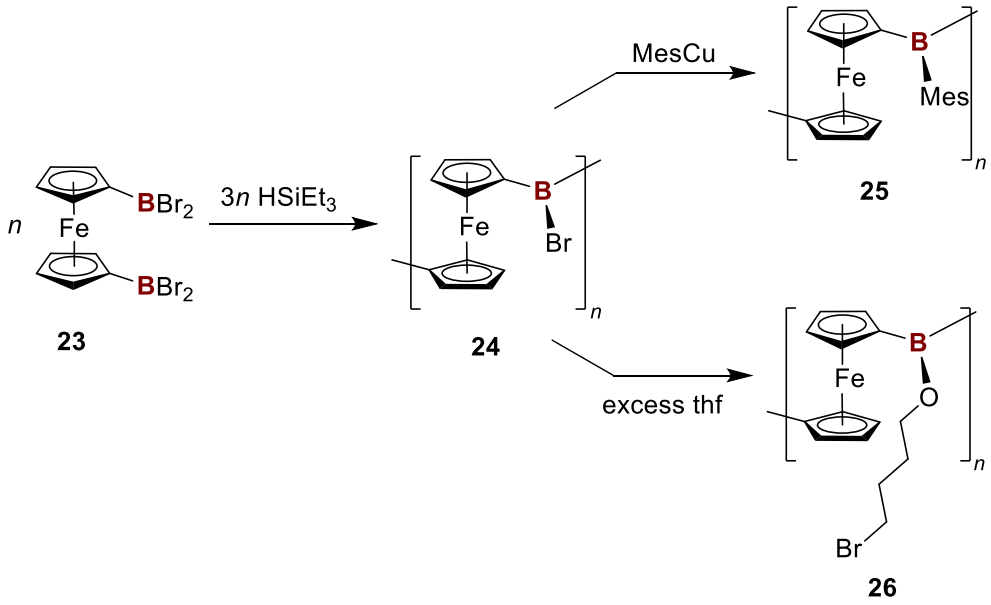

The objective of my Ph.D. work was to prepare a new family of bora[1]ferrocenophanes by applying the recently developed method in the Müller group (see section 1.2.2). It was hoped that this approach would allow to widely vary the ligand attached to the bridging boron atom. In addition, as the approach makes use of alkyl groups attached to Cp rings, there was a chance to solve the existing solubility problems in this area (see section 1.2.3). Overall, the applied approach offered a chance to develop new boron-containing monomers that might lead to soluble

metallopolymers. This Ph.D. work was curiosity-driven research aiming at increasing the knowledge base in the area of strained sandwich compounds. The following paragraphs provide more details about the thoughts and tactics applied to pursue the objective of the work.

Past experiences in the preparation of group-13-element bridged [1]FCPs suggest that steric plays a very important role in the successful synthesis of isolable [1]FCP monomers and their tendency to form polymers (see section 1.2).[18c,30] I wanted to carry forward that knowledge in the synthesis of isolable bora[1]ferrocenophanes, which would still be reactive enough to form poly(ferrocenylborane)s. Due to the presence of vacant p orbitals on boron, it is important to protect the boron atom electronically and/or sterically in order to obtain targeted [1]FCPs. Thus, initially the research proposal was divided into two the two parts of (a) electronically stabilized boron (e.g., aminoboranes) and (b) sterically stabilized boron (e.g., alkyl- or arylboranes) (see Chart 1-6). Combined with these two classes of boron dihalides, the dilithioferrocene derivatives **16** (Chart 1-6) were chosen as starting materials for the salt-metathesis reactions. Advantages of such dilithioferrocene species over $fcLi_2 \cdot tmeda$ are again twofold: (a) the overall steric bulk can be fine-tuned from the sandwich unit, and (b) the introduction of alkyl groups in sandwich unit should increase the solubility in common organic solvents of produced [1]FCPs as well as that of the polymers. As mentioned before, the lack of solubility of polymers could not be overcome in previous investigations of bora[1]ferrocenophanes.[30] With this Ph.D. thesis at hand it was hoped that the large intrinsic strain of boron-bridged [1]ferrocenophanes could finally be applied for the preparation of new, potentially useful metallopolymers.

Chart 1-6. Proposed Starting Materials for the Synthesis of New Bora[1]ferrocenophanes

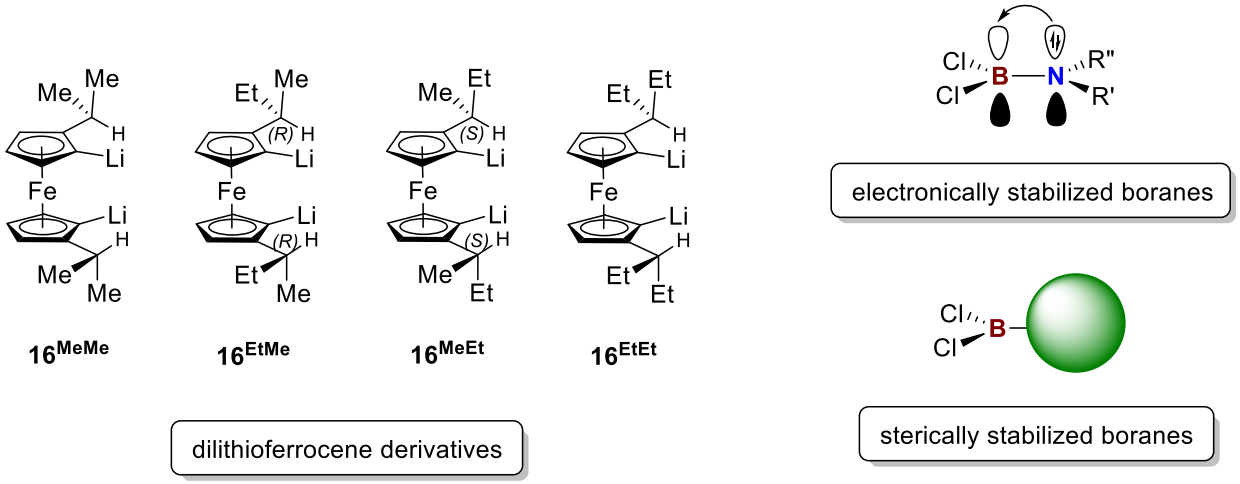

My Ph.D. work will be discussed in the following chapters in the form of four manuscripts.

Chapter 2:

Sadeh, S.; Bhattacharjee, H.; Khozeimeh Sarbisheh, E.; Quail, J. W.; Müller, J. *Chem.-Eur. J.* **2014,** *20*, 16320-16330.

Chapter 3:

Bhattacharjee, H.; Martell, J. D.; Khozeimeh Sarbisheh, E.; Sadeh, S.; Quail, J. W.; Müller, J. *Organometallics* **2016,** *35*, 2156-2164.

Chapter 4:

Bhattacharjee, H.; Dey, S.; Zhu, J.; Sun, W.; Müller, J. *Chem. Commun.* **2018**, *54*, 5562-5565.

Chapter 5:

Bhattacharjee, H.; Zhu, J.; Müller, J. manuscript under preparation.

In the first published manuscript (Chapter 2), we have reported on our strategy to employ amino(dichloro)boranes as a source of electronically stabilized boron and combined them with two alkyl-substituted dilithioferrocenes **16**$^{\mathbf{MeMe}}$ and **16**$^{\mathbf{EtEt}}$ (Chart 1-6) in respective salt-metathesis reactions. This resulted in a set of six new highly strained bora[1]ferrocenophanes, which were then used as monomers in thermal ROP to produce poly(ferrocenylborane)s. Both monomers and polymers are highly soluble in common organic solvents (such as hexanes, thf, CH_2Cl_2), however, the polymers are only of moderate molecular weight ($M_w \approx 10$ kDa). Along with these positive results, we also discovered 1,1′-bis(boryl)ferrocene species as major side products in such salt-metathesis reactions. In the quest of improving conversion rates towards targeted [1]FCPs by blocking the formation of 1,1′-bis(boryl)ferrocene species, we investigated the mechanism of such salt-metathesis reactions. We realized that temperature, speed of addition of amino(dichloro)-boranes, and alkyl groups on the applied dibromoferrocene species have an impact on the outcome of the product ratios.

We further investigated the mechanism, in particular, the effect of alkyl groups of the Cp moieties on the reaction outcome. We included two more dibromoferrocene derivatives (**16**$^{\mathbf{MeEt}}$ and **16**$^{\mathbf{EtMe}}$; Chart 1-6) in our studies and obtained further information on the reaction mechanism. This will be discussed in Chapter 3 (second published manuscript).

Moreover, we realized that in order to obtain isolable bora[1]ferrocenophanes an electronic π stabilization by a nitrogen donor of an amino group is essential. We utilized this knowledge further in our third published manuscript (Chapter 4) and reported the first examples of azabora[2]ferrocenophanes. In these species the bridging boron atom is electronically stabilized by a nitrogen atom, which is also a part of the bridge. However, these monomers turned out to be thermally robust and unreactive towards ROP.

From these results it seems apparent that an amino-substituted boron is essential to obtain isolable boron-bridged [*n*]FCPs. However, such π donor groups decrease the electrophilicity of the bridging boron atom, which might contribute significantly to a lack of reactivity of these species. For this reason, we sought to prepare bora[1]ferrocenophanes with sterically protected bridging boron. These explorations turned out to be challenging as the right amount of steric bulk and the proper conditions to synthesize and isolate such species required significant fine-tuning. In the final manuscript (Chapter 5), we report the synthesis and isolation of the first examples of bora[1]ferrocenophanes with sterically protected boron. These new [1]FCPs are highly strained and new record holders in ring tilting *α*. Moreover, one of these monomers resulted in a chiral poly(ferrocenylborane).

1.4 References

(1) (a) Manners, I. *Science* **2001**, *294*, 1664-1666. (b) Manners, I. *Synthetic Metal-Containing Polymers*; Wiley-VCH: Weinheim, 2004. (c) Whittell, G. R.; Manners, I. *Adv. Mater.* **2007**, *19*, 3439-3468. (d) Bellas, V.; Rehahn, M. *Angew. Chem., Int. Ed.* **2007**, *46*, 5082-5104. (e) Williams, K. A.; Boydston, A. J.; Bielawski, C. W. *Chem. Soc. Rev.* **2007**, *36*, 729-744. (f) Krüger, R. A.; Baumgartner, T. *Dalton Trans.* **2010**, *39*, 5759-5767. (g) Wong, W. Y.; Harvey, P. D. *Macromol. Rapid Commun.* **2010**, *31*, 671-713. (h) Whittell, G. R.; Hager, M. D.; Schubert, U. S.; Manners, I. *Nat. Mater.* **2011**, *10*, 176-188. (i) Zhou, J.; Whittell, G. R.; Manners, I. *Macromolecules* **2014**, *47*, 3529-3543. (j) Hailes, R. L. N.; Oliver, A. M.; Gwyther, J.; Whittell, G. R.; Manners, I. *Chem. Soc. Rev.* **2016**, *45*, 5358-5407. (k) Winter, A.; Schubert, U. S. *Chem. Soc. Rev.* **2016**, *45*, 5311-5357.

(2) (a) Schacher, F. H.; Rupar, P. A.; Manners, I. *Angew. Chem., Int. Ed.* **2012**, *51*, 7898-7921. (b) Wang, L.; Cole, M.; Li, J.; Zheng, Y.; Chen, Y. P.; Miller, K. P.; Decho, A. W.; Benicewicz, B.

C. *Polym. Chem.* **2015**, *6*, 248-255. (c) Li, Y.; Krentz, T. M.; Wang, L.; Benicewicz, B. C.; Schadler, L. S. *ACS Appl. Mater. Interfaces* **2014**, *6*, 6005-6021.

(3) (a) Tamm, M.; Kunst, A.; Bannenberg, T.; Herdtweck, E.; Sirsch, P.; Elsevier, C. J.; Ernsting, J. M. *Angew. Chem., Int. Ed.* **2004**, *43*, 5530-5534. (b) Tamm, M. *Chem. Commun.* **2008**, 3089-3100. (c) Braunschweig, H.; Kupfer, T. *Acc. Chem. Res.* **2010**, *43*, 455-465. (d) Braunschweig, H.; Breitling, F. M.; Gullo, E.; Kraft, M. *J. Organomet. Chem.* **2003**, *680*, 31-42. (e) Braunschweig, H.; Kupfer, T. *Eur. J. Inorg. Chem.* **2012**, *2012*, 1319-1332. (f) Adams, C. J.; Braunschweig, H.; Fuss, M.; Kraft, K.; Kupfer, T.; Manners, I.; Radacki, K.; Whittell, G. R. *Chem.-Eur. J.* **2011**, *17*, 10379-10387. (g) Tagne Kuate, A. C.; Daniliuc, C. G.; Jones, P. G.; Tamm, M. *Eur. J. Inorg. Chem.* **2012**, *2012*, 1727-1733. (h) Braunschweig, H.; Damme, A.; Demeshko, S.; Dück, K.; Kramer, T.; Krummenacher, I.; Meyer, F.; Radacki, K.; Stellwag-Konertz, S.; Whittell, G. R. *J. Am. Chem. Soc.* **2015**, *137*, 1492-1500. (i) Russell, A. D.; Musgrave, R. A.; Stoll, L. K.; Choi, P.; Qiu, H.; Manners, I. *J. Organomet. Chem.* **2015**, *784*, 24-30.

(4) Kealy, T. J.; Pauson, P. L. *Nature* **1951**, *168*, 1039-1040.

(5) Rinehart, K. L.; Curby, R. J. *J. Am. Chem. Soc.* **1957**, *79*, 3290-3291.

(6) Rinehart, K. L.; Frerichs, A. K.; Kittle, P. A.; Westman, L. F.; Gustafson, D. H.; Pruett, R. L.; McMahon, J. E. *J. Am. Chem. Soc.* **1960**, *82*, 4111-4112.

(7) Osborne, A. G.; Whiteley, R. H. *J. Organomet. Chem.* **1975**, *101*, C27-C28.

(8) Foucher, D. A.; Tang, B.-Z.; Manners, I. *J. Am. Chem. Soc.* **1992**, *114*, 6246-6248.

(9) Bellas, V.; Rehahn, M. *Angew. Chem., Int. Ed.* **2007**, *46*, 5082-5104.

(10) Kulbaba, K.; Manners, I. *Macromol. Rapid Commun.* **2001**, *22*, 711-724.

(11) (a) Paquet, C.; Cyr, P. W.; Kumacheva, E.; Manners, I. *Chem. Commun.* **2004**, 234-235. (b) Paquet, C.; Cyr, P. W.; Kumacheva, E.; Manners, I. *Chem. Mater.* **2004**, *16*, 5205-5211.

(12) Rulkens, R.; Lough, A. J.; Manners, I.; Lovelace, S. R.; Grant, C.; Geiger, W. E. *J. Am. Chem. Soc.* **1996**, *118*, 12683-12695.

(13) Puzzo, D. P.; Arsenault, A. C.; Manners, I.; Ozin, G. A. *Angew. Chem., Int. Ed.* **2009**, *121*, 961-965.

(14) Massey, J. A.; Temple, K.; Cao, L.; Rharbi, Y.; Raez, J.; Winnik, M. A.; Manners, I. *J. Am. Chem. Soc.* **2000**, *122*, 11577-11584.

(15) Wang, X. S.; Guerin, G.; Wang, H.; Wang, Y. S.; Manners, I.; Winnik, M. A. *Science* **2007**, *317*, 644-647.

(16) (a) Gilroy, J. B.; Gädt, T.; Whittell, G. R.; Chabanne, L.; Mitchels, J. M.; Richardson, R. M.; Winnik, M. A.; Manners, I. *Nat. Chem.* **2010**, *2*, 566-570. (b) Qiu, H.; Gao, Y.; Du, V. A.; Harniman, R.; Winnik, M. A.; Manners, I. *J. Am. Chem. Soc.* **2015**, *137*, 2375-2385.

(17) (a) Qiu, H.; Cambridge, G.; Winnik, M. A.; Manners, I. *J. Am. Chem. Soc.* **2013**, *135*, 12180-12183. (b) Qiu, H.; Hudson, Z. M.; Winnik, M. A.; Manners, I. *Science* **2015**, *347*, 1329-1332. (c) Hudson, Z. M.; Boott, C. E.; Robinson, M. E.; Rupar, P. A.; Winnik, M. A.; Manners, I. *Nat. Chem.* **2014**, *6*, 893-898. (d) Hudson, Z. M.; Lunn, D. J.; Winnik, M. A.; Manners, I. *Nat. Commun.* **2014**, *5*, 3372.

(18) (a) Herbert, D. E.; Mayer, U. F. J.; Manners, I. *Angew. Chem., Int. Ed.* **2007**, *46*, 5060-5081. (b) Musgrave, R. A.; Russell, A. D.; Manners, I. *Organometallics* **2013**, *32*, 5654-5667. (c) Bhattacharjee, H.; Müller, J. *Coord. Chem. Rev.* **2016**, *314*, 114-133.

(19) Ieong, N. S.; Manners, I. *Macromol. Chem. Phys.* **2009**, *210*, 1080-1086.

(20) (a) Honeyman, C. H.; Peckham, T. J.; Massey, J. A.; Manners, I. *Chem. Commun.* **1996**, 2589-2590. (b) Peckham, T. J.; Massey, J. A.; Honeyman, C. H.; Manners, I. *Macromolecules* **1999**, *32*, 2830-2837. (c) Mizuta, T.; Onishi, M.; Miyoshi, K. *Organometallics* **2000**, *19*, 5005-5009. (d)

Mizuta, T.; Imamura, Y.; Miyoshi, K. *J. Am. Chem. Soc.* **2003**, *125*, 2068-2069. (e) Patra, S. K.; Whittell, G. R.; Nagiah, S.; Ho, C.-L.; Wong, W.-Y.; Manners, I. *Chem.-Eur. J.* **2010**, *16*, 3240-3250.

(21) Herbert, D. E.; Mayer, U. F. J.; Gilroy, J. B.; Lopez-Gómez, M. J.; Lough, A. J.; Charmant, J. P. H.; Manners, I. *Chem.-Eur. J.* **2009**, *15*, 12234-12246.

(22) (a) Bishop, J. J.; Davison, A.; Katcher, M. L.; Lichtenberg, D. W.; Merrill, R. E.; Smart, J. C. *J. Organomet. Chem.* **1971**, *27*, 241-249. (b) Wrighton, M. S.; Palazzotto, M. C.; Bocarsly, A. B.; Bolts, J. M.; Fischer, A. B.; Nadjo, L. *J. Am. Chem. Soc.* **1978**, *100*, 7264-7271.

(23) Brandt, P. F.; Rauchfuss, T. B. *J. Am. Chem. Soc.* **1992**, *114*, 1926-1927.

(24) Rulkens, R.; Gates, D. P.; Balaishis, D.; Pudelski, J. K.; McIntosh, D. F.; Lough, A. J.; Manners, I. *J. Am. Chem. Soc.* **1997**, *119*, 10976-10986.

(25) Fischer, A. B.; Kinney, J. B.; Staley, R. H.; Wrighton, M. S. *J. Am. Chem. Soc.* **1979**, *101*, 6501-6506.

(26) Seyferth, D.; Withers, H. P. *J. Organomet. Chem.* **1980**, *185*, C1-C5.

(27) Foucher, D. A.; Manners, I. *Macromol. Rapid Commun.* **1993**, *14*, 63-66.

(28) Jäkle, F.; Rulkens, R.; Zech, G.; Foucher, D. A.; Lough, A. J.; Manners, I. *Chem.-Eur. J.* **1998**, *4*, 2117-2128.

(29) Braunschweig, H.; Dirk, R.; Müller, M.; Nguyen, P.; Resendes, R.; Gates, D. P.; Manners, I. *Angew. Chem., Int. Ed.* **1997**, *36*, 2338-2340.

(30) Berenbaum, A.; Braunschweig, H.; Dirk, R.; Englert, U.; Green, J. C.; Jäkle, F.; Lough, A. J.; Manners, I. *J. Am. Chem. Soc.* **2000**, *122*, 5765-5774.

(31) Eaborn, C.; Smith, J. D. *J. Chem. Soc., Dalton Trans.* **2001**, 1541-1552.

(32) (a) Schachner, J. A.; Lund, C. L.; Quail, J. W.; Müller, J. *Organometallics* **2005**, *24*, 785-787. (b) Schachner, J. A.; Lund, C. L.; Quail, J. W.; Müller, J. *Organometallics* **2005**, *24*, 4483-4488.

(33) Lund, C. L.; Schachner, J. A.; Quail, J. W.; Müller, J. *Organometallics* **2006**, *25*, 5817-5823.

(34) Schachner, J. A.; Tockner, S.; Lund, C. L.; Quail, J. W.; Rehahn, M.; Müller, J. *Organometallics* **2007**, *26*, 4658-4662.

(35) Schachner, J. A.; Orlowski, G. A.; Quail, J. W.; Kraatz, H.-B.; Müller, J. *Inorg. Chem.* **2006**, *45*, 454-459.

(36) Schachner, J. A.; Lund, C. L.; Burgess, I. J.; Quail, J. W.; Schatte, G.; Müller, J. *Organometallics* **2008**, *27*, 4703-4710.

(37) Sadeh, S.; Schatte, G.; Müller, J. *Chem.-Eur. J.* **2013**, *19*, 13408-13417.

(38) (a) Yoshifuji, M.; Kamijo, K.; Toyota, K. *Tetrahedron Lett.* **1994**, *35*, 3971-3974. (b) Bagh, B.; Gilroy, J. B.; Staubitz, A.; Müller, J. *J. Am. Chem. Soc.* **2010**, *132*, 1794-1795. (c) Bagh, B.; Schatte, G.; Green, J. C.; Müller, J. *J. Am. Chem. Soc.* **2012**, *134*, 7924-7936.

(39) (a) Schwink, L.; Knochel, P. *Chem.-Eur. J.* **1998**, *4*, 950-968. (b) Kang, J.; Lee, J. H.; Im, K. S. *J. Mol. Catal. A: Chem.* **2003**, *196*, 55-63.

(40) Corey, E. J.; Bakshi, R. K.; Shibata, S. *J. Am. Chem. Soc.* **1987**, *109*, 5551-5553.

(41) Marquarding, D.; Klusacek, H.; Gokel, G.; Hoffmann, P.; Ugi, I. *J. Am. Chem. Soc.* **1970**, *92*, 5389-5393.

(42) Bailey, W. F.; Luderer, M. R.; Jordan, K. P. *J. Org. Chem.* **2006**, *71*, 2825-2828.

(43) Bagh, B.; Sadeh, S.; Green, J. C.; Müller, J. *Chem.-Eur. J.* **2014**, *20*, 2318-2327.

(44) (a) Heilmann, J. B.; Qin, Y.; Jäkle, F.; Lerner, H.-W.; Wagner, M. *Inorg. Chim. Acta* **2006**, *359*, 4802-4806. (b) Cheng, F.; Jäkle, F. *Polym. Chem.* **2011**, *2*, 2122-2132. (c) Lorenz, T.; Crumbach, M.; Eckert, T.; Lik, A.; Helten, H. *Angew. Chem., Int. Ed.* **2017**, *56*, 2780-2784. (d)

Heilmann, J. B.; Scheibitz, M.; Qin, Y.; Sundararaman, A.; Jäkle, F.; Kretz, T.; Bolte, M.; Lerner, H. W.; Holthausen, M. C.; Wagner, M. *Angew. Chem., Int. Ed.* **2006**, *45*, 920-925. (e) Helten, H. *Chem.-Eur. J.* **2016**, *22*, 12972-12982. (f) Entwistle, C. D.; Marder, T. B. *Angew. Chem., Int. Ed.* **2002**, *41*, 2927-2931.

(45) Khozeimeh Sarbisheh, E.; Bhattacharjee, H.; Cao, M. P. T.; Zhu, J.; Müller, J. *Organometallics* **2017**, *36*, 614-621.

(46) (a) Jäkle, F. *Coord. Chem. Rev.* **2006**, *250*, 1107-1121. (b) Jäkle, F. *Chem. Rev.* **2010**, *110*, 3985-4022. (c) Chen, P.; Lalancette, R. A.; Jäkle, F. *J. Am. Chem. Soc.* **2011**, *133*, 8802-8805. (d) Baggett, A. W.; Guo, F.; Li, B.; Liu, S. Y.; Jäkle, F. *Angew. Chem., Int. Ed.* **2015**, *54*, 11191-11195. (e) Ayhan, O.; Eckert, T.; Plamper, F. A.; Helten, H. *Angew. Chem., Int. Ed.* **2016**, *55*, 13321-13325. (f) Resendiz-Lara, D. A.; Stubbs, N. E.; Arz, M. I.; Pridmore, N. E.; Sparkes, H. A.; Manners, I. *Chem. Commun.* **2017**, *53*, 11701-11704.

2 Chiral Bora[1]ferrocenophanes: Syntheses, Mechanistic Insights, and Ring-Opening Polymerizations

2.1 Author Contribution and Relation to the Research Objectives

This work was done in collaboration with Dr. Saeid Sadeh, Dr. Elaheh Khozeimeh Sarbisheh, and Prof. J. Wilson Quail. Dr. Sadeh synthesized di(isopropyl)dibromoferrocene (**15^{MeMe}**) and all the boron-bridged [1]FCPs (**27^{R1R2}**), and performed complete characterization of [1]FCPs, DSC, and thermal ROP studies. Dr. Khozeimeh Sarbisheh synthesized di(3-pentyl)dibromoferrocene (**15^{EtEt}**). All single-crystal X-ray analyses were performed by Prof. Quail. I synthesized di(isopropyl)dibromoferrocene (**15^{MeMe}**) and all three dichloro(amino)boranes (R′R″NBCl$_2$). I synthesized and completely characterized the 1,1′-bis(boryl)ferrocenes (**28^{R1R2}**). I also performed UV-Vis spectrophotometric analyses for all strained bora[1]ferrocenophanes and 1,1′-bis(boryl)ferrocenes. Moreover, I assisted Dr. Saeid Sadeh on many experiments such as DSC, elemental analysis, thermal ROP, and salt-metathesis reactions. Furthermore, I contributed on editing and referencing the manuscript, which was written by Prof. Jens Müller, and also compiled the supporting information for the compounds that I synthesized.

In this manuscript, we reported a new family of bora[1]ferrocenophanes (**27^{R1R2}**), equipped with different alkyl groups on the Cp moieties and different amino substituents on the bridging boron atom, which resulted in soluble poly(ferrocenylborane)s. Moreover, detailed investigations provided mechanistic insight into the formation of bora[1]ferrocenophanes. The key compounds of this approach are the enantiomerically pure ferrocene dibromides (**15^{MeMe}** and **15^{EtEt}**). Dichloroboranes with π-donor substituents on boron, specifically amino(dichloro)boranes

*t*Bu(SiMe$_3$)NBCl$_2$, *i*Pr$_2$NBCl$_2$, and Et$_2$NBCl$_2$, were chosen in the synthesis of boron-bridged [1]FCPs.

Six different boron-bridged [1]FCPs were targeted from the salt-metathesis reactions between three amino(dichloro)boranes [Et$_2$NBCl$_2$, *t*Bu(SiMe$_3$)NBCl$_2$, and *i*Pr$_2$NBCl$_2$] and the two alkylated dibromoferrocenes. The alkyl groups on these [1]FCPs helped to increase the solubilities of the obtained polymers, however, they were of low molecular weight and not pure linear polymers. The thermal stability of monomers is so high that the required temperatures for ROP lead to extrusion of iron.

In this work we obtained a better insight into the outcome of the salt-metathesis reactions. For instance, reactions of Et$_2$NBCl$_2$ and the dilithioferrocene derivatives proceed nearly quantitatively to yield the corresponding [1]FCPs **27^{R1R2}**. While the similar reactions with the amino(dichloro)boranes *t*Bu(SiMe$_3$)NBCl$_2$ and *i*Pr$_2$NBCl$_2$ led to the formation of significant amounts of 1,1′-bis(boryl)ferrocenes (**28^{R1R2}**) as side products. It was realized that the product ratio **27^{R1R2}**:**28^{R1R2}** strongly depends on the reaction temperature and the rate of addition of the boron dihalide solution. Further investigation on this led us to an improved reaction condition which favours the formation of the targeted [1]FCPs.

The following is a verbatim copy[d,e] of the published article Sadeh, S.; Bhattacharjee, H.; Khozeimeh Sarbisheh, E.; Quail, J. W.; Müller, J. *Chem.-Eur. J.* **2014**, *20*, 16320-16330.

[d] Reproduced with permission from Sadeh, S.; Bhattacharjee, H.; Khozeimeh Sarbisheh, E.; Quail, J. W.; Müller, J. *Chem.-Eur. J.* **2014**, *20*, 16320-16330. Copyright © 2014 John Wiley & Sons.
[e] Compound numbers and some chemical drawings were changed to maintain a uniform style in the thesis.

2.2 Abstract

A series of new boron-bridged [1]ferrocenophanes ([1]FCPs) was prepared by salt-metathesis reactions between enantiomerically pure dilithioferrocenes and amino(dichloro)boranes [Et_2NBCl_2, iPr_2NBCl_2, or tBu(Me_3Si)$NBCl_2$]. The dilithioferrocenes were prepared *in situ* by lithium–bromine exchange from the respective planar-chiral dibromides (S_p,S_p)-[1-Br-2-(HR^1R^2C)H_3C_5]$_2$Fe (R^1R^2 = Me_2 or Et_2). In most of the cases, mixtures of the targeted [1]FCPs **27** and the unwanted 1,1′-bis(boryl)ferrocenes **28** were formed. The product ratio depends on the bulkiness of the amino group, the speed of addition of the amino(dichloro)borane, the alkyl group on Cp rings, and in particular on the reaction temperature. The formation of strained [1]FCPs is strongly favoured by increased reaction temperatures. Secondly, $CHEt_2$ groups at Cp rings favoured the formation of the targeted [1]FCPs stronger than $CHMe_2$ groups. These discoveries open up new possibilities to further suppress the formation of unwanted byproducts by a careful choice of the reaction temperature and through tailoring the bulkiness of CHR_2 groups on ferrocene. Thermal ring-opening polymerizations of selected boron-bridged [1]FCPs gave metallopolymers with a M_w of 10 kDa (GPC).

2.3 Introduction

During the last two decades, significant advances have been made towards incorporating boron into polymeric materials. Many research efforts have been concentrated on materials for optoelectronic applications with boron being a part of an extended π system.[1] There has been tremendous progress in this area, which is partly due to the development of new synthetic procedures and the application of bulky aryl groups to protect the acidic boron center [for example, 2,4,6-trimethylphenyl (Mes) or 2,4,6-triisopropylphenyl (Tip)]. A particularly elegant method to incorporate main-group

elements into a polymer backbone is that of ring-opening polymerization (ROP) of strained sandwich compounds.[2] Significant advances in the synthesis and purification of monomers and in polymerization methods were made during the last two decades, in particular for the class of ferrocenophanes (FCPs).[3] The most developed strained sandwich compounds are silicon-bridged [1]FCPs (**G^{R}**; Figure 2-1), which can undergo living polymerization,[2,4] allowing the preparation of block copolymers. Poly(ferrocenyldimethylsilane) (**PFS** with $SiMe_2$; Figure 2-1) is partially crystalline, causing block copolymers to form rod-shaped micelles in block-selective solvents with PFS as the core. These micelles are living and grow to larger micelles of uniform lengths through the addition of further unimers. This bottom-up approach has been recently applied for the fabrication of uniform nanomaterials.[5] In contrast to the advanced use of silicon-bridged [1]FCPs, other strained sandwich compounds are far less developed, and only [1]FCPs bridged by germanium[6] and phosphorus,[7] and [2]FCPs bridged by carbon[8] could be polymerized with control over molecular weights and molecular weight distributions. Many other strained sandwich compounds were polymerized but a variety of problems brought these endeavors to a standstill. A common encountered problem is the lack of synthetic flexibility. Often, for the targeted polymers, non-encumbered ligands at bridging elements are needed; however, many strained monomers are only accessible with sterically encumbered bridging moieties.[9,10] Another common problem is the lack of solubility of prepared metallopolymers. Recently, we tackled both problems simultaneously through the introduction of isopropyl groups adjacent to the bridging element, which provide steric protection and act as solubilizing groups (**K**; Figure 2-1).[11,12]

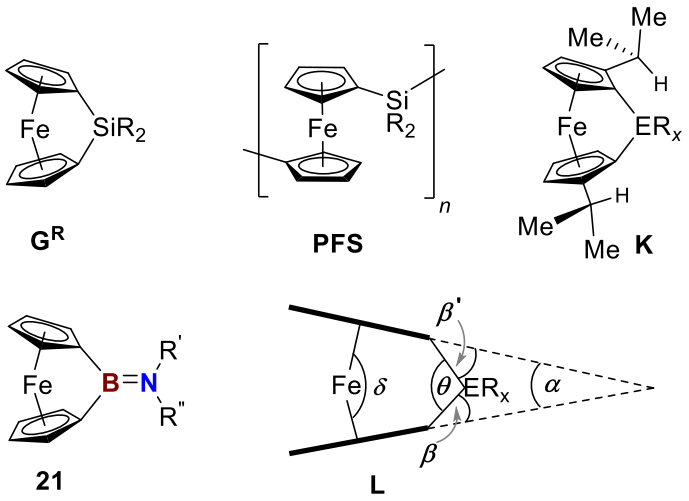

Figure 2-1. Known [1]ferrocenophanes (**G^{R}**, **K**, **21**), polyferrocenylsilane (**PFS**), and common distortion angles (**L**).[3b] **K**: ER_x = BN*i*Pr$_2$, Ga(2-$Me_2NCH_2C_6H_4$), In[6-(Me_2NCH_2)-2,4-*t*$Bu_2C_6H_2$], $SiMe_2$, Sn*t*Bu_2; **21**: NR′R″ = N($SiMe_3$)$_2$; N*t*Bu($SiMe_3$); N*i*Pr$_2$.

A particularly interesting family of strained sandwich compounds is that of boron-bridged [1]FCPs: they are the only known [1]FCPs bridged by a 2nd period element.[3c,13] Before we started working in this area, only three bora[1]ferrocenophanes were known (**21**; Figure 2-1); the BN($SiMe_3$)$_2$-bridged species showed with 32.4(2)° the largest α tilt angle of all known FCPs (**L**; Figure 2-1). These three boron-bridged [1]FCPs could be polymerized thermally, but the resulting materials were insoluble in organic solvents, and this chemistry came to a halt.[13b,14] The authors concluded that high-molecular-weight polymers might be accessible if boron-bridged [1]FCPs can be prepared with smaller substituents at boron.[13b]

Herein, we report on a new family of boron-bridged [1]FCPs, equipped with different alkyl groups on the Cp moieties. These investigations not only resulted in soluble poly(ferrocenylborane)s but also provided mechanistic insights into the formation of [1]FCPs. Furthermore, we solved the puzzle why the measured strain energy for these record holders in Cp tilting is significantly lower than expected.[13b]

2.4 Results and Discussion

As mentioned before, we recently described [1]FCPs equipped with two *i*Pr groups in α positions on the Cp rings (**K**, Figure 2-1). The alkyl groups were introduced through a well-developed multistep diastereoselective synthesis based on Ugi amine chemistry,[15] with the key steps shown in Scheme 2-1.[16,17] We now employed the same method to introduce 3-pentyl instead of the isopropyl groups (Scheme 2-1).

Scheme 2-1. Formation of Bora[1]ferrocenophanes **27^{R1R2}**

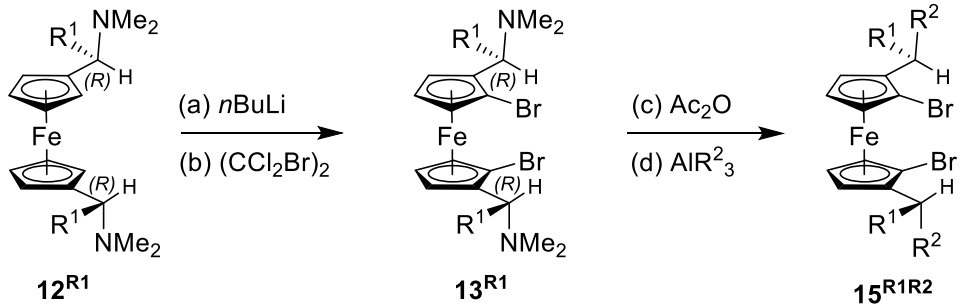

12^{R1} **13^{R1}** **15^{R1R2}** **27^{R1R2}**

R'/R"	CHR^{1}R^2 = CHMe$_2$	CHR^{1}R^2 = CHEt$_2$
Et/Et	**27a^{MeMe}**	**27a^{EtEt}**
*i*Pr/*i*Pr	**27b^{MeMe}**	**27b^{EtEt}**
*t*Bu/Me$_3$Si	**27c^{MeMe}**	**27c^{EtEt}**

The key compounds of this approach are the enantiomerically pure ferrocene dibromides **15^{MeMe}** and **15^{EtEt}** (Scheme 2-1). Whereas the isopropyl-containing dibromide **15^{MeMe}** had been prepared for the first time by us,[11] the 3-pentyl decorated species **15^{EtEt}** is already known.[18] We obtained **15^{EtEt}** as a crystalline solid and obtained single crystals for structural analysis by X-ray diffraction (Figure 2-2; Supporting Information, Tables S1 and S2). As expected, the molecular

structure of **15**$^{\mathbf{EtEt}}$ did not reveal any surprises. Its structure is very similar to that of **15**$^{\mathbf{MeMe}}$,[11] including the conformation of the alkyl groups, a fact that will become important for the later discussion (see mechanistic insights below). Both dibromides, **15**$^{\mathbf{MeMe}}$ and **15**$^{\mathbf{EtEt}}$, were prepared as enantiomerically pure species exhibiting planar chirality (S_p,S_p isomers).

Recently, we had shown that addition of 2.1 equivalents of *n*BuLi to **15**$^{\mathbf{MeMe}}$ in a solvent mixture of thf/hexanes (1:9) results in a clean lithium-bromide exchange (Scheme 2-1);[11,19] expectedly, **15**$^{\mathbf{EtEt}}$ can be lithiated with the same method. It is worth noting that the resulting Li_2fc^{iPr} (**16**$^{\mathbf{MeMe}}$) and $Li_2fc^{3\text{-Pen}}$ (**16**$^{\mathbf{EtEt}}$**)**, respectively, do not precipitate, even though most of the solvent in the mixture is hexane (fc^{iPr} = (S_p,S_p)-2,2′-(*i*PrH_3C_5)$_2$Fe; $fc^{3\text{-Pen}}$ = (S_p,S_p)-2,2′- [(Et_2CH)H_3C_5]$_2$Fe).

As shown in Scheme 2-1, the so-prepared dilithio species Li_2fc^{iPr} and $Li_2fc^{3\text{-Pen}}$, respectively, were reacted with the amino-boranes Et_2NBCl_2, *i*Pr_2NBCl_2, and *t*Bu(Me_3Si)$NBCl_2$ resulting in six bora[1]ferrocenophanes.[20] Whereas species **27a-c**$^{\mathbf{EtEt}}$ and **27b**$^{\mathbf{MeMe}}$ were isolated as pure solids in yields between 48 and 65%, species **27a**$^{\mathbf{MeMe}}$ and **27c**$^{\mathbf{MeMe}}$ could only be obtained as impure oils containing small amounts of the hydrolysis byproduct (*i*PrH_4C_5)$_2$Fe. The three [1]FCPs equipped with *i*Pr groups on Cp (**27a-c**$^{\mathbf{MeMe}}$) are volatile under vacuum at 55–95 °C and were obtained either by sublimation (**27b**$^{\mathbf{MeMe}}$) or by flask-to-flask condensation (**27a**$^{\mathbf{MeMe}}$ and **27c**$^{\mathbf{MeMe}}$). It seems that the lack of formation of crystals of the latter two species prohibited further purification. The three [1]FCPs equipped with 3-pentyl groups were isolated as crystalline products (**27a**$^{\mathbf{EtEt}}$ and **27b**$^{\mathbf{EtEt}}$) or as a solid powder (**27c**$^{\mathbf{EtEt}}$) from hexane solutions at −80 °C.[21] All six [1]FCPs are highly soluble in common organic solvents.

The six [1]FCPs show similar signal patterns in NMR spectra. For example, the compounds equipped with either Et_2NB- or *i*Pr_2NB-bridging moieties show three Cp signals in ^{1}H NMR spectra, as expected for these C_2-symmetric species. The signals for Cp protons were found in the ranges of

δ = 3.43–3.56 (α-CH), 4.26–4.30 (β-CH), and 4.52–4.57 (β-CH) ppm. Each of the two *t*Bu(Me$_3$Si)NB-bridged species (**27c^{MeMe}** and **27c^{EtEt}**) reveal their lower symmetry by a set of three pairs of signals that occur in similar ranges as the peaks for the C_2-symmetric [1]FCPs. The most indicative spectroscopic data for the presence of a strained FCP are the ^{13}C resonances of the *ipso*-carbon bound to boron, which were found as broad signals in the range of δ = 39.9 to 45.5 ppm. Similar values were reported for the known bora[1]ferrocenophanes (**21**; Figure 2-1).[13]

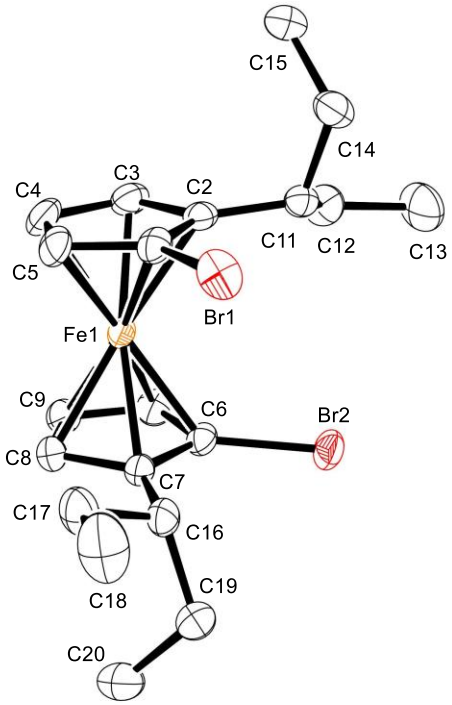

Figure 2-2. Molecular structure of **15^{EtEt}** with thermal ellipsoids at 50% probability level. Hydrogen atoms are omitted for clarity. For bond lengths and angles, see the Supporting Information, Table S2.

Employing the aminoboranes *i*Pr$_2$NBCl$_2$ and *t*Bu(Me$_3$Si)NBCl$_2$ to prepare respective [1]FCPs (Scheme 2-1) led to the formation of significant amounts of bis(boryl)ferrocenes (**28^{R1R2}**; Scheme 2-2). The four compounds **28b^{MeMe}**, **28c^{MeMe}**, **28b^{EtEt}**, and **28c^{EtEt}** were identified by ^{1}H NMR spectroscopy in reaction mixtures (see the Supporting Information for NMR spectra). In salt-metathesis reactions with Et$_2$NBCl$_2$ (Scheme 2-1), we could not identify bis(boryl)ferrocenes, as the

two Et_2NB-bridged [1]FCPs **27a^{MeMe}** and **27a^{EtEt}** formed with such high conversions that the small peaks of byproducts in the proton NMR spectra could not reliably be assigned to the expected bis-(boryl)ferrocenes (see the Supporting Information for NMR spectra). To fully characterize some of these bis-(boryl)ferrocenes, we prepared **28b^{MeMe}** and **28c^{MeMe}** selectively by a reverse order of addition; that is, a solution of the dilithio species Li_2fc^{iPr} was added to a solution of 3 equivalents of iPr_2NBCl_2 and tBu(Me$_3$Si)$NBCl_2$, respectively, at 0 °C. After filtration and removal of solvents, the crude products were almost pure. Further purification by crystallization gave yields of 55% (**28b^{MeMe}**) and 53% (**28c^{MeMe}**). These low yields are caused by the high solubility of both species in organic solvents, resulting in inefficient crystallizations. Both species sublime under vacuum but require higher temperatures (120 °C oil bath temperature) than their [1]FCP cousins **27b^{MeMe}** and **27c^{MeMe}**.

Scheme 2-2. Byproducts of the Salt-Metathesis Reaction (see Scheme 2-1). CHR^1R^2 = $CHMe_2$, $CHEt_2$; R′/R″ = Et/Et (**28a^{R1R2}**), *i*Pr/*i*Pr (**28b^{R1R2}**), *t*Bu/$SiMe_3$ (**28c^{R1R2}**)

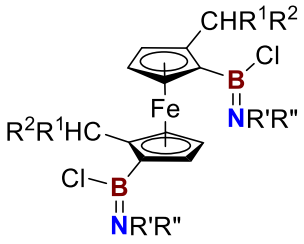

28^{R1R2}

Both bis(boryl)ferrocene species show in ^{11}B NMR spectra with 38.0 (**28b^{MeMe}**) and 45.3 ppm (**28c^{MeMe}**) chemical shifts that are in the expected range for this type of substitution at boron.[22] ^{1}H and ^{13}C NMR spectra of both species exhibit signal pattern that match those expected for C_2-symmetrical molecules. It is noteworthy that **28c^{MeMe}**, equipped with the tBu(Me$_3$Si)N group, could show *cis* and *trans* isomers caused by the BN double bonds. The fact that only one signal pattern was observed in ^{1}H and ^{13}C NMR spectroscopy either means that only one isomer is present or that

fast *cis-trans* isomerization occurs in solution. However, such a fast conversion is not expected. For example, the [1]FCPs bridged by *t*Bu(Me$_3$Si)NB moieties (**27c^{MeMe}** and **27c^{EtEt}**) do not exhibit fast rotations around the BN double bond even though, because of the substitution pattern, the B atoms in these strained compounds are expected to be less Lewis acidic compared to the B atoms of the bis(boryl)ferrocene **28c^{MeMe}**.

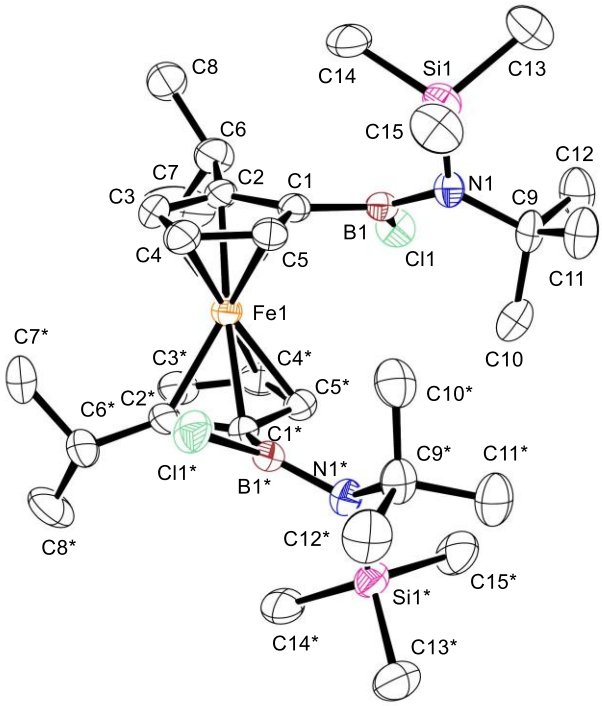

Figure 2-3. Molecular structure of **28c^{MeMe}** with thermal ellipsoids at 50% probability level. Hydrogen atoms are omitted for clarity. Selected bond lengths [Å] and bond angles [°] for **28c^{MeMe}**: B1–C1 = 1.817(4); B1–Cl1 = 1.817(4); B1–N1 = 1.420(5); C1-B1-Cl1 = 116.6(3); Cl1-B1-N1 = 120.7(3); N1-B1-C1 = 122.7(3); B1-N1-Si1 = 116.9(2); Si1-N1-C9 = 120.4(2); C9-N1-B1 = 121.9(3). See also the Supporting Information, Table S3.

Crystals suitable for single-crystal X-ray analysis of **28c^{MeMe}** were obtained by vacuum sublimation (Figure 2-3; Supporting Information, Tables S1 and S3).[23] This chiral species crystallizes in the orthorhombic space group *C*222$_1$ revealing *C*$_2$-symmetrical molecules. The B1–N1 distance of 1.420(5) Å is slightly longer than a typical BN double bond of 1.41 Å.[24] An elongation is expected as the coordination plane around boron is significantly twisted to that around

nitrogen (Cl1-B1-N1-Si1 133.3(2)°). This clearly is the result of steric congestion: twisting of the amino group to optimize the BN π-bonding is impossible as the Me_3Si group would sterically interfere with the Cp ring.

2.4.1 Mechanistic Insight

Recently, we prepared the *i*Pr_2NB-bridged species **27b^{MeMe}**,[11] which we could isolate in a low yield of 20% by vacuum sublimation from the crude reaction mixture. This yield was matching the result obtained from ^{1}H NMR spectroscopy of the crude reaction mixture, where the 1,1′-bis(boryl)ferrocene **28b^{MeMe}** (Scheme 2-2) was the major product.[11] In the first attempts to prepare the new [1]FCPs **27a^{MeMe}**, **27c^{MeMe}**, and **27a-c^{EtEt}**, we used similar conditions as those used for the synthesis of **27b^{MeMe}**; namely, after the lithiation of **15^{MeMe}** and **15^{EtEt}**, respectively, at 0 °C in mixtures of thf and hexanes (1:9), the ice bath was removed and a solution of the aminoborane was added dropwise during 10 min through a cannula from a second Schlenk flask. Table 2-1 shows approximate ratios between targeted [1]FCPs (**27**; Scheme 2-1) and the unwanted bis(boryl)ferrocenes (**28**; Scheme 2-2) as determined by ^{1}H NMR spectroscopy from reaction mixtures. However, the reaction conditions could not be controlled very well. First, the speed of addition varied from experiment to experiment as a cannula transfer cannot be controlled perfectly. Second, removing the ice bath from the solution of the dilithio species before addition of the dichloride also creates some uncertainties, as the temperature during the salt-metathesis reaction is not controlled. We also noticed that the characteristic deep red colour of the [1]FCPs did not appear instantaneously with addition of the amino(dichloro)borane and it seemed that increased temperatures were required. Therefore, we immersed the solution of the dilithio species in a heated oil bath at 50 °C. After a warm-up period of 10 min, the solution of a respective amino(dichloro)borane was added dropwise during 10 min using a syringe pump. These new con-

ditions not only allowed an almost perfect control over the reaction conditions, and therefore led to reliable ratios between species **27** and **28**, but also led to a significant change of these ratios in favour of the targeted [1]FCPs (**27**).

Of course, we optimized the reaction conditions stepwise. First, the speed of addition was controlled by applying a syringe pump, but the reaction temperature was kept low (0 °C to room temperature). However, the product ratios were not affected significantly. Second, the reaction temperature was first raised to ambient temperature by exchanging the ice bath by a water bath which significantly favoured the formation of the targeted [1]FCPs; a further increase to 50 °C gave even better product ratios of **27** to **28** (Table 2-1). This temperature effect confirms that the reaction path yielding [1]FCPs (**27**) has a higher activation energy than that leading to bis-(boryl)ferrocenes (**28**). As the formation of lithium chloride in salt-metathesis reactions is irreversible, the formation of products must be kinetically controlled. An obvious reaction mechanism is illustrated in Scheme 2-3 and will be used to interpret the effects of reaction conditions on the product ratios.

Table 2-1. Measured Product Ratios of [1]FCPs (**27**) and Bis(boryl)ferrocenes (**28**) [a]

		Reaction temperature [b]	
$CHR^1R^2/NR'R''$ [c]		0 °C → RT	50 °C
$CHMe_2/NiPr_2$	**27b^{MeMe}:28b^{MeMe}**	1.0:2.4 [d]	1.0:0.59
$CHMe_2/NtBu(SiMe_3)$	**27c^{MeMe}:28c^{MeMe}**	1.0:1.4	1.0:0.47
$CHEt_2/NiPr_2$	**27b^{EtEt}:28b^{EtEt}**	1.0:0.81	1.0:0.30
$CHEt_2/NtBu(SiMe_3)$	**27c^{EtEt}:28c^{EtEt}**	1.0:0.52	1.0:0.12

[a] Approximate ratios determined by ^{1}H NMR spectroscopy (samples were taken from aliquots of the reaction mixture, 20 min after the addition of $R'R''NBCl_2$). [b] See text for discussion. [c] See Scheme 2-1 and 2-2. [d] A ratio of 1.0:3.5 was found before[11] for allegedly the same reaction conditions used for the ratios shown here for the 0 °C → room temperature (r.t.) conditions, which indicates that such reaction conditions cannot be reproduced well (see text for discussion).

The common intermediate, the monoborylated species $\mathbf{I^{27\text{-}28}}$ (Scheme 2-3), can either react intramolecularly to form a [1]FCP (**27**) or intermolecularly with a second equivalent amino-(dichloro)borane to give a bis(boryl)ferrocene (**28**). The rate of formation of **28** will be favoured by increased concentrations of R′R″$NBCl_2$, whereas that of the intramolecular ring-closure to **27** does not depend on it. To favour the formation of the [1]FCPs **27**, the concentration of R′R″$NBCl_2$ must be kept as low as possible, and therefore a solution of this reagent should be added slowly to the solution of the dilithioferrocene.[25] However, a low reaction bath temperature (for example, 0 °C) will result in a low rate for the ring-closure reaction toward **27** so that significant amounts of the intermediate $\mathbf{I^{27\text{-}28}}$ are present and can compete with the dilithioferrocene species for R′R″$NBCl_2$. An increase of the temperature to 50 °C increases the rate of the intramolecular ring-closure (Scheme 2-3) the strongest, and consequently results in a reduced concentration of $\mathbf{I^{27\text{-}28}}$, which, on the other hand, will negatively affect the rate of the formation of bis(boryl)ferrocenes **28**. The rate of the intramolecular ring-closure exhibits the highest activation energy makes sense from two points of view. First, in this step strain is introduced and it can be assumed that some amount of this strain is already established in the transition state. Second, the rate of a salt metathesis should correlate with the electrophilicity of the borane species. As the electrophilicity of the boryl group of the intermediate $\mathbf{I^{27\text{-}28}}$ with only one chloride substituent is lower than that of the starting borane R′R″$NBCl_2$, a higher activation energy is expected for the intramolecular ring-closure. This conclusion can only be drawn if in both paths (intra- and intermolecular) steric influences are similar (see discussion below).

Scheme 2-3. Reaction Mechanism

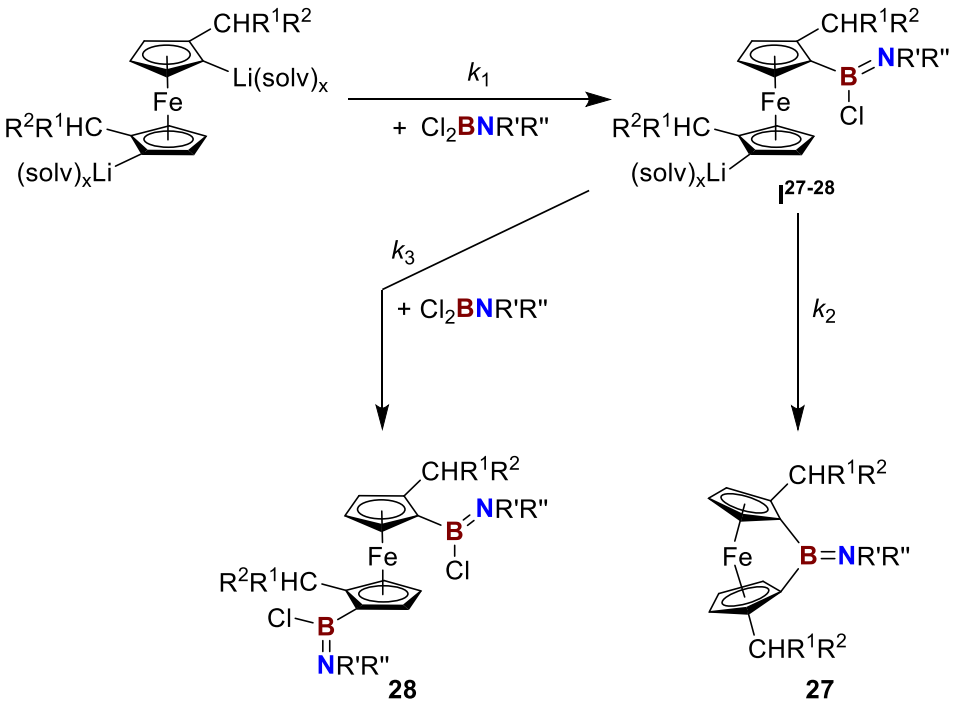

As shown in Table 2-1, the ratios between species **27** and **28** change significantly with an increase of the reaction temperature to 50 °C: for the two cases with *i*Pr groups on ferrocene, the bis(boryl)ferrocene **28** is the major species at lower temperature, whereas at higher temperature, it is the minor product. This is also reflected in the yields of isolated product. For example, the [1]FCP **27b**$^{\mathbf{MeMe}}$ was prepared before using the "low temperature" (0 °C to room temperature) procedure with a yield of isolated product of 20%.[11] With the improved procedure (50 °C), the yield increased to 53% (see Experimental Section).

A comparison of respective product ratios obtained from Li_2fc^{iPr} with those from $Li_2fc^{3\text{-Pen}}$ reveals the influence of alkyl groups on the ferrocene moiety (Table 2-1). For all of the cases, the 3-pentyl equipped sandwich species resulted in higher conversions to the targeted [1]FCPs; for example, for the *i*Pr$_2$N-substituted species the product ratios **27**:**28** under optimized reaction conditions were 1.0:0.59 (**27b**$^{\mathbf{MeMe}}$:**28b**$^{\mathbf{MeMe}}$) and 1.0:0.30 (**27b**$^{\mathbf{EtEt}}$:**28b**$^{\mathbf{EtEt}}$). This trend can be

rationalized by an analysis of the conformation of the alkyl groups on the ferrocene moiety. The most stable conformation of the alkyl groups CHR^1R^2 (R^1R^2 = Me_2, Et_2) on the ferrocene moiety shows that one of the two R groups is approximately in the same plane as a Cp ring, whereas the second R group is oriented away from iron and nearly perpendicular to a Cp ring. The four known molecular structures of [1]FCPs equipped with the fc^{iPr} moiety,[11] and the structures of the dibromide species **15**$^{\mathbf{MeMe}}$ [11] and **15**$^{\mathbf{EtEt}}$ (Figure 2-2) all show the described orientation of the alkyl groups. Presumably, this conformation is thermodynamically favoured because repulsive interactions of the alkyl groups (R = Me or Et) with iron are minimized by orienting the small H atom towards iron. As a first approximation, for a particular amino(dichloro)borane the rate constant k_2 for the intramolecular ring-closure (Scheme 2-3) should be unaffected by the type of alkyl group on the ferrocene moiety: for the *i*Pr as well as for the 3-pentyl groups, H atoms of the alkyl groups point to the inner parts of the sandwich where the ring-closure happens. However, the rate constants k_1 and k_3 will be affected by the type of alkyl group for the following reasons. It can be assumed that the borane R′R″$NBCl_2$ approaches a lithiated Cp ring from the least-hindered side, which will be opposite to the Fe atom. This means that one R group of CH R^1R^2 will point approximately in the direction of the incoming amino(dichloro)borane, and for steric reasons R = Et should give lower rate constants than R = Me. In summary, 3-pentyl groups suppress the formation of bis(boryl)ferrocene derivates (k_3; Scheme 2-3) more effectively than *i*Pr groups. A similar effect should occur for the formation of the intermediate **I**$^{\mathbf{27\text{-}28}}$ (k_1). However, the rate constant k_2 for the ring-closure reaction towards [1]FCPs does not depend on the type of alkyl group.

2.4.2 Improved Synthesis of the [1]FCP *i*Pr$_2$NBfc

Equipped with these mechanistic insights, we reinvestigated the preparation of the known boron-bridged [1]FCP *i*Pr_2NBfc (fc = $(H_4C_5)_2Fe$; **21** in Figure 2-1).[13] As the authors did not mention any

byproducts,[13] we wanted to find out if bis-(boryl)ferrocenes are the major byproducts and if temperature has a similar positive influence on the yield of the targeted [1]FCP. The [1]FCP *i*Pr$_2$NBfc had been prepared by a dropwise addition of a hexane solution of *i*Pr$_2$NBCl$_2$ to a suspension of dilithioferrocene (Li$_2$fc·tmeda) in hexanes at room temperature, followed by filtration and crystallization at −50 °C (yield of isolated product: 38%).[13b] We repeated the preparation of *i*Pr$_2$NBfc following these published reaction conditions as close as possible. Analysis of the reaction mixture by ^{1}H NMR spectroscopy revealed the presence of the two major products *i*Pr$_2$NBfc and 1,1′-[Cl(*i*Pr$_2$N)B]$_2$fc in an approximate ratio of 1.0:2.4 (Supporting Information, Figure S32). Employing our optimized conditions (syringe pump/50 °C) ^{1}H NMR spectroscopy revealed that the targeted [1]FCP was formed as a major product, with only minimal amounts of the unwanted 1,1′-[Cl(*i*Pr$_2$N)B]$_2$fc (Supporting Information, Figure S33). Crystallization at low temperature gave pure *i*Pr$_2$NBfc in a yield of 74%, which is nearly double that previously reported (38%). This species has a similar vapor pressure as the alkyl-decorated [1]FCPs **27a-c^{MeMe}** and can be sublimed under vacuum at oil bath temperature of 70 °C.

2.4.3 Thermal Properties of [1]FCPs

The thermal properties of the four pure [1]FCPs **27b^{MeMe}** and **27a-c^{EtEt}** were investigated by differential scanning calorimetry (DSC). However, the enthalpy of ring-opening polymerization (ΔH_{ROP}) could not be measured for species **27b^{MeMe}**. In each run, a broad, serrated endothermic peak around the melting point of **27b^{MeMe}** (m.p. 68–70 °C) indicated the evaporation and loss of the starting compound (Supporting Information, Figure S37). At the end of each run, some material was clearly visible at the outside of the aluminum crucible. Despite multiple attempts, aluminum crucibles could not be sealed well enough for **27b^{MeMe}**. In contrast, the DSC measurements of the 3-pentyl substituted species **27a-c^{EtEt}** were not accompanied by any loss of species, and their

thermograms were obtained. Species **27a**$^{\mathbf{EtEt}}$ and **27b**$^{\mathbf{EtEt}}$ gave defined exothermic peaks, whereas **27c**$^{\mathbf{EtEt}}$, equipped with the bulky *t*Bu(Me$_3$Si)NB-bridging moiety, revealed multiple exothermic peaks with the main peak being very broad (Supporting Information, Figure S36).

The DSC thermograms of **27a**$^{\mathbf{EtEt}}$ and **27b**$^{\mathbf{EtEt}}$ show melt endotherms followed by exothermic peaks indicative of ROP at ca. 205 and 222 °C (onset), respectively (Figure 2-4; Supporting Information, Figures S34 and S35). However, the measured enthalpies ΔH_{ROP} of −75(±5) (**27a**$^{\mathbf{EtEt}}$) and −63(±5) kJ mol^{-1} (**27b**$^{\mathbf{EtEt}}$) are significantly lower than expected. For comparison, the Me$_2$Si-bridged [1]FCP with a tilt angle α of 20.8(5)°[26] showed ΔH_{ROP} of about −80 kJ mol^{-1},[27] whereas the sulfur-bridged [1]FCP[28] with an angle α of 31.05(10)° showed ΔH_{ROP} of −130(±20) kJ mol^{-1}. On the basis of the tilt angle α, boron-bridged [1]FCPs should be similarly strained as the sulfur-bridged species.[29, 3a] Only for one of the three known bora[1]ferrocenophanes could a ΔH_{ROP} value be determined, and the ΔH_{ROP} of −95 kJ mol^{-1} for (Me$_3$Si)$_2$NBfc[13b] was also lower than expected. The authors rationalized the reduced enthalpy by the presence of "side group interactions" between the sterically demanding amino groups, which presumably resulted in substantial destabilization of the polymer relative to the monomer.

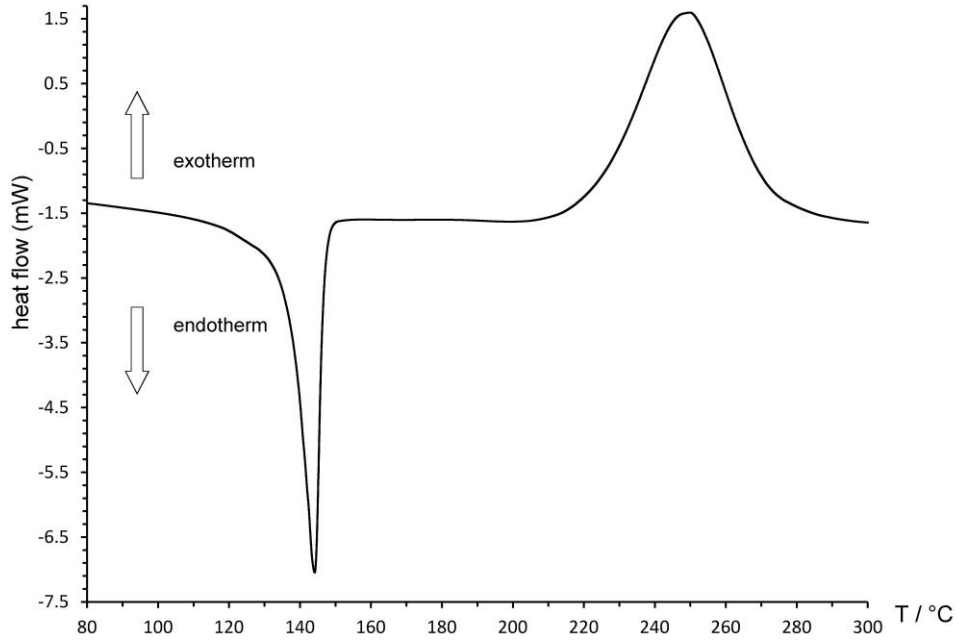

Figure 2-4. Differential scanning calorimetry (DSC) thermogram of **27b^{EtEt}** (heating rate: 10 °C min^{-1}; T_{ROP} (onset) = 222 °C; ΔH_{ROP} = −63(±5) kJ mol^{-1}).

We investigated the products of a DSC run of species **27b^{EtEt}**. The content of the aluminum crucible was extracted with C_6D_6, resulting in a yellow solution from which particles separated. As these particles were attracted towards a magnet, it can be assumed that they are made of iron. This result corresponded with our observations in thermal ROP of **27a^{EtEt}** and **27b^{EtEt}**, where always elemental iron was found (see Experimental Section and the discussion below). The thermal extrusion of iron from the starting compound presumably is a radical process, which is either only slightly exothermic of even endothermic. Thus, the measured exothermy in DSC thermograms is not representative of the intrinsic strain of [1]FCPs, as a clean ring-opening reaction is not occurring. The known boron-bridged [1]FCPs (**21**; Figure 2-1) and the four species **27b^{MeMe}** and **27a-c^{EtEt}** all exhibit exothermic peaks in DSC thermograms at similar onset temperatures (200 °C for $(Me_3Si)_2$NBfc),[13b] and it is expected that each compound undergoes a similar decomposition to produce iron particles. This expectation was met when we measured a DSC thermogram of the

known [1]FCP *i*Pr$_2$NBfc (T_{ROP}(onset) ≈ 180 °C; Supporting Information, Figure S38). The product mixture in the crucible after a DSC run clearly showed the presence of iron particles. As already described by Braunschweig and Manners et al., the overlap of the endothermic and the exothermic peaks prevents extracting a reliable ΔH_{ROP} value.[13b] However, we estimated the exothermy of the process to be approximately −73 kJ mol^{-1} (Supporting Information, Figure S38).

2.4.4 Ring-Opening Polymerization of 27a^{EtEt} and 27b^{EtEt}

Species **27a**^{EtEt} and **27b**^{EtEt} were selected for thermal ROP experiments as both compounds showed the most promising exothermic peaks in DSC measurements. Each compound was heated in a flame-sealed NMR tube for 1.5 h, resulting in a colour change from red to orange. The obtained glassy solids were dissolved in thf, leaving magnetic particles behind (iron). As expected, ^{1}H NMR spectra of the products showed broad peaks. Characterization of (**27a**^{EtEt})$_x$ and (**27b**^{EtEt})$_x$ by gel permeation chromatography (GPC) revealed one main fraction and other smaller fractions of lower molecular weights that interfered with system peaks of the GPC system. The main fraction exhibited molecular weights (M_w) relative to polystyrene of about 10 kDa (Supporting Information, Tables S4 and S5; Figure S39–S41). For both products, elemental analysis gave carbon values that were significantly lower than expected for polymers (**27a**^{EtE})$_x$ and (**27b**^{EtEt})$_x$. These results can be interpreted by assuming that the [1]FCPs undergo ROP, but this process does not result in pure polymers as unavoidable extrusion of iron gives byproducts of low M_w that could not be removed. Furthermore, the extrusion of iron must go hand-in-hand with formation of radicals and it is feasible that they result in chain terminations so that high molecular weights could not be obtained.

2.5 Conclusions

A series of new boron-bridged [1]FCPs was prepared by salt-metathesis reactions between the enantiomerically pure dilithioferrocenes Li$_2$fc^{iPr} and Li$_2$fc$^{3\text{-Pen}}$ and the three

amino(dichloro)boranes Et_2NBCl_2, *i*Pr_2NBCl_2, and *t*Bu(Me_3Si)$NBCl_2$. In case of the sterically bulky amino groups *i*Pr_2N and *t*Bu(Me_3Si)N, ^{1}H NMR spectroscopy of reaction mixtures revealed that, along with the targeted strained [1]FCPs (**27**), 1,1′-bis(boryl)ferrocenes (**28**) formed in significant amounts. The product ratio of **27**:**28** depends on the bulkiness of the amino group, the speed of addition of the amino(dichloro)borane, the alkyl group on Cp rings, and in particular on the reaction temperature. Salt-metathesis reactions are kinetically controlled and the product ratio **27**:**28** reflects relative rates between the ring-closure of the monoborylated intermediate $\mathbf{I}^{\mathbf{27\text{-}28}}$ (Scheme 2-3) to form the [1]FCPs **27** and the reaction of intermediate $\mathbf{I}^{\mathbf{27\text{-}28}}$ with amino(dichloro)borane to give the 1,1′-bis(boryl)ferrocenes **28**. The fact that increased reaction temperature favours the formation of **27** more strongly reveals that this pathway has the highest activation barrier. This makes sense as some of the strain present in the [1]FCP **27** must already be built-up in the transition state leading to this species. Using the optimized reaction temperature of 50 °C for the preparation of the known bora[1]ferrocenophane *i*Pr_2NBfc increased the reported yield by nearly 100%. Also, initial investigations with phosphorus-bridged [1]FCPs revealed that an increased reaction temperature of 50 °C significantly favours their formation in salt-metathesis reactions.[30] To the best of our knowledge, despite the numerous reports of the preparation of strained sandwich compounds, employing increased reaction temperatures has not been reported. Probably, researchers targeting strained species expect a thermally sensitive species, and therefore tend to apply low temperatures for respective salt-metathesis reactions. Our results suggest that increased reaction temperatures should strongly be considered in future syntheses of [1]FCPs.

The measured product ratios of **27**:**28** shed some light on the influence of the alkyl groups CHR^1R^2 on the Cp rings. In all cases, $CHEt_2$ groups favoured the formation of the targeted [1]FCPs stronger than $CHMe_2$ groups. This effect reveals that the choice of CHR_2 mainly influences the

rates of the intermolecular reactions, leading to the intermediate **I**[27-28] and the bis(boryl)ferrocenes **28** (Scheme 2-3), while the intramolecular ring-closure towards [1]FCPs (**27**) is unaltered. This discovery opens up new possibilities to further suppress the formation of unwanted byproducts through tailoring the bulkiness of CHR_2 groups on ferrocene.

Thermal ROP of bora[1]ferrocenophanes occurred and gave soluble polymers. However, the required high temperatures also resulted in extrusion of elemental iron, a fact that explains why the determined exothermy in DSC measurements were lower than expected for these highly strained species.

Our current efforts are concentrated on the preparation of boron-bridged [1]FCPs equipped with aryl groups at boron. We believe that this approach will result in species with increased Lewis acidity at boron, which probably will result in lower activation energies for ROP.

2.6 Experimental Section

General procedures. Syntheses of all compounds were carried out using standard Schlenk and glovebox techniques unless mentioned otherwise. Solvents were dried using an MBraun Solvent Purification System and stored under nitrogen over 3 Å molecular sieves. All solvents for NMR spectroscopy were degassed (freeze-pump-thaw method) prior to use and stored under nitrogen over 3 Å molecular sieves. ^{1}H and ^{13}C NMR spectra were recorded on a 500 MHz Bruker Avance NMR spectrometer at 25 °C in C_6D_6 or $CDCl_3$. ^{1}H chemical shifts were referenced to the residual protons of the deuterated solvents (δ = 7.15 ppm for C_6D_6 and 7.26 ppm for $CDCl_3$); ^{13}C chemical shifts were referenced to the C_6D_6 signal at δ = 128.00 ppm or the $CDCl_3$ signal at δ = 77.00 ppm. Assignments for all compounds were supported by additional NMR experiments (DEPT, HMQC, COSY). As signals of Cp protons show a fine structure, all signals were called multiplets. Mass

spectra were measured on a VG 70SE and were reported in the form *m/z* (rel intens) [M^+] where *m/z* is the observed mass. The intensities are reported relative to the most-intense peak and M^+ is the molecular-ion peak or a fragment; only characteristic mass peaks are listed. For isotopic pattern, only the mass peak of the isotopoloque or isotope with the highest natural abundance is listed. Elemental analyses were performed on a Perkin Elmer 2400 CHN Elemental Analyzer using V_2O_5 to promote complete combustion. UV/Vis spectra were measured at ambient temperature with dry, degassed solvents, using a Varian Cary 50 Bio UV/Vis spectrophotometer. Cannula transfer of a solution of the boron dihalides (0 °C → r.t. method; see Results and Discussion) was performed by applying a small N_2 pressure difference between two Schlenk flasks that were connected through a fluoropolymer tubing by inserting both ends into septa. For controlled addition of solutions of boron dihalides a syringe pump has been used (Sage Instruments, model 355).

Reagents. The compounds ferrocene (98%), *n*BuLi (2.5 M in hexanes), *i*Pr_2NBCl_2, and $AlEt_3$ (1.9 M in toluene) were purchased from Sigma Aldrich. 1,2-Dibromotetrachloroethane (Alfa Aesar, 98%) and silica gel 60 (EMD, Geduran, particle size 0.040–0.063 mm) were purchased from VWR. The compounds Et_2NBCl_2,[31] *t*Bu(Me_3Si)$NBCl_2$,[32] (*R*,*R*)-1,1′-bis(*α*-*N*,*N*-dimethylaminopropyl)ferrocene (**12^{Et}**),[33] and (S_p,S_p)-1,1′-dibromo-2,2′-di(isopropyl)ferrocene (**15^{MeMe}**)[11] were prepared as described in the literature. The species (LiH_4C_5)$_2$Fe·2/3tmeda,[34] (*R*,*R*,S_p,S_p)-2,2′-bis(*α*-*N*,*N*-dimethylaminopropyl)-1,1′-dibromoferrocene (**13^{Et}**),[18] (*R*,*R*,S_p,S_p)-2,2′-bis(*α*-acetoxyethyl)-1,1′-dibromoferrocene,[18] and (S_p,S_p)-1,1′-dibromo-2,2′-bis(3-pentyl)ferrocene (**15^{EtEt}**)[18] were synthesized according to literature procedure with some alterations (see Supporting Information for details).

Thermal Studies. DSC analyses were performed on a TA Instruments Q20 at a heating rate of 10 °C/min. The samples, sealed in hermetic aluminum pans, were tared using a balance with a repeatability of 0.1 mg (AB204-S Mettle Toledo). DSC data was analyzed with TA Instruments Universal Analysis 2000 software.

GPC Analyses. Chromatograms were recorded on a Viscotek 350 HT-GPC system (Malvern) that was used at low temperature (column temperature of 37.5 °C; thf; flowrate = 1.0 mL min^{-1}; calibrated for polystyrene standards). The instrument was equipped with the following Viscotek components: autosampler (Model 430 Vortex), degasser (model 7510), two pumps (model 1122), 7° and 90° light scattering detectors, refractometer, and viscometer. GPC columns cover the range of M_w of 500 to 10,000,000 g mol^{-1} (three main columns: Plgel 10 µM MIXED-B LS 300 × 7.5 mm; one guard column: 10 µM GUARD 50 × 7.5 mm; Agilent Technologies). Samples were dissolved in thf and filtered through 0.2 µm syringe PTFE filters before GPC analysis.

Synthesis of 27a^{MeMe}. *n*BuLi (2.5 M in hexanes, 0.88 mL, 2.2 mmol) was added dropwise to a cold (0 °C) solution of **15**^{MeMe} (0.447 g, 1.04 mmol) in a mixture of thf (1.0 mL) and hexanes (9.0 mL). The reaction mixture was stirred at 0 °C for 30 min, resulting in an orange solution. The cold bath was removed and replaced with a preheated oil bath (50 °C), followed by stirring of the solution for 10 min. A solution of Et_2NBCl_2 (0.167 g, 1.09 mmol) in hexanes (10 mL) was added dropwise within 10 min applying a syringe pump. The reaction colour changed from orange to dark-red along with formation of a white precipitate. After the reaction mixture was stirred at r.t. for 20 min, all volatiles were removed, and the resulting red residue was dissolved in hexanes (10 mL). After the removal of LiCl by filtration, the solvent was removed under vacuum, followed by a flask-to-flask condensation (55 °C oil bath temperature; p ≈ 10^{-2} mbar) to yield **27a**^{MeMe} as a red oil, which was contaminated with about 7% of (iPrH$_4$C$_5$)$_2$Fe (0.256 g of total mass; 0.241g (calc)

of pure **27a^{MeMe}**; 66% yield; see Figure S7–S9). ^{1}H NMR (C_6D_6): δ = 1.04 (t, 6H, $NCH_2C\underline{H}_3$), 1.17 [d, 6H, $CH(C\underline{H}_3)_2$], 1.31 [d, 6H, $CH(C\underline{H}_3)_2$], 2.34 [sept, 2H, $C\underline{H}(CH_3)_2$], 3.41 (m, 4H, $NC\underline{H}_2CH_3$), 3.43 (m, 2H, CH-α of Cp), 4.29 (m, 2H, CH-β of Cp), 4.52 (m, 2H, CH-β of Cp) ppm; ^{13}C NMR (C_6D_6): δ = 15.83 ($NCH_2\underline{C}H_3$), 21.87 [$CH(\underline{C}H_3)_2$], 27.57 [$CH(\underline{C}H_3)_2$], 30.20 [$\underline{C}H(CH_3)_2$], 39.9 (br., *ipso*-Cp, B), 41.78 ($N\underline{C}H_2CH_3$), 71.33 (C-β of Cp), 76.13 (C-β of Cp), 80.03 (C-α of Cp), 101.03 (*ipso*-Cp, *i*Pr); ^{11}B NMR (C_6D_6): δ = 40.0 ppm.

Synthesis of 27a^{EtEt}. *n*BuLi (2.5 M in hexanes, 0.85 mL, 2.1 mmol) was added dropwise to a cold (0 °C) solution of **15^{EtEt}** (0.490 g, 1.01 mmol) in a mixture of thf (1.0 mL) and hexanes (9.0 mL). The reaction mixture was stirred at 0 °C for 30 min, resulting in an orange solution. The cold bath was removed and replaced with a preheated oil bath (50 °C), followed by stirring of the solution for 10 min. A solution of Et_2NBCl_2 (0.161 g, 1.05 mmol) in hexanes (10 mL) was added dropwise within 10 min applying a syringe pump. The reaction colour changed from orange to dark-red along with formation of a white precipitate. After the reaction mixture was stirred at r.t. for 20 min, all volatiles were removed, and the resulting red residue was dissolved in hexanes (10 mL). After the removal of LiCl by filtration, the resulting solution was concentrated to around 4 mL and left at −80 °C for 48 h, resulting in **27a^{EtEt}** as a dark-red precipitate (0.260 g, 63%). ^{1}H NMR (C_6D_6): δ = 0.83 [t, 6H, $CH(CH_2C\underline{H}_3)_2$], 1.02 [t, 6H, $CH(CH_2C\underline{H}_3)_2$ or $NCH_2C\underline{H}_3$], 1.05 [t, 6H, $NCH_2C\underline{H}_3$ or $CH(CH_2C\underline{H}_3)_2$], 1.50–1.70 [m, 6H, $CH(C\underline{H}_2CH_3)_2$], 2.11 [m, 2H, $C\underline{H}(CH_2CH_3)_2$], 2.19 [m, 2H, $CH(C\underline{H}_2CH_3)_2$], 3.45 (m, 2H, $NC\underline{H}_2CH_3$) 3.53 (m, 2H, CH-α of Cp), 3.56 (m, 2H, $NC\underline{H}_2CH_3$), 4.28 (m, 2H, CH-β of Cp), 4.57 (m, 2H, CH-β of Cp) ppm; ^{13}C NMR (C_6D_6): δ = 9.74 [$CH(CH_2\underline{C}H_3)_2$], 12.99 [$CH(CH_2\underline{C}H_3)_2$], 15.64 ($NCH_2\underline{C}H_3$), 25.51 [$CH(\underline{C}H_2CH_3)_2$], 29.16 [$CH(\underline{C}H_2CH_3)_2$], 40.7 (br., *ipso*-Cp, B), 41.60 ($N\underline{C}H_2CH_3$), 42.52 [$\underline{C}H(CH_2CH_3)_2$], 73.31 (C-$\beta$ of Cp), 76.38 (C-β of Cp), 79.98 (C-α of Cp), 100.13 (*ipso*-Cp, 3-pentyl) ppm; ^{11}B NMR (C_6D_6): δ

= 40.3 ppm; MS (70 eV): *m/z* (%): 407 (100) [M^+]; HRMS (70 eV; *m/z*): calcd for $C_{24}H_{38}BFeN$: 407.2441; found: 407.2444; UV/Vis (hexanes): λ_{max} (ε) = 496 nm (478 L mol^{-1} cm^{-1}); elemental analysis calcd (%) for $C_{24}H_{38}BFeN$ (407.22): C 70.79, H 9.41, N 3.44; found: C 70.06, H 9.68, N 3.45.

Optimized synthesis of 27b^{MeMe}.[11] *n*BuLi (2.5 M in hexanes, 0.85 mL, 2.1 mmol) was added dropwise to a cold (0 °C) solution of **15^{MeMe}** (0.433 g, 1.01 mmol) in a mixture of thf (1.0 mL) and hexanes (9.0 mL). The reaction mixture was stirred at 0 °C for 30 min, resulting in an orange solution. The cold bath was removed and replaced with a preheated oil bath (50 °C), followed by stirring of the solution for 10 min. A solution of *i*Pr_2NBCl_2 (0.190 g, 1.04 mmol) in hexanes (10 mL) was added dropwise within 10 min applying a syringe pump. The reaction colour changed from orange to dark-red along with formation of a white precipitate. After the reaction mixture was stirred at r.t. for 20 min, all volatiles were removed, and the resulting red residue was dissolved in hexanes (10 mL). All solids were removed by filtration, solvents were removed under vacuum, and the product sublimed (80 °C oil bath temperature; p ≈ 10^{-2} mbar) to give red-purple crystals (0.202 g, 53%). Spectroscopic data were matching those published.[11]

Synthesis of 27b^{EtEt}. *n*BuLi (2.5 M in hexanes, 0.84 mL, 2.1 mmol) was added dropwise to a cold (0 °C) solution of **15^{EtEt}** (0.485 g, 1.00 mmol) in a mixture of thf (1.0 mL) and hexanes (9.0 mL). The reaction mixture was stirred at 0 °C for 30 min, resulting in an orange solution. The cold bath was removed and replaced with a preheated oil bath (50 °C), followed by stirring of the solution for 10 min. A solution of *i*Pr_2NBCl_2 (0.190 g, 1.04 mmol) in hexanes (10 mL) was added dropwise within 10 min applying a syringe pump. The reaction colour changed from orange to dark-red along with formation of a white precipitate. After the reaction mixture was stirred at r.t. for 20 min, all volatiles were removed, and the resulting red residue was dissolved in hexanes (10 mL).

After the removal of LiCl by filtration, the resulting solution was concentrated to around 8 mL and left at −80 °C for 16 h, resulting in **27b^{EtEt}** as dark-red crystals (0.289 g, 65%). ^{1}H NMR (C_6D_6): δ = 0.78 [t, 6H, CH($CH_2C\underline{H}_3$)$_2$], 1.03 [t, 6H, CH($CH_2C\underline{H}_3$)$_2$], 1.25 [d, 6H, CH_3 of CH($C\underline{H}_3$)$_2$], 1.30 [d, 6H, CH_3 of CH($C\underline{H}_3$)$_2$], 1.64 [m, 4H, CH($C\underline{H}_2CH_3$)$_2$], 1.77 [m, 2H, CH($C\underline{H}_2CH_3$)$_2$], 2.24 [m, 4H, CH($C\underline{H}_2CH_3$)$_2$ and C$\underline{H}$(CH_2CH_3)$_2$], 3.54 (m, 2H, CH-α of Cp), 4.03 [sept, 2H, C$\underline{H}$(CH_3)$_2$], 4.26 (m, 2H, CH-β of Cp), 4.55 (m, 2H, CH-β of Cp) ppm; ^{13}C NMR (C_6D_6): δ = 8.78 [CH($CH_2\underline{C}H_3$)$_2$], 13.13 [CH($CH_2\underline{C}H_3$)$_2$], 24.40 [CH($\underline{C}H_3$)$_2$], 24.66 [CH($\underline{C}H_3$)$_2$], 25.00 [CH($\underline{C}H_2CH_3$)$_2$], 27.98 [CH($\underline{C}H_2CH_3$)$_2$], 40.6 (br., *ipso*-Cp, B), 41.75 [$\underline{C}$H(CH_2CH_3)$_2$], 48.06 [$\underline{C}$H(CH_3)$_2$], 73.59 (C-β of Cp), 76.39 (C-β of Cp), 79.70 (C-α of Cp), 99.64 (*ipso*-Cp, 3-pentyl) ppm; ^{11}B NMR (C_6D_6): δ = 41.2 ppm; MS (70 eV): *m/z* (%): 435 (100) [M^+], 326 (18) [M^+ − BN*i*Pr$_2$ + 2H]; HRMS (70 eV; *m/z*): calcd for $C_{26}H_{42}BFeN$: 435.2760; found: 435.2759; UV/Vis (hexanes): λ_{max} (ε) = 494 nm (457 L mol^{-1} cm^{-1}); elemental analysis calcd (%) for $C_{26}H_{42}BFeN$ (435.27): C 71.74, H 9.73, N 3.22; found: C 70.91, H 9.77, N 3.19.

Synthesis of 27c^{MeMe}. *n*BuLi (2.5 M in hexanes, 0.89 mL, 2.2 mmol) was added dropwise to a cold (0 °C) solution of **15^{MeMe}** (0.451 g, 1.05 mmol) in a mixture of thf (1.0 mL) and hexanes (9.0 mL). The reaction mixture was stirred at 0 °C for 30 min, resulting in an orange solution. The cold bath was removed and replaced with a preheated oil bath (50 °C), followed by stirring of the solution for 10 min. A solution of [*t*Bu(Me_3Si)N]BCl_2 (0.238 g, 1.05 mmol) in hexanes (10 mL) was added dropwise within 10 min applying a syringe pump. The reaction colour changed from orange to red along with formation of a white precipitate. After the reaction mixture was stirred at r.t. for 20 min, all volatiles were removed, and the resulting red residue was dissolved in hexanes (15 mL). After the removal of LiCl by filtration, solvents were removed under vacuum. Flask-to-flask condensation (95 °C oil bath temperature; p ≈ 10^{-2} mbar) resulted in condensation of **27c^{MeMe}**

contaminated with (iPrH$_4$C$_5$)$_2$Fe and small amounts of other unknown impurities (0.192 g; see Figure S16–S18). ^{1}H NMR (C_6D_6): δ = 0.46 (s, 9H, SiMe$_3$), 1.23 [2d, 6H, CH(C<u>H</u>$_3$)$_2$], 1.38 [2d, 6H, CH(C<u>H</u>$_3$)$_2$], 1.57 (s, 9H, tBu), 2.40 [m, 2H, C<u>H</u>(CH$_3$)$_2$], 3.40 (m, 1H, CH-α of Cp), 3.41 (m, 1H, CH-α of Cp), 4.26 (m, 1H, CH-β of Cp), 4.28 (m, 1H, CH-β of Cp), 4.49 (m, 2H, CH-β of Cp) ppm; ^{13}C NMR (C_6D_6): δ = 7.77 (SiMe$_3$), 22.77 [CH(<u>C</u>H$_3$)$_2$], 22.84 [CH(<u>C</u>H$_3$)$_2$], 26.88 [CH(<u>C</u>H$_3$)$_2$], 27.14 [CH(<u>C</u>H$_3$)$_2$], 29.75 [<u>C</u>H(CH$_3$)$_2$], 30.02 [<u>C</u>H(CH$_3$)$_2$], 34.77 [C(<u>C</u>H$_3$)$_3$], 44.1 (br., *ipso*-Cp, B), 45.3 (br., *ipso*-Cp, B), 57.86 [<u>C</u>(CH$_3$)$_3$], 71.10 (C-β of Cp), 71.22 (C-β of Cp), 75.75 (C-β of Cp), 75.86 (C-β of Cp), 78.12 (C-α of Cp), 79.34 (C-α of Cp), 98.80 (*ipso*-Cp, *i*Pr), 99.47 (*ipso*-Cp, *i*Pr) ppm; ^{11}B NMR (C_6D_6): δ = 46.1 ppm.

Synthesis of 27c^{EtEt}. nBuLi (2.5 M in hexanes, 0.85 mL, 2.1 mmol) was added dropwise to a cold (0 °C) solution of **15^{EtEt}** (0.488 g, 1.01 mmol) in a mixture of thf (1.0 mL) and hexanes (9.0 mL). The reaction mixture was stirred at 0 °C for 30 min, resulting in an orange solution. The cold bath was removed and replaced with a preheated oil bath (50 °C), followed by stirring of the solution for 10 min. A solution of [tBu(Me$_3$Si)N]BCl$_2$ (0.237 g, 1.05 mmol) in hexanes (10 mL) was added dropwise within 10 min applying a syringe pump. The reaction colour changed from orange to dark-red along with formation of a white precipitate. After the reaction mixture was stirred at r.t. for 20 min, all volatiles were removed, and the resulting red residue was dissolved in hexanes (15 mL). After the removal of LiCl by filtration, the resulting solution was concentrated to around 8 mL and left at −80 °C for 16 h, resulting in **27c^{EtEt}** as a dark-red precipitate (0.234 g, 48%). ^{1}H NMR (C_6D_6): δ = 0.47 (s, 9H, SiMe$_3$), 0.80 [t, 6H, CH(CH$_2$C<u>H</u>$_3$)$_2$], 1.02 [t, 3H, CH(CH$_2$C<u>H</u>$_3$)$_2$], 1.06 [t, 3H, CH(CH$_2$C<u>H</u>$_3$)$_2$], 1.60 [s, 9H, C(C<u>H</u>$_3$)$_3$], 1.69 [m, 4H, CH(C<u>H</u>$_2$CH$_3$)$_2$], 1.82 [m, 2H, CH(C<u>H</u>$_2$CH$_3$)$_2$], 2.13–2.34 [m, 4H, CH(C<u>H</u>$_2$CH$_3$)$_2$ and C<u>H</u>(CH$_2$CH$_3$)$_2$], 3.43 (m, 1H, CH-α of Cp), 3.47 (m, 1H, CH-α of Cp), 4.25 (m, 1H, CH-β of Cp), 4.26 (m, 1H, CH-β of Cp), 4.50 (m, 1H,

CH-β of Cp), 4.51 (m, 1H, CH-β of Cp) ppm; ^{13}C NMR (C_6D_6): δ = 7.70 ($SiMe_3$), 8.86 [$CH(CH_2\underline{C}H_3)_2$, 9.00 [$CH(CH_2\underline{C}H_3)_2$], 13.08 [$CH(CH_2\underline{C}H_3)_2$], 13.20 [$CH(CH_2\underline{C}H_3)_2$], 24.70 [$CH(\underline{C}H_2CH_3)_2$], 25.10 [$CH(\underline{C}H_2CH_3)_2$], 27.47 [$CH(\underline{C}H_2CH_3)_2$], 27.95 [$CH(\underline{C}H_2CH_3)_2$], 34.73 [$C(\underline{C}H_3)_3$], 41.82 [$\underline{C}H(CH_2CH_3)_2$], 42.01 [$\underline{C}H(CH_2CH_3)_2$], 42.2 (br., *ipso*-Cp, B), 45.5 (br., *ipso*-Cp, B), 57.87 [$\underline{C}(CH_3)_3$], 73.61 (C-β of Cp), 73.81 (C-β of Cp), 75.71 (C-β of Cp), 75.75 (C-β of Cp), 78.75 (C-α of Cp), 79.13 (C-α of Cp), 97.10 (*ipso*-Cp, 3-pentyl), 98.24 (*ipso*-Cp, 3-pentyl) ppm; ^{11}B NMR (C_6D_6): δ = 46.5 ppm; MS (70 eV): *m/z* (%): 479 (100) [M^+], 423 (12) [M^+ − *t*Bu + H]; HRMS (70 eV; *m/z*): calcd for $C_{27}H_{46}BFeNSi$: 479.2842; found: 479.2842; UV/Vis (hexanes): λ_{max} (ε) = 487 nm (507 L mol^{-1} cm^{-1}); elemental analysis calcd (%) for $C_{27}H_{46}BFeNSi$ (479.40): C 67.64, H 9.67, N 2.92; found: C 66.64, H 9.78, N 2.87.

Synthesis of bis(boryl)ferrocene 28b^{MeMe}. *n*BuLi (2.5 M in hexanes, 0.88 mL, 2.2 mmol) was added dropwise to a cold (0 °C) solution of **15^{MeMe}** (0.447 g, 1.04 mmol) in a mixture of thf (1.0 mL) and hexanes (9.0 mL). The reaction mixture was stirred at 0 °C for 30 min, resulting in an orange solution, and added to a solution (0 °C) of *i*Pr_2NBCl_2 (0.570 g, 3.13 mmol) in hexanes (10 mL) within 5 min via a cannula. The reaction mixture was stirred at 0 °C for 30 min, warmed to r.t., and stirred for another 30 min. All volatiles were removed and the resulting yellow residue was dissolved in hexanes (10 mL). LiCl was removed by filtration and washed with hexanes (2 × 5.0 mL), followed by removal of solvents under vacuum to leave a crystalline orange solid behind. This solid was dissolved in hexanes (2.0 mL) and the solution was left at −22 °C for 6 days to give a small amount of crystals. The flask with the partly crystallized product was then left for 8 days at −80 °C to yield orange crystals of **28b^{MeMe}** (0.324 g, 55%). Note that the high solubility of **28b^{MeMe}** in hexanes causes a mediocre yield (see Figure S22–S24). ^{1}H NMR (C_6D_6): δ = 0.73 [d, 6H, $CH(C\underline{H}_3)_2$], 0.96 [d, 6H, $CH(C\underline{H}_3)_2$], 1.13 [d, 6H, $CH(C\underline{H}_3)_2$], 1.34 [d, 6H, $CH(C\underline{H}_3)_2$],

1.48 [d, 6H, CH(C<u>H</u>$_3$)$_2$], 1.54 [d, 6H, CH(C<u>H</u>$_3$)$_2$], 3.16 [sept, 2H, C<u>H</u>(C<u>H</u>$_3$)$_2$], 3.40 [sept, 2H, C<u>H</u>(C<u>H</u>$_3$)$_2$], 4.23 [sept, 2H, C<u>H</u>(C<u>H</u>$_3$)$_2$], 4.25 (m, 2H, CH of Cp), 4.29 (m, 2H, CH of Cp), 4.50 (m, 2H, CH of Cp) ppm; ^{13}C NMR (C_6D_6): δ = 21.23 [CH(<u>C</u>H$_3$)$_2$], 21.60 [CH(<u>C</u>H$_3$)$_2$], 22.05 [CH(<u>C</u>H$_3$)$_2$], 23.66 [CH(<u>C</u>H$_3$)$_2$], 23.71 [CH(<u>C</u>H$_3$)$_2$], 27.09 [CH(<u>C</u>H$_3$)$_2$], 27.16 [<u>C</u>H(CH$_3$)$_2$], 46.22 [<u>C</u>H(CH$_3$)$_2$], 51.88 [<u>C</u>H(CH$_3$)$_2$], 67.82 (CH of Cp), 71.19 (CH of Cp), 75.92 (CH of Cp), 76.8 (br., *ipso*-Cp, B), 102.28 (*ipso*-Cp, *i*Pr) ppm; ^{11}B NMR (C_6D_6): δ = 38.0 ppm; MS (70 eV): *m/z* (%): 560 (100) [M^+]; HRMS (70 eV; *m/z*): calcd for $C_{28}H_{48}B_2Cl_2FeN_2$: 560.2759; found: 560.2759; UV/Vis (hexanes): λ_{max} (ε) = 450 nm (216 L mol^{-1} cm^{-1}); elemental analysis calcd (%) for $C_{28}H_{48}B_2Cl_2FeN_2$ (561.07): C 59.94, H 8.62, N 4.99; found: C 60.13, H 8.95, N 4.95.

Synthesis of bis(boryl)ferrocene 28c^{MeMe}. *n*BuLi (2.5 M in hexanes, 0.86 mL, 2.1 mmol) was added dropwise to a cold (0 °C) solution of **15^{MeMe}** (0.435 g, 1.02 mmol) in a mixture of thf (1.0 mL) and hexanes (9.0 mL). The reaction mixture was stirred at 0 °C for 30 min, resulting in an orange solution, and added to a solution (0 °C) of [*t*Bu(Me$_3$Si)N]BCl$_2$ (0.689 g, 3.05 mmol) in hexanes (10 mL) within 5 min via a cannula. The reaction mixture was stirred at 0 °C for 30 min, warmed to r.t., and stirred for another 30 min. All volatiles were removed and the resulting yellow residue was dissolved in hexanes (10 mL). LiCl was removed by filtration and washed with hexanes (2 × 5.0 mL), followed by removal of solvents under vacuum to leave a crystalline orange solid behind. This solid was dissolved in hexanes (2.0 mL) and the solution was left at −22 °C for 6 days to give a small amount of crystals. The flask with the partly crystallized product was then left for 8 days at −80 °C to yield orange crystals of **28c^{MeMe}** (0.351 g, 53%, after two batches of crystallization). Note that the high solubility of **28c^{MeMe}** in hexanes causes a mediocre yield (see Figure S25–S27). ^{1}H NMR (C_6D_6): δ = 0.20 (s, 18H, SiMe$_3$), 1.12 [d, 6H, CH(C<u>H</u>$_3$)$_2$], 1.31 [d, 6H, CH(C<u>H</u>$_3$)$_2$], 1.64 (s, 18H, *t*Bu), 1.60 (s, 9H, *t*Bu), 3.56 [sept, 2H, C<u>H</u>(CH$_3$)$_2$], 4.33 (m, 2H, CH of

Cp), 4.55 (m, 2H, CH of Cp), 4.56 (m, 2H, CH of Cp) ppm; ^{13}C NMR (C_6D_6): δ = 6.64 ($SiMe_3$), 22.57 [$CH(\underline{C}H_3)_2$], 26.55 [$CH(\underline{C}H_3)_2$], 26.84 [$\underline{C}H(CH_3)_2$], 33.45 [$C(\underline{C}H_3)_3$], 57.07 [$\underline{C}(CH_3)_3$], 74.13 (C of Cp), 75.28 (C of Cp; two peaks overlapping), 77.4 (br., *ipso*-Cp, B), 102.08 (*ipso*-Cp, *i*Pr) ppm; ^{11}B NMR (C_6D_6): δ = 45.3; MS (70 eV): *m/z* (%): 648 (69) [M^+], 459 (22) [M^+ − $BClN(SiMe_3)(t\text{Bu})$ + H], 403 (14) [M^+ − $BClN(SiMe_3)(t\text{Bu})$ − *t*Bu + 2H]; HRMS (70 eV; *m/z*): calcd for $C_{30}H_{56}B_2Cl_2FeN_2Si_2$: 648.2896; found: 648.2897; UV/Vis (hexanes): λ_{max} (ε) = 463 nm (474 L mol^{-1} cm^{-1}); elemental analysis calcd (%) for $C_{30}H_{56}B_2Cl_2FeN_2Si_2$ (648.32): C 55.49, H 8.69, N 4.31; found: C 55.52, H 9.14, N, 4.19.

Optimized synthesis of *i*Pr$_2$NBfc. A solution of *i*Pr$_2$NBCl$_2$ (0.577 g, 3.17 mmol) in hexanes (10 mL) was added dropwise within 10 min applying a syringe pump to a slurry dilithioferrocene·2/3tmeda (0.876 g, 3.18 mmol) in hexanes (40 mL). The reaction mixture was stirred at this temperature for another 15 min. After the removal of LiCl by filtration, the resulting solution was concentrated to around 40 mL and left at −80 °C for 16 h, resulting in *i*Pr$_2$NBfc as a dark-red precipitate (0.691 g, 74%). ^{1}H NMR data matches the reported data.[13b]

Thermal ring-opening polymerization of 27a^{EtEt}. Monomer **27a^{EtEt}** (110 mg) was heated to 240 °C for 90 min in a flame-sealed Pyrex NMR tube. The dark-red crystalline powder turned into a dark-orange immobile solid, which was partially soluble in toluene, benzene, and thf. From this part on all manipulations were done under ambient atmosphere. The resulting compound was dissolved in thf (1.0 mL) and precipitated into dry methanol (20 mL) in a Schlenk flask. The methanol phase was syringed off, and the precipitate was taken-up in thf (1.0 mL). This resulted in a suspension that contained particles that were attracted toward an external magnet. This suspension was precipitated into dry methanol (20 mL), the organic phase was syringed off, and the precipitate was taken-up in thf (1.0 mL). This process was repeated one more time. The pre-

purified product was taken-up in thf (1.0 mL), and magnetic particles were filtered off by using a 0.2 μm syringe PTFE filter (diameter of 25 mm). This filtration procedure was repeated two more time. After all volatiles were removed, and the product was obtained as an orange solid **(27a^{EtEt})$_x$** (80 mg; ca. 73%). ^{1}H NMR (C_6D_6): δ = 0.55–1.25 [m, 12H, $NCH_2C\underline{H}_3$ and $CH(CH_2C\underline{H}_3)_2$], 1.44–1.91 [m, 6H, $CH(C\underline{H}_2CH_3)_2$], 2.05–2.53 [m, 4H, $C\underline{H}(CH_2CH_3)_2$ and $CH(C\underline{H}_2CH_3)_2$], 3.21–3.77 [m, 6H, $NC\underline{H}_2CH_3$) and CH-α of Cp], 3.86–4.31 (m, 4H, CH-β of Cp) ppm; UV/Vis (thf): λ_{max} = 455 nm; elemental analysis calcd (%) for $C_{24}H_{38}BFeN$ (407.24): C 70.79, H 9.41, N 3.44; found: C 68.92, H 9.49, N 2.87 (see main text for discussion on purity).

Thermal ring-opening polymerization of 27b^{EtEt}. Monomer **27b^{EtEt}** (103 mg) was heated to 260 °C for 90 min in a flame-sealed Pyrex NMR tube. The dark-red crystalline powder turned into a dark-orange immobile solid, which was partially soluble in toluene, benzene, and thf. The crude product was purified as described for **27a^{EtEt}** (3 times precipitation; 3 times filtration; removal of volatiles) to afford the product as an orange solid **(27b^{EtEt})$_x$** (72 mg; ca. 70%). ^{1}H NMR (C_6D_6): δ = 0.53–2.10 [m, 30H, $CH(CH_2C\underline{H}_3)_2$, $CH(C\underline{H}_3)_2$, and $CH(C\underline{H}_2CH_3)_2$], 2.23–2.43 [m, 4H, $CH(C\underline{H}_2CH_3)_2$ and $C\underline{H}(CH_2CH_3)_2$], 3.54 [m, 8H, CH-$\alpha$ of Cp and $C\underline{H}(CH_3)_2$] ppm; UV/Vis (thf): λ_{max} = 460 nm; elemental analysis calcd for $C_{26}H_{42}BFeN$ (435.27): C 71.74, H 9.73, N 3.22; found: C 67.25, H 9.51, N 2.49 (see main text for discussion on purity).

Crystal Structure Determinations. Single crystals were coated with Paratone-N oil, mounted using a Micromount (*MiTeGen*—Microtechnologies for Structural Genomics), and frozen in the cold stream of the Oxford Cryojet attached to the diffractometer. Crystal data were collected on a Bruker (Nonius) Kappa 4-Circle diffractometer (**28c^{MeMe}**: CCD model; **15^{EtEt}**: APEX2 model) at −100 °C, using monochromated Mo Kα radiation (λ = 0.71073 Å).

For compound **15**$^{\mathbf{EtEt}}$, an initial orientation matrix and cell was determined by ω scans, and the X-ray data were measured using ϕ and ω scans.[35] The frames were integrated with the Bruker SAINT software package.[36] Data reduction was performed with the APEX2 software package.[35] A multiscan absorption correction (SADABS) was applied.[36] The structure was solved by direct methods (SHELXS-2014) and refined using the Bruker SHELXL-2014 software package.[37]

For compound **28c**$^{\mathbf{MeMe}}$, an initial orientation matrix and cell was determined using ϕ scans and data were measured using ω scans.[38] Cell parameters were initially retrieved using the COLLECT software.[38] Refinement and data reduction were performed using the HKL DENZO and SCALEPACK software and a multiscan absorption correction was applied (SCALEPACK).[39] Transmission coefficients were calculated using SHELXL-2012.[37] The structure was solved using direct methods (SIR-2004)[37] and refined by full-matrix least-squares method on F^2 with SHELXL-2012.

For both compounds non-hydrogen atoms were refined anisotropically; hydrogen atoms were included at geometrically idealized positions but not refined. The isotropic thermal parameters of the hydrogen atoms were fixed at 1.5 or 1.2 times that of the preceding carbon atom. The final refined Flack parameter for both compounds indicates that the correct absolute structure was chosen.[40] Crystallographic data are summarized in Table S1. Thermal ellipsoid plots were prepared using ORTEP-3 for Windows.[41]

CCDC 1010995 (**15**$^{\mathbf{EtEt}}$) and 1010996 (**28c**$^{\mathbf{MeMe}}$) contain the supplementary crystallographic data for this paper. These data can be obtained free of charge from The Cambridge Crystallographic Data Centre via www.ccdc.cam.ac.uk/data_request/cif.

2.7 Associated Content

Supporting Information

Supporting information for this article is available on the WWW under http://dx.doi.org/10.1002/chem.201404222.

Acknowledgements

We thank the Natural Sciences and Engineering Research Council of Canada (NSERC Discovery Grant, JM) for support. We thank the Canada Foundation for Innovation (CFI) and the government of Saskatchewan for funding of the X-ray and NMR facilities in the Saskatchewan Structural Sciences Centre (SSSC). We thank Prof. S. R. Foley (GPC; University of Saskatchewan) and Prof. D. E. Ward (syringe pump; University of Saskatchewan) for making instruments available for our studies. We thank Dr. G. Schatte (SSSC) for crystallographic data of **28c**$^{\mathbf{MeMe}}$. We thank Dr. V. MacKenzie (DSC) and K. Thoms (CHN analysis and MS) for support and measurements.

2.8 References

(1) (a) Lorbach, A.; Hubner, A.; Wagner, M. *Dalton Trans.* **2012**, *41*, 6048-6063; (b) Tanaka, K.; Chujo, Y. *Macromol. Rapid Commun.* **2012**, *33*, 1235-1255; (c) Jäkle, F. *Chem. Rev.* **2010**, *110*, 3985-4022; (d) Matsumi, N.; Chujo, Y. *Polym. J.* **2008**, *40*, 77-89; (e) Jäkle, F. *Coord. Chem. Rev.* **2006**, *250*, 1107-1121; (f) Entwistle, C. D.; Marder, T. B. *Angew. Chem., Int. Ed.* **2002**, *41*, 2927-2931.

(2) Bellas, V.; Rehahn, M. *Angew. Chem., Int. Ed.* **2007**, *46*, 5082-5104.

(3) (a) Musgrave, R. A.; Russell, A. D.; Manners, I. *Organometallics* **2013**, *32*, 5654-5667; (b) Herbert, D. E.; Mayer, U. F. J.; Manners, I. *Angew. Chem., Int. Ed.* **2007**, *46*, 5060-5081; (c)

Braunschweig, H.; Kupfer, T. *Eur. J. Inorg. Chem.* **2012**, 1319-1332; (d) Braunschweig, H.; Kupfer, T. *Acc. Chem. Res.* **2010**, *43*, 455-465; (e) Tamm, M. *Chem. Commun.* **2008**, 3089-3100.

(4) (a) Rulkens, R.; Lough, A. J.; Manners, I. *J. Am. Chem. Soc.* **1994**, *116*, 797-798; (b) Ni, Y. Z.; Rulkens, R.; Manners, I. *J. Am. Chem. Soc.* **1996**, *118*, 4102-4114.

(5) (a) Hudson, Z. M.; Lunn, D. J.; Winnik, M. A.; Manners, I. *Nat. Commun.* **2014**, *5*, 3372; (b) Qiu, H.; Cambridge, G.; Winnik, M. A.; Manners, I. *J. Am. Chem. Soc.* **2013**, *135*, 12180-12183; (c) Rupar, P. A.; Chabanne, L.; Winnik, M. A.; Manners, I. *Science* **2012**, *337*, 559-562; (d) Rupar, P. A.; Cambridge, G.; Winnik, M. A.; Manners, I. *J. Am. Chem. Soc.* **2011**, *133*, 16947-16957; (e) Qian, J.; Guerin, G.; Lu, Y.; Cambridge, G.; Manners, I.; Winnik, M. A. *Angew. Chem., Int. Ed.* **2011**, *50*, 1622-1625; (f) Patra, S. K.; Ahmed, R.; Whittell, G. R.; Lunn, D. J.; Dunphy, E. L.; Winnik, M. A.; Manners, I. *J. Am. Chem. Soc.* **2011**, *133*, 8842-8845; (g) He, F.; Gädt, T.; Manners, I.; Winnik, M. A. *J. Am. Chem. Soc.* **2011**, *133*, 9095-9103; (h) Gilroy, J. B.; Patra, S. K.; Mitchels, J. M.; Winnik, M. A.; Manners, I. *Angew. Chem., Int. Ed.* **2011**, *50*, 5851-5855; (i) Gädt, T.; Schacher, F. H.; McGrath, N.; Winnik, M. A.; Manners, I. *Macromolecules* **2011**, *44*, 3777-3786; (j) Presa Soto, A.; Gilroy, J. B.; Winnik, M. A.; Manners, I. *Angew. Chem., Int. Ed.* **2010**, *49*, 8220-8223; (k) Gilroy, J. B.; Gädt, T.; Whittell, G. R.; Chabanne, L.; Mitchels, J. M.; Richardson, R. M.; Winnik, M. A.; Manners, I. *Nat. Chem.* **2010**, *2*, 566-570; (l) Gädt, T.; Ieong, N. S.; Cambridge, G.; Winnik, M. A.; Manners, I. *Nat. Mater.* **2009**, *8*, 144-150; (m) Wang, X. S.; Guerin, G.; Wang, H.; Wang, Y. S.; Manners, I.; Winnik, M. A. *Science* **2007**, *317*, 644-647; (n) Wang, H.; Lin, W.; Fritz, K. P.; Scholes, G. D.; Winnik, M. A.; Manners, I. *J. Am. Chem. Soc.* **2007**, *129*, 12924-12925; (o) Cao, L.; Manners, I.; Winnik, M. A. *Macromolecules* **2002**, *35*, 8258-8260; (p) Massey, J. A.; Temple, K.; Cao, L.; Rharbi, Y.; Raez, J.; Winnik, M. A.; Manners, I. *J. Am. Chem. Soc.* **2000**, *122*, 11577-11584.

(6) Ieong, N. S.; Manners, I. *Macromol. Chem. Phys.* **2009**, *210*, 1080-1086.

(7) (a) Honeyman, C. H.; Peckham, T. J.; Massey, J. A.; Manners, I. *Chem. Commun.* **1996**, 2589-2590; (b) Peckham, T. J.; Massey, J. A.; Honeyman, C. H.; Manners, I. *Macromolecules* **1999**, *32*, 2830-2837; (c) Mizuta, T.; Onishi, M.; Miyoshi, K. *Organometallics* **2000**, *19*, 5005-5009; (d) Mizuta, T.; Imamura, Y.; Miyoshi, K. *J. Am. Chem. Soc.* **2003**, *125*, 2068-2069; (e) Patra, S. K.; Whittell, G. R.; Nagiah, S.; Ho, C.-L.; Wong, W.-Y.; Manners, I. *Chem.-Eur. J.* **2010**, *16*, 3240-3250.

(8) Herbert, D. E.; Mayer, U. F. J.; Gilroy, J. B.; Lopez-Gomez, M. J.; Lough, A. J.; Charmant, J. P. H.; Manners, I. *Chem.-Eur. J.* **2009**, *15*, 12234-12246.

(9) For aluminum- and gallium-bridged strained sandwich compounds see: (a) Schachner, J. A.; Lund, C. L.; Quail, J. W.; Müller, J. *Organometallics* **2005**, *24*, 785-787; (b) Lund, C. L.; Schachner, J. A.; Quail, J. W.; Müller, J. *Organometallics* **2006**, *25*, 5817-5823; (c) Schachner, J. A.; Tockner, S.; Lund, C. L.; Quail, J. W.; Rehahn, M.; Müller, J. *Organometallics* **2007**, *26*, 4658-4662; (d) Bagh, B.; Schatte, G.; Green, J. C.; Müller, J. *J. Am. Chem. Soc.* **2012**, *134*, 7924-7936; (e) Bagh, B.; Gilroy, J. B.; Staubitz, A.; Müller, J. *J. Am. Chem. Soc.* **2010**, *132*, 1794-1795.

(10) For tin-bridged strained sandwich compounds see: (a) Rulkens, R.; Lough, A. J.; Manners, I. *Angew. Chem., Int. Ed. Engl.* **1996**, *35*, 1805-1807; (b) Jäkle, F.; Rulkens, R.; Zech, G.; Foucher, D. A.; Lough, A. J.; Manners, I. *Chem.-Eur. J.* **1998**, *4*, 2117-2128; (c) Sharma, H. K.; Cervantes-Lee, F.; Mahmoud, J. S.; Pannell, K. H. *Organometallics* **1999**, *18*, 399-403; (d) Jäkle, F.; Rulkens, R.; Zech, G.; Massey, J.; Manners, I. *J. Am. Chem. Soc.* **2000**, *122*, 4231-4232; (e) Baumgartner, T.; Jäkle, F.; Rulkens, R.; Zech, G.; Lough, A. J.; Manners, I. *J. Am. Chem. Soc.* **2002**, *124*, 10062-10070.

(11) Sadeh, S.; Schatte, G.; Müller, J. *Chem.-Eur. J.* **2013**, *19*, 13408-13417.

(12) Bagh, B.; Sadeh, S.; Green, J. C.; Müller, J. *Chem.-Eur. J.* **2014**, *20*, 2318-2327.

(13) (a) Braunschweig, H.; Dirk, R.; Müller, M.; Nguyen, P.; Resendes, R.; Gates, D. P.; Manners, I. *Angew. Chem., Int. Ed. Engl.* **1997**, *36*, 2338-2340; (b) Berenbaum, A.; Braunschweig, H.; Dirk, R.; Englert, U.; Green, J. C.; Jäkle, F.; Lough, A. J.; Manners, I. *J. Am. Chem. Soc.* **2000**, *122*, 5765-5774.

(14) Only in the case of the *i*Pr$_2$NB-bridged [1]FCP soluble material of low molecular weight was obtained; see Ref. 13b.

(15) Marquarding, D.; Klusacek, H.; Gokel, G.; Hoffmann, P.; Ugi, I. *J. Am. Chem. Soc.* **1970**, *92*, 5389-5393.

(16) Schwink, L.; Knochel, P. *Chem.-Eur. J.* **1998**, *4*, 950-968.

(17) For a recent review on planar-chiral ferrocenes see: Schaarschmidt, D.; Lang, H. *Organometallics* **2013**, *32*, 5668-5704.

(18) Kang, J.; Lee, J. H.; Im, K. S. *J. Mol. Catal. A.* **2003**, *196*, 55-63.

(19) This lithiation method was recently described for aromatic bromides; see Bailey, W. F.; Luderer, M. R.; Jordan, K. P. *J. Org. Chem.* **2006**, *71*, 2825-2828.

(20) Species **27b$^{\mathbf{MeMe}}$** was described before; see Ref. 11.

(21) Species **27a$^{\mathbf{EtEt}}$**, **27b$^{\mathbf{EtEt}}$**, and **27c$^{\mathbf{EtEt}}$** could be not be sublimed directly from reaction mixtures. However, the purified compounds could be sublimed in high vacuum.

(22) Nöth, H.; Wrackmeyer, B. Nuclear Magnetic Resonance Spectroscopy of Boron Compounds. In *NMR: Basic Principles and Progress*, Diehl, P.; Fluck, E.; Kosfeld, R., Eds.; Spinger: Berlin Heidelberg New York, 1978; Vol. 14.

(23) For related borylated sandwich compounds please see Braunschweig, H.; Kupfer, T.; Lutz, M.; Radacki, K. *J. Am. Chem. Soc.* **2007**, *129*, 8893-8906.

(24) Paetzold, P. I. *Adv. Inorg. Chem.* **1987**, *31*, 133-137.

(25) A decrease of the concentration of the amino(dichloro)borane solution should slow down the rate of formation of **28**. However, in our hands, using higher dilution did not show the expected effect; instead, salt-metathesis reactions proceeded less cleanly as with higher concentrated R′R″NBCl$_2$ solutions. We assume that the high moisture sensitivity of this chemistry sets the limits on the concentration range that can be used.

(26) Finckh, W.; Tang, B.-Z.; Foucher, D. A.; Zamble, D. B.; Ziembinski, R.; Lough, A.; Manners, I. *Organometallics* **1993**, *12*, 823-829.

(27) Foucher, D. A.; Tang, B.-Z.; Manners, I. *J. Am. Chem. Soc.* **1992**, *114*, 6246-6248.

(28) Rulkens, R.; Gates, D. P.; Balaishis, D.; Pudelski, J. K.; McIntosh, D. F.; Lough, A. J.; Manners, I. *J. Am. Chem. Soc.* **1997**, *119*, 10976-10986.

(29) Green, J. C. *Chem. Soc. Rev.* **1998**, *27*, 263-271.

(30) Sadeh, S.; Khozeimeh Sarbisheh, E.; Cao, My P. T.; Müller J., unpublished results.

(31) Niedenzu, K.; Dawson, J. W. *J. Am. Chem. Soc.* **1959**, *81*, 3561-3564.

(32) Neilson, R. H.; Wells, R. L. *Synth. React. Inorg. Met.-Org. Chem.* **1973**, *3*, 283-289.

(33) Almena Perea, J. J.; Lotz, M.; Knochel, P. *Tetrahedron: Asymmetry* **1999**, *10*, 375-384.

(34) Butler, I. R.; Cullen, W. R.; Ni, J.; Rettig, S. J. *Organometallics* **1985**, *4*, 2196-2201.

(35) Bruker *APEX2*, 2014.3–0 ed; Bruker AXS Inc., 2014.

(36) Bruker *SAINT and SADABS*, v8.34a ed; Bruker AXS Inc., 2013.

(37) (a) Sheldrick, G. M. *SHELXL, Program for the Solution of Crystal Structures*; University of Göttingen: Germany; (b) Sheldrick, G. M. *Acta Crystallogr., Sect. A: Found. Crystallogr.* **2008**, *64*, 112-122.

(38) Nonius, B. V. *Nonius Collect*, Nonius BV, Delft, The Netherlands: Delft, The Netherlands, 1998.

(39) Otwinowski, Z.; Minor, W. Methods in Enzymology. In *Macromolecular Crystallography, Part A*; Carter, C. W.; Sweet, R. M., Eds.; Academic Press: London, 1997; Vol. 276, pp 307-326.

(40) (a) Flack, H. D.; Bernardinelli, G. *Acta Crystallogr. Sect. A* **1999**, *55*, 908-915; (b) Parsons, S.; Flack, H. D.; Wagner, T. *Acta Crystallogr. Sect. B* **2013**, *69*, 249-259.

(41) Farrugia, L. J. *J. Appl. Crystallogr.* **1997**, *30*, 565.

3 Insight into the Formation of Highly Strained [1]Ferrocenophanes with Boron in Bridging Position

3.1 Author Contribution and Relation to the Research Objectives

This work was done in collaboration with Jonathon D. Martell, Dr. Elaheh Khozeimeh Sarbisheh, Prof. J. Wilson Quail, and Prof. Jens Müller. Mr. Martell synthesized (*S*,*S*)-di(2-butyl)dibromoferrocene (**15**$^{\mathbf{MeEt}}$); Dr. Khozeimeh Sarbisheh synthesized (*R*,*R*)-di(2-butyl)dibromoferrocene (**15**$^{\mathbf{EtMe}}$) and di(3-pentyl)dibromoferrocene (**15**$^{\mathbf{EtEt}}$). Single crystal X-ray analysis of **27b**$^{\mathbf{EtEt}}$ was performed by Prof. Quail. All the DFT calculations were done by Prof. Müller. I synthesized di(isopropyl)dibromoferrocene (**15**$^{\mathbf{MeMe}}$), dichloro(diisopropylamino)-borane, and performed all the salt-metathesis reactions for the mechanistic investigation. I compiled the entire experimental section and the supporting information for this manuscript. Moreover, I contributed on referencing and performed rigorous editing of the manuscript, which was written by Prof. Müller.

This work is the continuation to the previous manuscript (Chapter 2). Detailed investigation during the optimization of the reaction conditions provided a mechanistic insight into the formation of bora[1]ferrocenophanes. The proposed mechanism explained the effect of reaction conditions on the obtained product ratios. The mechanism supports that both an increased reaction temperature and a slower addition rate of the amino(dichloro)borane solution enhance the chance of formation of the [1]FCP, which matches with the experimental observations. Moreover, bulkier groups at the Cp rings favour the formation of the [1]FCPs. Under identical reaction conditions, the 3-pentyl equipped sandwich species suppresses the formation of the 1,1′-bis(boryl)species better than the corresponding *i*Pr equipped species. The effect of the CHR^1R^2 groups of the Cp rings on the reaction outcome was rationalized by analyzing their preferred conformation. The

known single-crystal X-ray analysis data of [1]FCPs and dibromoferrocenes equipped with CHR^1R^2 groups all revealed the same conformation. In the most stable conformation of the alkyl groups CHR^1R^2, one of the R groups (R^1) is approximately in the same plane as the Cp ring, whereas the other R group (R^2) is pointed away from the iron and nearly perpendicular to the Cp ring (see Chart 3-1).

Our intent was to test the hypothesis that the alkyl group R^2, and not R^1, affects the outcome of the salt-metathesis reaction. In order to do so, enantiomerically pure dibromoferrocenes with different R^1 and R^2 groups were prepared. The four different ferrocene dibromides were then used as precursors for the respective dilithiated species, which were prepared *in situ* and reacted with $i Pr_2NBCl_2$. Our previously developed procedure was followed for all the salt-metathesis reactions. The obtained product ratios clearly support our hypothesis that the alkyl group that is oriented approximately perpendicular to the Cp ring (R^2) affects the outcome of the salt-metathesis reaction. These experimental results are also supported by DFT calculations.

The following is a verbatim copy[f,g] of the published article Bhattacharjee, H.; Martell, J. D.; Khozeimeh Sarbisheh, E.; Sadeh, S.; Quail, J. W.; Müller, J. *Organometallics* **2016,** *35*, 2156-2164.

[f] Reproduced with permission from Bhattacharjee, H.; Martell, J. D.; Khozeimeh Sarbisheh, E.; Sadeh, S.; Quail, J. W.; Müller, J. *Organometallics* **2016,** *35,* 2156-2164. Copyright © 2016 American Chemical Society.

[g] Compound numbers and some chemical drawings were changed to maintain a uniform style in the thesis.

3.2 Abstract

Four planar-chiral, enantiomerically pure ferrocene dibromides (**15^{R1R2}**; [(CHR^{1}R^2)BrH$_3$C$_5$]$_2$Fe) equipped with two CHR^{1}R^2 groups in α position to bromine were synthesized. From the four C_2 symmetrical species, two are already known [CHR^{1}R^2 = CHMe$_2$ (**15^{MeMe}**), CHEt$_2$ (**15^{EtEt}**)] and two are new compounds [CHR^{1}R^2 = *R*-CHEtMe (**15^{EtMe}**), *S*-CHMeEt (**15^{MeEt}**)]. The dibromides **15^{R1R2}** were *in situ* converted into dilithio ferrocene derivatives and reacted with Cl$_2$BN*i*Pr$_2$ resulting in mixtures of bora[1]ferrocenophanes (**27b^{R1R2}**) and 1,1′-bis(boryl)ferrocenes (**28b^{R1R2}**). The aim of this investigation was to test the hypothesis that the alkyl group that is oriented approximately perpendicular to the Cp ring, i.e., R^2, affects the outcome of the salt-metathesis reaction. The obtained product ratios **27b^{R1R2}**:**28b^{R1R2}** were determined by ^{1}H NMR spectroscopy and revealed that systems with the same R^2 group gave similar **27b^{R1R2}**:**28b^{R1R2}** ratios (1.0:0.51 and 1.0:0.49 for R^2 = Me; 1.0:0.30 and 1.0:0.27 for R^2 = Et), confirming the hypothesis. Shown by DFT calculations (B3PW91/6-311+G(d,p)), reaction paths resulting in either product **27b^{R1R2}** or product **28b^{R1R2}** are both concerted steps.

3.3 Introduction

The first known strained ferrocenophane with a single atom in bridging position was already reported in 1975,[1] however, it took almost 20 years before the capability of these species to produce metallopolymers of high molecular weight through ring-opening polymerization (ROP) was realized.[2] Since this key discovery, different methodologies for ROP have been developed,[3] as well as many new strained sandwich compounds have been prepared.[4] The largest known family of strained sandwich compounds is that of [*n*]ferrocenophanes ([*n*]FCPs), which are usually prepared either by the so-called "salt-metathesis route" or the more rarely applied "flytrap route"

(Scheme 3-1).[4b] One reason why the salt-metathesis route is so popular is due to the fact that dilithioferrocene, stabilized by tmeda, can be made in one step from commercially available reagents.[5] However, in cases where the needed reagent $(R_xE)_nX_2$ (X = Cl, Br; Scheme 3-1) is not available or does not allow nucleophilic substitution on the element E, the flytrap route is often applied.[4b,f] Reported yields for isolated [1]FCPs, obtained from a salt-metathesis route, vary widely. This is not surprising as a combination of two bifunctional reagents can result in a multitude of different products. In addition to the targeted [1]FCP, other cyclic products ([1^n]FCPs) as well as noncyclic species, like small molecules or oligomers, can be formed. Depending on the case, other reasons might exist for obtaining a targeted [1]FCP in a low yield. For example, a [1]FCP could be so reactive that under its formation conditions ROP is initiated to result in oligomers or polymers and, hence, resulting in a diminished amount of [1]FCP for isolation.[6] In the vast majority of publications dealing with the salt-metathesis route toward [1]FCPs byproducts are not discussed. However, identification of byproducts in a chemical reaction and understanding their origin is an important step to rationally optimize a synthetic procedure. Recently, we used this approach and optimized the synthesis of new boron-bridged [1]FCPs and equipped with a more profound understanding of the salt-metathesis reaction, the reported yield of the known bora[1]ferrocenophane iPr$_2$NB(H$_4$C$_5$)$_2$Fe could nearly be doubled.[7]

Scheme 3-1. Synthesis of [*n*]Ferrocenophanes

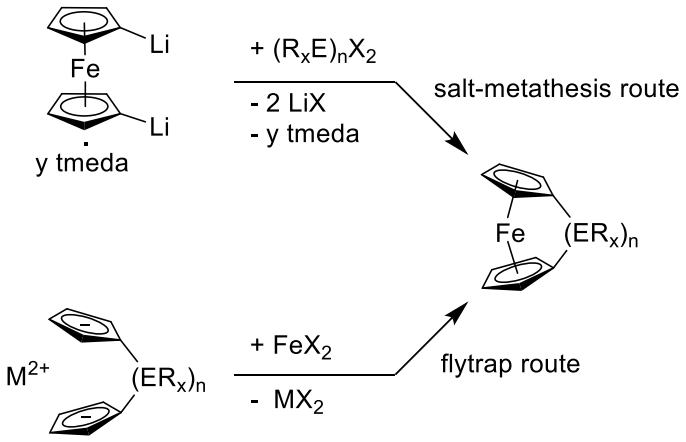

Herein, we describe a mechanistic study of the salt-metathesis route toward boron-bridged [1]FCPs using experimental and theoretical methods. We believe that our findings are of general importance and are relevant to the formation of other [1]FCPs by the salt-metathesis approach.

3.4 Results and Discussion

Recently, we prepared new bora[1]ferrocenophanes (**27**) through a salt-metathesis approach and applied three different amino groups at boron and two different sets of CHR_2 substituents on Cp rings (Scheme 3-2).[7d] In the course of these investigations, we discovered that 1,1′-bis(boryl)-ferrocenes (**28**) formed in addition to the targeted strained [1]FCPs (**27**).[7c,d] Determination of the product ratios **27**:**28** by ^{1}H NMR spectroscopy led to the proposed mechanism as shown in Scheme 3-2 with the following experimental results. First, increasing the reaction temperature favours the formation of the targeted [1]FCP (**27**) over that of the unstrained byproduct (**28**). Second, under identical conditions, the larger $CHEt_2$ groups led to higher conversions to the targeted [1]FCPs compared to reactions when the smaller $CHMe_2$ groups were employed. The temperature effect demonstrated that the reaction path leading to species **27** was associated with the higher activation barrier compared to that leading to 1,1′-bis(boryl)ferrocenes (**28**). This fact was rationalized based

on the proposed mechanism shown in Scheme 3-2.[7d] The common intermediate **I**[27–28] can either react with additional amino(dichloro)borane to give species **28** or take part in an intramolecular ring closure to give the targeted species **27**. As in the step leading to **27** strain is introduced, one can assume that some amount of this strain is already established in the transition state. Furthermore, the rate of a salt metathesis should correlate with the electrophilicity of the borane species. The electrophilicity of the borane for the ring-closure reaction is lower than that of the amino(dichloro)borane leading to the unstrained byproduct **28**. Both parts, the buildup of strain and the lower electrophilicity, should result in a higher activation barrier for the formation of **27**.[7d]

Scheme 3-2. Recently Investigated Preparation of Boron-Bridged [1]FCPs [a]

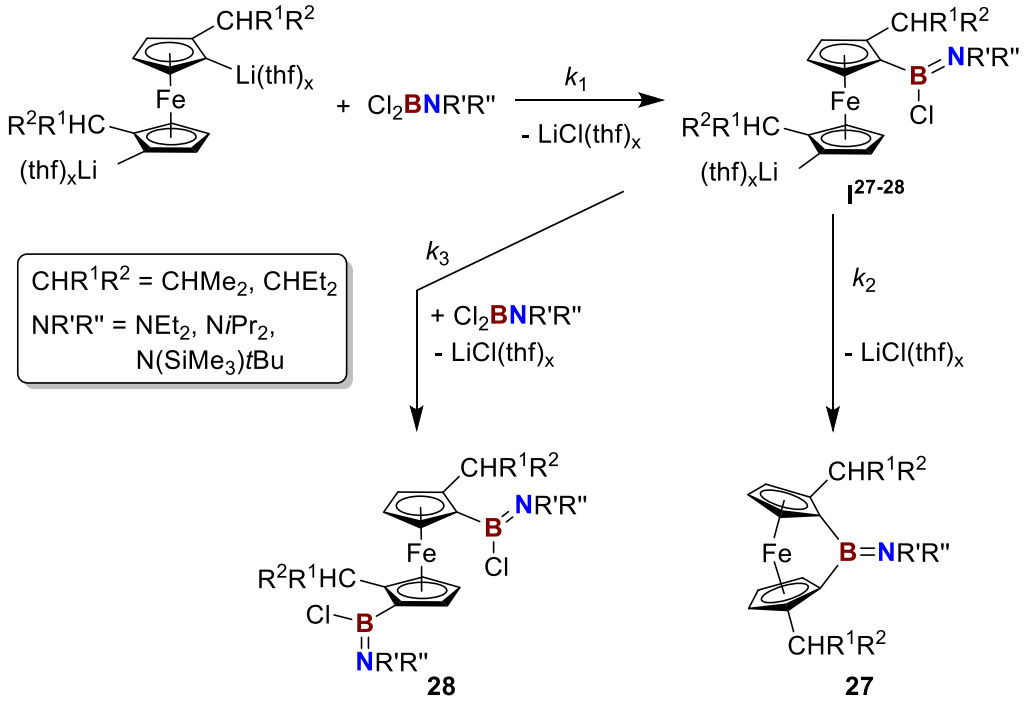

[a] Adopted from ref 7d.

The more puzzling effect was that of the CHR_2 groups on Cp rings, which was explained by considering their preferred conformation.[7d] The known single-crystal X-ray analysis data of [1]FCPs and dibromoferrocenes equipped with CHR_2 (R = Me, Et) groups all revealed the same

conformation.[7c,d] This is illustrated in Chart 3-1 with a drawing of a dibromoferrocene derivative and a Newman projection for one of the two CHR_2 groups. One of the two R groups (R^1) is approximately in the same plane as a Cp ring, whereas the second R group (R^2) is oriented away from iron and nearly perpendicular to the Cp ring. We assumed[7d] that for a particular amino(dichloro)borane the rate constant k_2 for the intramolecular ring closure (Scheme 3-2) should be unaffected by the type of alkyl group on the ferrocene moiety, because independent of the CHR^1R^2 alkyl groups only H atoms point to the inner parts of the sandwich where the ring closure happens. However, this is different for the rate constants k_1 and k_3. We assumed that the amino(dichloro)borane approaches a lithiated Cp ring from the least-hindered side, i.e., opposite to iron, with the result that the R^2 group of CHR^1R^2 will point approximately in the direction of the incoming amino(dichloro)borane. Hence, for steric reasons, R^2 = Et should give lower rate constants than R^2 = Me. In short, the effect of the CHR^1R^2 groups on the product ratio **27**:**28** was interpreted as a steric effect that influences the rate constant k_3 but not k_2 (Scheme 3-2).[7d]

Chart 3-1. Conformation of CHR^1R^2 Moieties

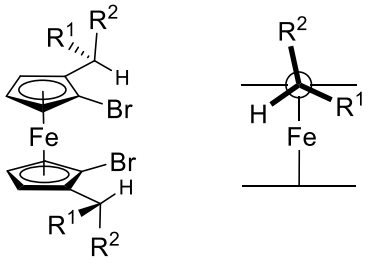

We set out to further test the proposed mechanism experimentally and theoretically for a deeper understanding of the salt-metathesis approach toward strained sandwich compounds. Our intent was an improved understanding of the effect of the CHR^1R^2 groups on the outcome of the salt-metathesis reactions so that this effect could be used in future syntheses of strained sandwich compounds.

3.4.1 Experimental Results

In order to test the hypothesis that the alkyl group that is oriented approximately perpendicular to the Cp ring, R^2 (Chart 3-1), and not R^1, affects the outcome of the salt-metathesis reaction, enantiomerically pure dibromoferrocene derivatives with different R^1 and R^2 groups were prepared first. As shown in Chart 3-2, in addition to the known species **15**$^{\mathbf{MeMe}}$[7c] and **15**$^{\mathbf{EtEt}}$[7d] the "hybrids" in form of the two stereoisomers **15**$^{\mathbf{EtMe}}$ and **15**$^{\mathbf{MeEt}}$ were prepared. Similar as the known species **15**$^{\mathbf{MeMe}}$ and **15**$^{\mathbf{EtEt}}$ had been prepared, the two new dibromoferrocene derivatives were obtained using the Ugi-amine approach (Scheme 3-3).[7c,d,8] This methodology allows the introduction of both groups separately: R^1 is introduced in the first step by a Friedel–Crafts acylation of ferrocene, and R^2 is introduced in the last step (d in Scheme 3-3).

Chart 3-2. Chiral Dibromoferrocenes **15**$^{\mathbf{R1R2}}$ *a*

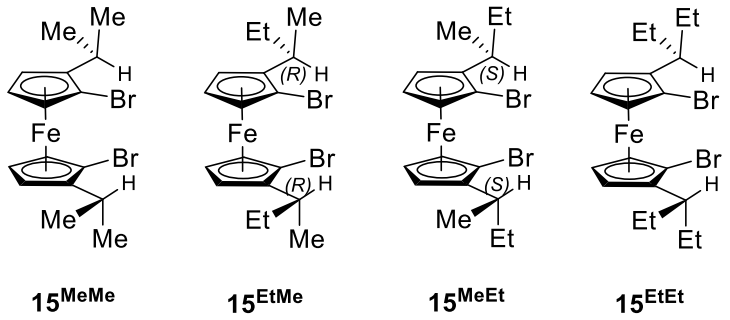

15$^{\mathbf{MeMe}}$ **15**$^{\mathbf{EtMe}}$ **15**$^{\mathbf{MeEt}}$ **15**$^{\mathbf{EtEt}}$

a **15**$^{\mathbf{MeMe}}$ and **15**$^{\mathbf{EtEt}}$ are known compounds.[7c,d]

The four different dibromides **15**$^{\mathbf{R1R2}}$ were used as precursors for the respective dilithiated species, which were in situ prepared and reacted with Cl_2BN*i*Pr_2 (Scheme 3-3). As the focus of our investigation was on the reaction mechanism rather than the synthesis of new strained bora[1]ferrocenophanes, from the two new bora[1]ferrocenophanes only **27b**$^{\mathbf{MeEt}}$ was isolated and characterized by NMR spectroscopy, elemental analysis, and mass spectrometry. Not surprisingly,

its NMR data compares very well with that of the known species **27b**$^{\mathbf{MeMe}}$ and **27b**$^{\mathbf{EtEt}}$ (for a discussion see refs 7c and 7d).

Scheme 3-3. Synthesis of [1]FCPs **27b**$^{\mathbf{R1R2}}$

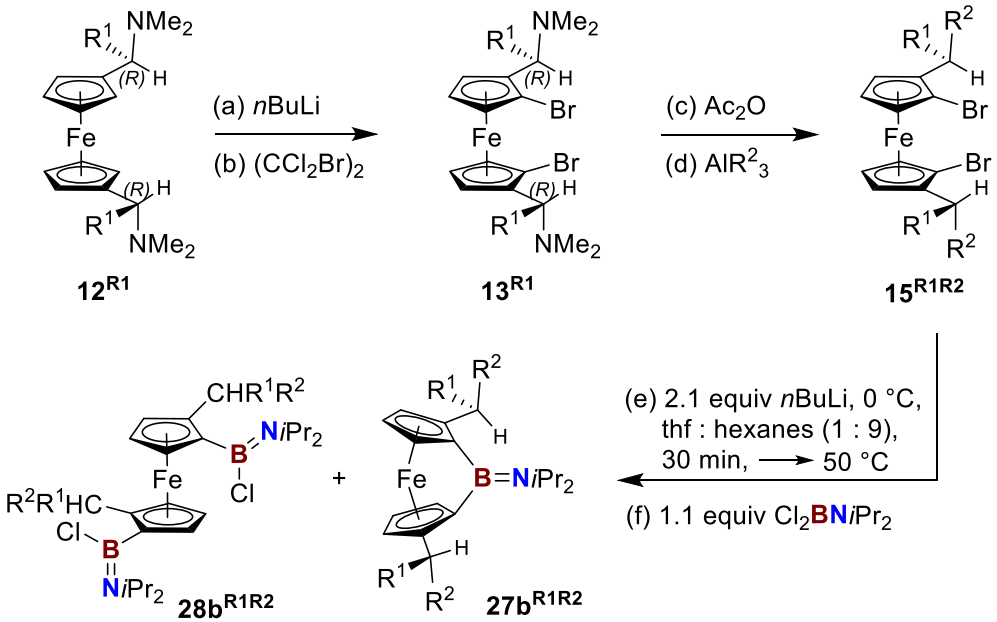

When the synthesis and isolation of the [1]FCP **27b**$^{\mathbf{EtEt}}$ had been reported, also single crystals were obtained and solving of the molecular structure by single-crystal X-ray analysis was attempted.[7d] However, due to molecular disorder, the structure could not be solved. Recently, we were able to model the disorder and, therefore, the molecular structure of **27b**$^{\mathbf{EtEt}}$ is presented here. Figure 3-1 exhibits an ORTEP plot of **27b**$^{\mathbf{EtEt}}$, while crystallographic data can be found in Table S1 (Supporting Information). It is not surprising that the molecular structure of **27b**$^{\mathbf{EtEt}}$ is very similar to the known structure of **27b**$^{\mathbf{MeMe}}$.[7c] This can be best illustrated by a comparison of the common distortion angles of α = 31.2(9), β/β' = 36.00(13)/35.20(12), δ = 156.3(9), and θ = 103.38(15)° for **27b**$^{\mathbf{EtEt}}$ (Figure 3-1) which are, as expected, similar to the respective values in **27b**$^{\mathbf{MeMe}}$ (α = 31.9(2), β/β' = 36(1)/35(1), δ = 155(2), θ = 103.0(3)°).[7c]

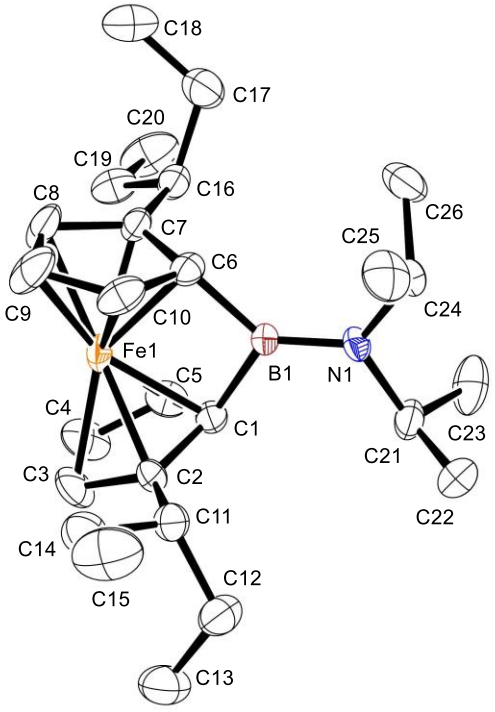

Figure 3-1. Molecular structure of **27b^{EtEt}** with thermal ellipsoids at 50% probability level. Hydrogen atoms are omitted for clarity. Only the major component of the disordered structure is shown. The common distortion angles are α = 31.2(9), β/β' = 36.00(13)/35.20(12), δ = 156.3(9), and θ = 103.38(15)° (for the definition of distortion angles and additional data see Table S3 in Supporting Information).[4b,7c] For bond lengths [Å] and angles [deg] see Table S2 (Supporting Information).

In order to obtain information about the influence of the CHR^1R^2 groups on the outcome of the salt-metathesis reaction, ratios between the two products **27b^{R1R2}** and **28b^{R1R2}** were measured by ^{1}H NMR spectroscopy. To collect meaningful data, reaction conditions had been controlled as precise as possible. Therefore, all experiments were done on the same scale, using the same conditions; each experiment was repeated multiple times to get reliable data. As indicated in Scheme 3-3, the dilithioferrocene derivatives were prepared from precursors **15^{R1R2}** in a mixture of thf and hexanes[9] through addition of 2.1 equiv of *n*BuLi. After 30 min of stirring, the cold bath was replaced by a 50 °C prewarmed oil bath and, after 10 min of allowing thermal equilibration, a hexane solution of 1.1 equiv of Cl_2BNiPr_2 was added dropwise with a syringe pump over 10 min.

This procedure was developed in the course of our last investigation of boron-bridged [1]FCPs.[7d] Even though this investigation already included the use of **15**$^{\mathbf{MeMe}}$ and **15**$^{\mathbf{EtEt}}$ and measurement of the respective product ratios **27b**$^{\mathbf{R1R2}}$ to **28b**$^{\mathbf{R1R2}}$, we remeasured both ratios to make sure that all four product ratios were measured under the same conditions (Table 3-1).

Table 3-1. Product Ratios of [1]FCPs (**27b**$^{\mathbf{R1R2}}$) and Bis(boryl)ferrocenes (**28b**$^{\mathbf{R1R2}}$) [a]

CHR^1R^2	Products	Ratio
$CHMe_2$	**27b**$^{\mathbf{MeMe}}$:**28b**$^{\mathbf{MeMe}}$	1.0:0.51
R-CHEtMe	**27b**$^{\mathbf{EtMe}}$:**28b**$^{\mathbf{EtMe}}$	1.0:0.49
S-CHMeEt	**27b**$^{\mathbf{MeEt}}$:**28b**$^{\mathbf{MeEt}}$	1.0:0.30
$CHEt_2$	**27b**$^{\mathbf{EtEt}}$:**28b**$^{\mathbf{EtEt}}$	1.0:0.27

[a] Determined by ^{1}H NMR spectroscopy (see Experimental Section for details)

The **27b**$^{\mathbf{R1R2}}$:**28b**$^{\mathbf{R1R2}}$ product ratios in Table 3-1 show that the $CHEt_2$ groups result in the highest relative amounts of a [1]FCP (**27b**$^{\mathbf{EtEt}}$), whereas the $CHMe_2$ groups lead to the poorest performance. Moreover, the two systems with R^2 = Me ($CHMe_2$ and *R*-CHEtMe) give very similar ratios; the same can be said for the two systems with R^2 = Et ($CHEt_2$ and *S*-CHMeEt). These results support our hypothesis that the alkyl group that is oriented approximately perpendicular to the Cp ring (R^2; Charts 3-1 and 3-2) affects the outcome of the salt-metathesis reaction. Even though the effects of the CHR^1R^2 groups were relatively small, we explored the reaction mechanism using DFT calculations with the hope to better understand the origin of the effects.

3.4.2 Theoretical Results

The reaction mechanism of the salt-metathesis reactions was explored employing DFT calculations. Initial calculations were performed on the popular B3LYP/6-31G(d) level of theory. At first, in a series of calculations different conformers with respect to rotation of the CHR^1R^2 group were explored. This was needed in order to use the conformers of lowest energy as starting

geometries for the investigation of the reaction mechanism. The dibromoferrocenes **15^{R1R2}** were used as model compounds and rotation around the Cp−CHR^{1}R^2 bond of one of the two CHR^{1}R^2 groups was investigated by relaxed potential energy surface scans, which resulted in three minima. The optimized structures of these conformers and their relative energies are illustrated in Figure 3-2 for the dibromide **15^{MeMe}**. If in solution only these three conformers would be present, the preferred conformer (conf-A) would make up 98.5% of the entire mixture. This does not come as a surprise as all known molecular structures of compounds equipped with CHR^{1}R^2 groups show this preferred conformation, including the new structure shown in Figure 3-1; R^1 lies approximately in the same plane as the Cp ring and R^2 is oriented away from iron and nearly perpendicular to the Cp ring. For R^1 or R^2 being Et the presence of additional C−C bonds resulted in other possible conformers, which were investigated using the method described above. In short, for all cases the preferred conformation is that where the alkyl group is as far as possible away from iron (e.g., see Figure 3-1).

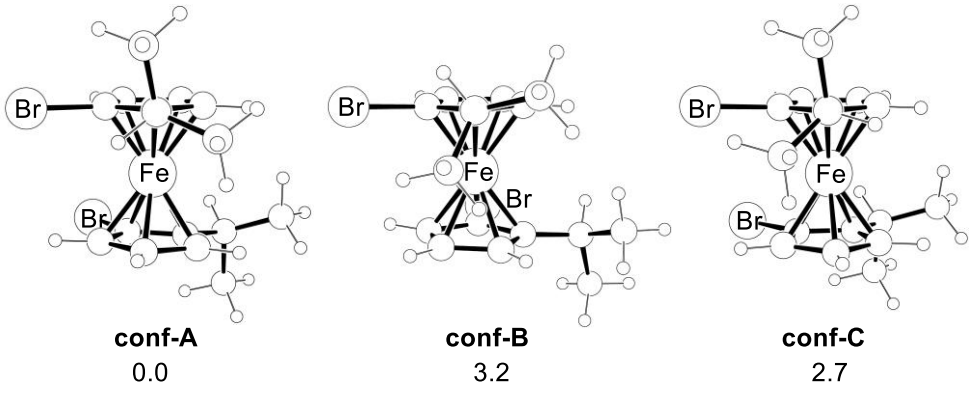

Figure 3-2. Relative standard free energies ($\Delta G°$ in kcal mol^{-1} at B3LYP/6-31G(d)) of three conformations in **15^{MeMe}** with respect to the rotation of one $CHMe_2$ group.

Equipped with the knowledge about conformers, ground-and transition-state geometries were first optimized at the B3LYP/6-31G(d) and, finally, calculated at the B3PW91/6-311+G(d,p) level of theory (Scheme 3-4). The motivation to use a different functional came from a recent

benchmark study,[10] where it was shown that the popular B3LYP method performed worse than the average of tested functionals. In particular, B3LYP is a poor choice for reaction energies, however, its precursor B3PW91 performed as one of the best of the tested hybrid functionals.[10] In addition, an important selection criterion for us was to compare optimized ground-state geometries of known, strained [1]FCPs to their known molecular structures. Using several recommended functionals[10] available in GAUSSIAN 09, B3PW91 was one of the best methods (Table S3 in Supporting Information). Salt-metathesis reactions were performed using the solvent mixture of hexanes/ thf (9/1) and, therefore, thf must be coordinated to lithium (Scheme 3-2). As a starting point to optimize the geometry of the intermediate $\mathbf{I}^{\mathbf{27-28}}$ we assumed that three thf molecules fill-up the coordination sphere to form a common 4-fold coordinated lithium ion. Even though geometries could be optimized, thf was replaced by the less flexible Me_2O to avoid problems associated with the presence of multiple isomers through different conformations of thf molecules. As illustrated in Scheme 3-4, the intramolecular ring closure to form $\mathbf{27b}^{\mathbf{R1R2}}$, as well as the intermolecular reaction to form $\mathbf{28b}^{\mathbf{R1R2}}$, both proceed through transition states with the formation of C−Li−Cl−B cycles as the common structural motif. In both reaction paths, when boron approaches the lithiated carbon atom, the Li−Cl distance decreases while the Li−C distance increases. This is illustrated in Figure 3-3 for both transition states ($\mathbf{TS}^{\mathbf{27}}$ and $\mathbf{TS}^{\mathbf{28}}$) for the $CHMe_2$ substituted species. In this process, the relative orientation of the $Li(OMe_2)_3$ moiety attached to one Cp ring in $\mathbf{I}^{\mathbf{27-28}}$ changes by bending away from the approaching boron-containing moiety. That is where the two reaction paths differ. For the intramolecular path, the $Li(OMe_2)_3$ moiety bends toward an open space away from the center of the molecule where iron is located. However, for the intermolecular path, the $Li(OMe_2)_3$ moiety must bend toward the center of the molecule which enforces the loss of one Me_2O ligand; the freed-up space around lithium gets occupied by

the iron-containing part of the molecule. One might be tempted to say that an electron donation from iron to lithium partially compensates for the loss of one Me_2O ligand. However, the calculated Fe−Li distances between 3.242 and 3.266 Å are significantly longer than known Fe−Li distances in systems where such an interaction was discussed.[11] The loss of one solvent molecule from lithium was found, when we searched for transition states performing relaxed potential energy surface scans along the B−C vector of the forming B−C bond. As the loss of one Me_2O was not accompanied by a pronounced energy barrier, this part of the mechanism was not investigated in further details. Finally, on the path from **TS^{28}** to **28b^{R1R2}**, LiCl gets eliminated in form of $(Me_2O)_3LiCl$ and the lost ligand molecule Me_2O now gets backfilled from the surrounding solvent molecules. We like to stress that the latter part is an assumption and the potential energy profile with respect to incoming Me_2O was not investigated.

Scheme 3-4. Calculated Free Energies of Ground- and Transition-State Species [a]

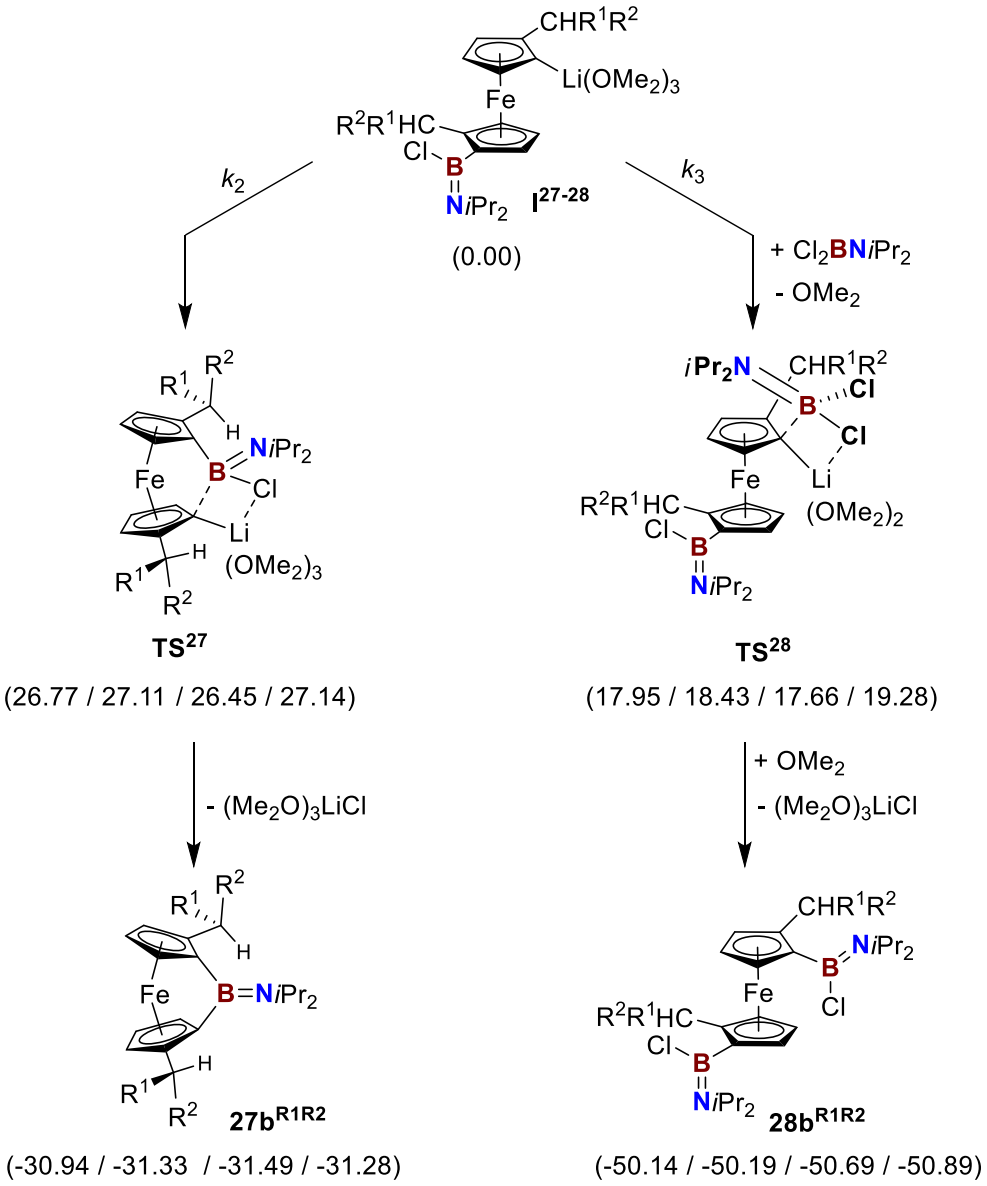

[a] Relative Δ*G*° values (B3PW91/6-311+G(d,p) in kcal mol^{-1}) in parenthesis shown for CHR^1R^2 in the order of $CHMe_2$ / *R*-CHEtMe / *S*-CHMeEt / $CHEt_2$ (see also Scheme S1 in Supporting Information).

Relative free energies (Δ*G*°) associated with the reaction mechanism are shown for the various species in Scheme 3-4 in parentheses. Activation energies for the ring-closure reaction toward species **27b^{R1R2}** are between 26.45 and 27.14 kcal mol^{-1} and expectedly larger than those of the path toward **28b^{R1R2}** (17.66 to 19.28 kcal mol^{-1}). Both ranges are very narrow as they span

0.7 and 1.6 kcal mol^{-1}, respectively. The formation of the strained [1]FCPs is associated with a higher activation barrier had also been proven experimentally. More important than the absolute values are the differences between free energies of the two transition states which cover just a narrow range of 8.8 ($CHMe_2$) to 7.9 ($CHEt_2$) kcal mol^{-1} [$\Delta\Delta G°$ = 8.8 ($CHMe_2$), 8.7 (*R*-CHEtMe), 8.8 (*S*-CHMeEt), 7.9 ($CHEt_2$) kcal mol^{-1}]. This matches the experimental results where it was found that the $CHMe_2$ substituted system gave the worst product ratio of **27b**$^{\mathbf{R1R2}}$:**28b**$^{\mathbf{R1R2}}$ (1.00:0.51; Table 3-1), while the $CHEt_2$ substituted system gave the best product ratio (1.00:0.27; Table 3-1). However, other details of the experimentally determined order of product ratios are not reflected in the DFT results. According to the calculation, the $CHMe_2$ and the *S*-CHMeEt substituted system both should lead to the same product ratios, contradicting the experimental findings that the *S*-CHMeEt system behaves similar as the $CHEt_2$ system (see Table 3-1). Even though the experimentally determined effects of the CHR^1R^2 groups are significant, they are small, which means that they must be caused by small differences between the free activation energies of the two competing reaction paths. The maximum calculated difference in the set of $\Delta\Delta G°$ values of 0.9 kcal mol^{-1} is very small and its meaning should not be overinterpreted.

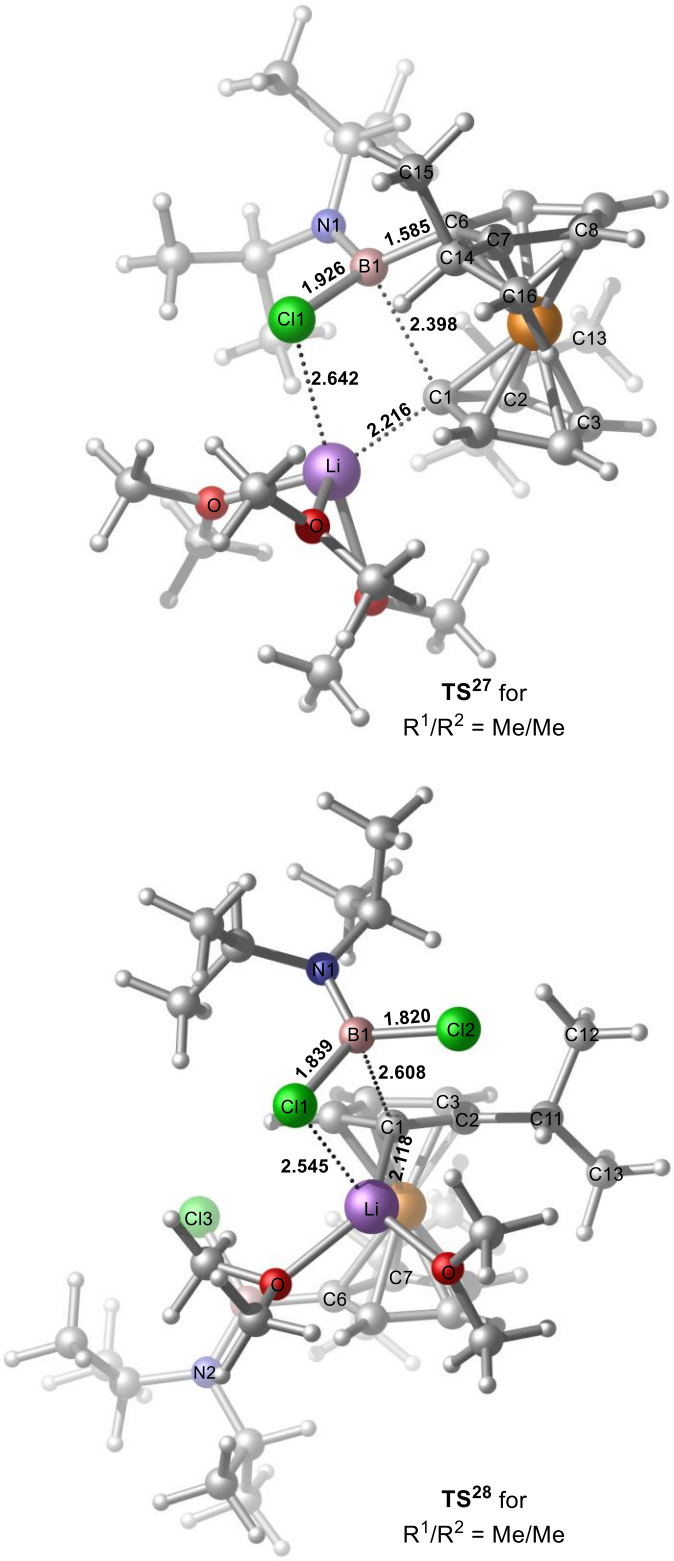

Figure 3-3. Bond lengths in Å for **TS**^{27} and **TS**^{28} illustrated for the $CHMe_2$ substituted species (R^1/R^2 = Me/Me).

These small energetic differences between related species in the set of the four CHR^1R^2-substituted systems are reflected in small structural differences. Whereas an illustration of the two transition states **TS[27]** and **TS[28]** for the $CHMe_2$-substituted species can be seen in Figure 3-3, Table 3-2 provides an overview of selected structural parameters. The distances between the atoms of the newly forming B−C bond (B1−C1) are shorter for the intramolecular ring-closure reaction (**TS[27]**; 2.383−2.398 Å) than for the intermolecular reaction (**TS[28]**; 2.603−2.609 Å). Both sets of values are significantly longer than the sum of the covalent radii (1.60 Å) or the already present B−C bonds in **TS[27]** (1.585−1.587 Å) or **TS[28]** (1.565 Å). The lithium-chlorine distances of the newly forming bond (Li−Cl1), 2.620−2.677 Å (**TS[27]**) and 2.539−2.548 Å (**TS[28]**), are also longer than a completely formed bond like in $ClLi(OMe_2)_3$ (2.204 Å). However, both comparisons indicate that in both transition states the formation of Li−Cl bonds is further progressed compared to the formation of B−C bonds. Table 3-2 also lists the two torsion angles C12−C11−C2−C3 and C15−C14−C7−C8 to illustrate the degree of rotation of the CHR^1R^2 groups in both transition states. The angles B1−N1−C1 and N1−B1− C1−C2 (Table 3-2 and Figure 3-3) are used to measure the relative orientation of the incoming Cl_2BNiPr_2 species with respect to the ferrocene moiety in **TS[28]**. Within the series of the four differently substituted systems, both angles do not change significantly.

3.5 Conclusions

Four planar-chiral, enantiomerically pure ferrocene dibromides (**15[R1R2]**) equipped with two CHR^1R^2 groups in α position to bromine (C_2 symmetry) were converted into dilithio ferrocene derivatives and reacted with Cl_2BNiPr_2. These salt-metathesis reactions resulted in mixtures of bora[1]ferrocenophanes (**27b[R1R2]**) and 1,1′-bis(boryl)ferrocenes (**28b[R1R2]**) (Scheme 3-3) and the

ratios **27b**$^{\mathbf{R1R2}}$:**28b**$^{\mathbf{R1R2}}$ were determined by ^{1}H NMR spectroscopy (Table 3-1). The aim of this investigation was to test the hypothesis that the alkyl group that is oriented approximately perpendicular to the Cp ring (R^2; Chart 3-1) affects the outcome of the salt-metathesis reaction. Therefore, in addition to the known species with CHR^1R^2 equal to $CHMe_2$ (**15**$^{\mathbf{MeMe}}$) or $CHEt_2$ (**15**$^{\mathbf{EtEt}}$), the "hybrids" equipped with *R*-CHEtMe (**15**$^{\mathbf{EtMe}}$) or *S*-CHEtMe groups (**15**$^{\mathbf{MeEt}}$) were employed. The measured **27b**$^{\mathbf{R1R2}}$:**28b**$^{\mathbf{R1R2}}$ product ratios clearly supported the hypothesis that R^2 (and not R^1) dictates the outcome of the salt-metathesis reaction (Table 3-1). In order to better understand this effect, the reaction mechanism had been investigated by DFT calculations (B3PW91/6-311+G(d,p)); however, the experimental findings could only partially be reproduced by theory. Even though our calculations failed to uncover the origin of the CHR^1R^2 effect, they clearly revealed that the two reaction paths starting from the common intermediate (**I**$^{\mathbf{27-28}}$) to either of the products (**27b**$^{\mathbf{R1R2}}$ or **28b**$^{\mathbf{R1R2}}$) both are concerted steps. In both transition states **TS**$^{\mathbf{27}}$ and **TS**$^{\mathbf{28}}$ (Figure 3-3), C−Li−Cl−B cycles are formed illustrating the fact of simultaneous bond breakage and formation. Both transition states have in common that the formation of Li−Cl bonds is further progressed compared to the formation of B−C bonds.

3.6 Experimental Section

General and Characterization Methods. If not mentioned otherwise, all syntheses were carried out using standard Schlenk and glovebox techniques. Solvents were dried using an MBraun Solvent Purification System and stored under nitrogen over 3 Å molecular sieves. All solvents for NMR spectroscopy were degassed (freeze-pump-thaw method) prior to use and stored under nitrogen over 3 Å molecular sieves. ^{1}H (500 MHz), ^{11}B (160 MHz), and ^{13}C (125 MHz) NMR spectra were recorded on 500 MHz Bruker Avance and 500 MHz Bruker Avance III HD NMR

spectrometers at 25 °C in C_6D_6 or $CDCl_3$. ^1H chemical shifts were referenced to the residual protons of the deuterated solvents (δ = 7.15 ppm for C_6D_6 and 7.26 ppm for $CDCl_3$); ^{13}C chemical shifts were referenced to the C_6D_6 signal at δ = 128.00 ppm or the $CDCl_3$ signal at δ = 77.00 ppm. ^{11}B NMR spectra were calibrated using $BF_3{\cdot}Et_2O$ (0.0 ppm) as external reference. Assignments for **15**$^{\mathbf{EtMe}}$, **15**$^{\mathbf{MeEt}}$, and **27b**$^{\mathbf{MeEt}}$ were supported by additional NMR experiments (DEPT, HMQC, COSY). As signals of Cp protons show a fine structure, all signals are designated as multiplets. High resolution mass data were obtained with a JEOL AccuTOF GCv 4G instrument using field desorption ionization (FDI). For the isotopic pattern, only the mass peak of the isotopoloque or isotope with the highest natural abundance is listed. Flash chromatography was performed with silica gel 60; mixed solvent eluents are reported as v/v solutions. Elemental analyses were performed on a PerkinElmer 2400 CHN Elemental Analyzer. For controlled addition of solutions of iPr$_2$NBCl$_2$ a syringe pump has been used (SAGE INSTRUMENT, model 355).

Reagents. Dichloro(diisopropylamino)borane,[12] (*R*,*R*,*S*$_p$,*S*$_p$)-2,2′-bis(*α*-acetoxyethyl)-1,1′-dibromoferrocene,[7c] (*R*,*R*,*S*$_p$,*S*$_p$)-2,2′-bis(*α*-acetoxypropyl)-1,1′-dibromoferrocene,[7d,13] (*S*$_p$,*S*$_p$)-1,1′-dibromo-2,2′-di(isopropyl)ferrocene (**15**$^{\mathbf{MeMe}}$),[7c] (*S*$_p$,*S*$_p$)-1,1′-dibromo-2,2′-di(3-pentyl)ferrocene (**15**$^{\mathbf{EtEt}}$)[7d,13] were synthesized as reported. Sodium potassium tartrate tetrahydrate (certified ACS crystalline) was purchased from Fisher Scientific. *n*BuLi (2.5 M in hexanes), triethylaluminum (25 wt.% in toluene), trimethylaluminum (2.0 M in hexanes) were purchased from Sigma Aldrich. Silica gel 60 (EMD, Geduran, particle size 0.040–0.063 mm) was used for column chromatography.

Synthesis of (*R*,*R*,*S*$_p$,*S*$_p$)-1,1′-Dibromo-2,2′-di(2-butyl)ferrocene (15$^{\mathbf{EtMe}}$). $AlMe_3$ (2.0 M in hexanes, 25.0 mL, 50 mmol) was added dropwise to a stirred solution of (*R*,*R*,*S*$_p$,*S*$_p$)-2,2′-bis(*α*-acetoxypropyl)-1,1′-dibromoferrocene (5.407 g, 9.938 mmol) in dry CH_2Cl_2 (100 mL) at –78 °C.

The reaction mixture was stirred for 1 h at −78 °C, warmed to r.t., and stirred for additional 20 min. The reaction mixture was added dropwise to a saturated aqueous solution of $NaHCO_3$ (250 mL) at 0 °C via cannula, followed by addition of a saturated aqueous solution of sodium potassium tartrate (150 mL). CH_2Cl_2 was removed using a rotary evaporator and replaced by Et_2O (150 mL). The mixture was stirred for 15 min and 1M HCl(aq) (100 mL) was added. The phases were separated and the aqueous phase was extracted with Et_2O (3 × 150 mL). The combined organic phases were washed with a saturated aqueous solution of $NaHCO_3$, water, and brine, respectively, dried over anhydrous Na_2SO_4, and concentrated using a rotary evaporator. The resulting red oil was further purified by column chromatography (hexanes; silica gel). The resulting red oil was crystallized from hexanes at ca. −22 °C. Collection of two batches of dark orange crystals gave product **15$^{\mathbf{EtMe}}$** (2.014 g, 44%). ^{1}H NMR (C_6D_6, 500 MHz): δ 0.99 [t, 6H, CH(CH_3)($CH_2C\underline{H}_3$)], 1.10 [d, 6H, CH($C\underline{H}_3$)(CH_2CH_3)], 1.22 [m, 2H, CH(CH_3)($C\underline{H}_2CH_3$)], 1.97 [m, 2H, CH(CH_3)($C\underline{H}_2CH_3$)], 2.53 [m, 2H, C$\underline{H}$(CH_3)(CH_2CH_3)], 3.70 (m, 2H, CH of Cp), 3.75 (m, 2H, CH of Cp), 4.14 ppm (m, 2H, CH of Cp). ^{13}C{^{1}H} NMR (C_6D_6, 125 MHz): δ 12.5 [CH(CH_3)($CH_2\underline{C}H_3$)], 20.6 [CH($\underline{C}H_3$)(CH_2CH_3)], 28.6 [CH(CH_3)($\underline{C}H_2CH_3$)], 32.7 [$\underline{C}$H(CH_3)(CH_2CH_3)], 65.6 (CH of Cp), 68.0 (CH of Cp), 73.8 (CH of Cp), 80.7 (*ipso*-C of Cp), 95.9 ppm (*ipso*-C of Cp). HRMS (FDI): *m/z* calcd for $C_{18}H_{24}Br_2Fe$, 453.9594; found, 453.9615. Elemental anal. calcd (%) for $C_{18}H_{24}Br_2Fe$ (456.043): C, 47.41; H, 5.30; found: C, 47.75; H, 5.32.

Synthesis of (*S*,*S*,*S*$_p$,*S*$_p$)-1,1′-Dibromo-2,2′-di(2-butyl)ferrocene (15$^{\mathbf{MeEt}}$). Et_3Al (25 wt. % in toluene, 27 mL, 51 mmol) was added dropwise to (*R*,*R*,*S*$_p$,*S*$_p$)-2,2′-bis(α-acetoxyethyl)-1,1′-dibromoferrocene (5.214 g, 10.10 mmol) in dry CH_2Cl_2 (100 mL) at −78 °C. The reaction mixture was stirred for 1 h at −78 °C, warmed to r.t. and stirred for 30 min. The reaction mixture was added dropwise to a saturated aqueous solution of $NaHCO_3$ (50 mL) at 0 °C via cannula, followed by

addition of a saturated aqueous solution of sodium potassium tartrate (50 mL). CH_2Cl_2 was removed using a rotary evaporator and replaced by Et_2O (100 mL). The mixture was stirred for 15 min and 1M HCl(aq) (25 mL) was added. The phases were separated and the aqueous phase was extracted with Et_2O (2 × 200 mL). The combined organic phases were washed with a saturated aqueous solution of $NaHCO_3$, water, brine, respectively, and then dried over anhydrous Na_2SO_4. All volatiles were removed to yield a red oil which was purified by column chromatography (hexanes; silica gel) to yield **15^{MeEt}** as a red oil (3.899 g, 85%). ^{1}H NMR ($CDCl_3$, 500 MHz): δ 0.81 [t, 6H, CH($CH_2C\underline{H}_3$)(CH_3)], 1.24–1.32 [m, 8H, CH($C\underline{H}_2CH_3$)($C\underline{H}_3$)], 1.45–1.53 [m, 2H, CH($C\underline{H}_2CH_3$)(CH_3)], 2.60–2.66 [m, 2H, C$\underline{H}$(CH_2CH_3)(CH_3)], 4.03 (m, 2H, CH of Cp), 4.05 (m, 2H, CH of Cp), and 4.22 ppm (m, 2H, CH of Cp). ^{13}C{^{1}H} NMR ($CDCl_3$, 125 MHz): δ 11.2 [CH($CH_2\underline{C}H_3$)(CH_3)], 18.3 [CH(CH_2CH_3)($\underline{C}H_3$)], 31.0 [CH($\underline{C}H_2CH_3$)(CH_3)], 31.8 [$\underline{C}$H(CH_2CH_3)(CH_3)], 65.2 (CH of Cp), 67.9 (CH of Cp), 74.1 (CH of Cp), 80.8 (*ipso*-C of Cp), and 94.2 (*ipso*-C of Cp) ppm. HRMS (FDI): *m/z* calcd for $C_{18}H_{24}Br_2Fe$: 453.9594; found: 453.9589. Elemental anal. calcd (%) for $C_{18}H_{24}Br_2Fe$ (456.043): C 47.41, H 5.30; found: C 48.05, H 5.29.

Synthesis of Boron-bridged [1]Ferrocenophane 27b^{MeMe}. *n*BuLi (2.5 M in hexanes, 0.44 mL, 1.1 mmol) was added dropwise to a cold (0 °C) solution of **15^{MeMe}** (0.222 g, 0.519 mmol) in a mixture of thf (0.5 mL) and hexanes (4.5 mL). The reaction mixture was stirred at 0 °C for 30 min, resulting in an orange solution. The cold bath was removed and replaced with a preheated oil bath (50 °C), followed by stirring of the solution for 10 min. A solution of *i*Pr_2NBCl_2 (0.105 g, 0.577 mmol) in hexanes (5.0 mL) was added dropwise within 10 min applying a syringe pump. The reaction colour changed from orange to dark-red along with formation of a white precipitate. After the addition of *i*Pr_2NBCl_2 was completed, the oil bath was removed and the reaction mixture

was slowly cooled to ambient temperature by continuous stirring at r.t. for 20 min. After that a ^{1}H NMR spectrum was measured from an aliquot of the reaction mixture. The ^{1}H NMR spectrum showed the corresponding signals for the compounds **27b^{MeMe}** and **28b^{MeMe}**, which matches with the NMR data provided in the literature.[7c,7d] ^{1}H NMR (C_6D_6, 500 MHz): **27b^{MeMe}**: δ 1.19 (d, 6H), 1.23 (d, 6H), 1.28 (d, 6H), 1.39 (d, 6H), 2.36–2.44 (m, 2H), 3.50 (br, 2H), 3.96–4.02 (m, 2H), 4.29 (m, 2H), 4.53 ppm (m, 2H); **28b^{MeMe}**: δ 0.73 (d, 6H), 0.96 (d, 6H), 1.13 (d, 6H), 1.34 (d, 6H), 1.48 (d, 6H), 1.55 (d, 6H), 3.11–3.19 (m, 2H), 3.34–3.44 (m, 2H), 4.20–4.27 (m, 2H), 4.25 (br, 2H), 4.29 (m, 2H), 4.50 ppm (m, 2H). The ratio between the compounds **27b^{MeMe}** and **28b^{MeMe}** was determined based on the integrations of the Cp signals (δ 3.50 and 4.50 ppm) as 1.0:0.51.

The above described procedure was used as a general procedure for all the following salt-metathesis reactions. Therefore, only the amounts of *n*BuLi, **15^{R1R2}**, and *i*Pr$_2$NBCl$_2$ used are mentioned.

Synthesis of Boron-bridged [1]Ferrocenophane 27b^{EtMe}. Amounts used: *n*BuLi (2.5 M in hexanes, 0.42 mL, 1.1 mmol), **15^{EtMe}** (0.229 g, 0.502 mmol), *i*Pr$_2$NBCl$_2$ (0.102 g, 0.561 mmol). ^{1}H NMR (C_6D_6, 500 MHz): **27b^{EtMe}**: δ 1.03 (t, 6H), 1.20 (d, 6H), 1.25 (d, 6H), 1.29 (d, 6H), 2.11–2.22 (m, 2H), 2.36–2.44 (m, 2H), 3.54 (br, 2H), 3.98–4.04 (m, 2H), 4.27 (br, 2H), 4.55 ppm (m, 2H). **28b^{EtMe}**: δ 0.74 (d, 6H), 0.96 (d, 6H), 1.08 (t, 6H), 1.15 (d, 6H), 1.49 (d, 6H), 1.55 (d, 6H), 3.10–3.19 (m, 4H), 4.22–4.29 (m, 2H), 4.27 (br, 2H), 4.34 (m, 2H), 4.54 ppm (m, 2H). Note: one multiplet for **27b^{EtMe}** could not be spotted clearly, most likely it is buried under the range δ 1.36–1.45 ppm (m, 2H). Two multiplets for **28b^{EtMe}** are presumably buried under the range δ 1.36–1.45 ppm (m, 4H). The ratio between the compounds **27b^{EtMe}** and **28b^{EtMe}** was determined based on the integrations of the Cp signals (δ 3.54 and 4.34 ppm) as 1.0:0.49.

Synthesis of Boron-bridged [1]Ferrocenophane 27b^{MeEt}. Amounts used: *n*BuLi (2.5 M in hexanes, 0.47 mL, 1.2 mmol), **15^{MeEt}** (0.256 g, 0.561 mmol), *i*Pr$_2$NBCl$_2$ (0.114 g, 0.627 mmol). A ^{1}H NMR spectrum of the reaction mixture showed the corresponding signals for compound **27b^{MeEt}** (see below) and signals for **5^{MeEt}** as follows ^{1}H NMR (C_6D_6, 500 MHz): δ 0.74 (d, 6H), 0.84 (t, 6H), 0.87 (d, 6H), 0.99 (d, 6H), 1.48 (d, 6H), 1.56 (d, 6H), 3.09–3.18 (m, 2H), 3.23–3.30 (m, 2H), 4.26 (br, 2H), 4.34 (br, 2H), 4.48 ppm (br, 2H). Note: three other multiplets for **5^{MeEt}** could not be spotted clearly, probably they are buried under the ranges δ1.44–1.51 and 4.23–4.32 ppm (m, 4H and 2H, respectively). The ratio between the compounds **27b^{MeEt}** and **5^{MeEt}** was determined based on the integrations of the Cp signals (δ3.51 and 4.48 ppm) as 1.0:0.30.

*Isolation of **27b^{MeEt}** from the Reaction Mixture.* All volatiles were removed from the reaction mixture and the resulting dark red residue was dissolved in hexanes (10 mL). LiCl was removed by filtration and washed with hexanes (2.0 mL). The resulting solution was concentrated to around 3.0 mL and left at −80 °C for 48 h, resulting in **27b^{MeEt}** as a dark-red precipitate (0.125 g, 55%). ^{1}H NMR (C_6D_6, 500 MHz): δ 0.91 [t, 6H, CH(CH$_3$)(CH$_2$C$\underline{H}_3$)], 1.24 [d, 6H, NCH(C$\underline{H}_3$)$_2$], 1.27 [d, 6H, NCH(C$\underline{H}_3$)$_2$], 1.31–1.41 [m, 2H, CH(CH$_3$)(C$\underline{H}_2$CH$_3$)], 1.39 [d, 6H, CH(C$\underline{H}_3$)(CH$_2$CH$_3$)], 1.73 [m, 2H, CH(CH$_3$)(C$\underline{H}_2$CH$_3$)], 2.24 [tq, 2H, C$\underline{H}$(CH$_3$)(CH$_2$CH$_3$)], 3.51 (m, 2H, CH-α of Cp), 4.00 [sept, 2H, NC$\underline{H}$(CH$_3$)$_2$], 4.28 (m, 2H, CH-β of Cp), 4.55 ppm (m, 2H, CH-β of Cp). ^{13}C{^{1}H} NMR (C_6D_6, 125 MHz): δ 11.7 [CH(CH$_3$)(CH$_2$$\underline{C}H_3$)], 18.6 [CH($\underline{C}H_3$)(CH$_2CH_3$)], 24.3 [NCH($\underline{C}H_3$)$_2$], 24.4 [NCH($\underline{C}H_3$)$_2$], 34.1 [CH(CH$_3$)($\underline{C}H_2CH_3$)], 36.2 [$\underline{C}$H(CH$_3$)(CH$_2CH_3$)], 40.2 (br, *ipso*-C of Cp, B), 48.0 [NCH(C$\underline{H}_3$)$_2$], 72.0 ($\underline{C}$H-β of Cp), 76.2 ($\underline{C}$H-β of Cp), 79.9 ($\underline{C}$H-α of Cp), 100.5 ppm (*ipso*-C of Cp, 2-butyl). ^{11}B NMR (C_6D_6, 160 MHz): δ 40.4 ppm. HRMS (FDI): *m/z* calcd for $C_{24}H_{38}BFeN$, 407.2447; found, 407.2430. Elemental anal. calcd (%) for $C_{24}H_{38}BFeN$ (407.230): C, 70.79; H, 9.41; N, 3.44; found: C, 70.68; H, 9.48; N, 3.30.

Synthesis of Boron-bridged [1]Ferrocenophane 27b^{EtEt}. Amounts used: *n*BuLi (2.5 M in hexanes, 0.44 mL, 1.1 mmol), **15^{EtEt}** (0.256 g, 0.529 mmol), *i*Pr$_2$NBCl$_2$ (0.111 g, 0.610 mmol). ^{1}H NMR of the reaction mixture shows the corresponding signals for the compound **27b^{EtEt}**, which matches with the NMR data provided in the literature.[7d] ^{1}H NMR (C_6D_6, 500 MHz): **27b^{EtEt}**: δ 0.79 (t, 6H), 1.04 (t, 6H), 1.26 (d, 6H), 1.30 (d, 6H), 1.60–1.69 (m, 4H), 1.74–1.82 (m, 2H), 2.21–2.29 (m, 4H), 3.56 (br, 2H), 4.00–4.06 (m, 2H), 4.27 (br, 2H), 4.56 ppm (br, 2H); **28b^{EtEt}**: δ 0.73 (d, 6H), 0.75 (t, 6H), 1.00 (d, 6H), 1.11 (t, 6H), 1.50 (d, 6H), 1.57 (d, 6H), 2.12–2.19 (m, 4H), 3.09–3.18 (m, 4H), 4.25 (br, 2H), 4.31–4.36 (m, 2H), 4.39 (br, 2H), 4.52 ppm (br, 2H). The ratio between the compounds **27b^{EtEt}** and **28b^{EtEt}** was determined based on the integrations of the Cp signals (δ 3.56 and 4.39 ppm) as 1.0:0.27.

Crystal Structure Determinations. A single crystal of **27b^{EtEt}** was coated with Paratone-N oil, mounted using a Micromount (MiTeGen—Microtechnologies for Structural Genomics), and frozen in the cold stream of an Oxford Cryojet attached to the diffractometer. Crystal data were collected on a Bruker APEX II diffractometer at −100 °C using monochromated Mo Kα radiation (λ = 0.71073 Å). An initial orientation matrix and cell was determined by ω scans, and the X-ray data were measured using ϕ and ω scans.[14] The frames were integrated with the Bruker SAINT soft-ware package.[15] Data reduction was performed with the APEX2 software package.[14] A multiscan absorption correction (SADABS) was applied.[15] The structure was solved by direct methods and refined using the Bruker SHELXL-2014 software package.[16] Non-hydrogen atoms were refined anisotropically; hydrogen atoms were included at geometrically idealized positions but not refined. The isotropic thermal parameters of the hydrogen atoms were fixed at 1.5 or 1.2 times that of the preceding carbon atom. The N[CH(CH$_3$)$_2$]$_2$ group in **27b^{EtEt}** was found to be disordered and modeled with a 68.6% and 31.4% occupancy. Crystallographic data are

summarized in Table S1, while bond lengths and bond angles are shown in Table S2 (Supporting Information). The ellipsoid plot was prepared using ORTEP-3 for Windows.[17] The common set of distortion angles in **27b**$^{\mathbf{EtEt}}$ was calculated using the programs PLATON.[18] The esds of all distortion angles that involve centroids of Cp rings (β, δ, and τ) are somewhat smaller than they should be, as esds on the positions of centroids were not included in the calculation.

DFT Calculations. All calculations were done employing the software package GAUSSIAN 09.[19] Initial calculations were performed on the B3LYP/6-31G(d) level of theory.[20] On this level relaxed potential energy surface scans and additional geometry optimizations to check that optimized transitions states correlate with the respective local minima, i.e., **TS**$^{\mathbf{27}}$ correlates with **I**$^{\mathbf{27–28}}$ and **27b**$^{\mathbf{R1R2}}$ while **TS**$^{\mathbf{28}}$ correlates with **I**$^{\mathbf{27–28}}$ and **28b**$^{\mathbf{R1R2}}$. Ground-state geometries of all possible isomers with respect to the conformation of the CHR^{1}R^2 groups were investigated so that the most stable conformer could be found. The most stable geometries were then finally optimized at the B3PW91/6-311+G(d,p) level.[20a,21] Frequency calculations were used to confirm minima and saddle points and provide thermodynamic information. An ultrafine grid (int = ultrafine) and tight requirements for geometry optimizations (opt = tight) were used for all final calculations. The notation used for free energies, $\Delta G°$, indicate standard conditions (p = 1 atm; T = 298.15 K). For the 1,1′-disubstituted ferrocene derivatives of type **I**$^{\mathbf{27–28}}$, **TS**$^{\mathbf{28}}$, and **28b**$^{\mathbf{R1R2}}$ several different isomers are possible that differ by the relative orientation of the two Cp moieties. However, these different isomers were not studied as only the relative and not the absolute values of free energies are important. Therefore, for each set of four species of each type **I**$^{\mathbf{27–28}}$, **TS**$^{\mathbf{28}}$, and **28b**$^{\mathbf{R1R2}}$, respectively, the same conformation with respect to the two Cp moieties were optimized. As discussed in the Results and Discussion section, the B3PW91 functional had been chosen based on the benchmark investigation of Grimme et al.[10] However, in contrast to this comprehensive

study, we did not include dispersion corrections. Inclusion of D3[22] or the later suggested D3(BJ)[23] correction resulted in calculated structures of [1]FCPs where the common set of distortion angles did not match the known values as good as without inclusion of dispersion corrections. Therefore, neither D3 nor D3(BJ) was included.

Graphical illustrations of calculated results were done with the help of ORTEP-3 for Windows (version 2.02)[17] and CYLview (version 1b).[24] Extraction of structural parameters from the calculated coordinates were done with the help of Mercury (version 3.7)[25] and CYLview (version 1b).[24]

3.7 Associated Content

Supporting Information

The Supporting Information is available free of charge on the ACS Publications website at DOI: 10.1021/acs.organo-met.6b00388.

Acknowledgements

We thank the Natural Sciences and Engineering Research Council of Canada (NSERC Discovery Grant, JM) for support. We thank the Canada Foundation for Innovation (CFI) and the government of Saskatchewan for funding of the X-ray and NMR facilities in the Saskatchewan Structural Sciences Centre (SSSC). For DFT calculations, we are grateful to WestGrid (www.westgrid.ca) and Compute Canada (www.computecanada.ca) for support. We thank K. Thoms (CHN analysis and MS) for support and measurements. We thank Dr. Jianfeng Zhu (SSSC) for his help.

3.8 References

(1) Osborne, A. G.; Whiteley, R. H. *J. Organomet. Chem.* **1975**, *101*, C27-C28.

(2) Foucher, D. A.; Tang, B.-Z.; Manners, I. *J. Am. Chem. Soc.* **1992**, *114*, 6246-6248.

(3) Bellas, V.; Rehahn, M. *Angew. Chem., Int. Ed.* **2007**, *46*, 5082-5104.

(4) Selected reviews: (a) Heo, R. W.; Lee, T. R. *J. Organomet. Chem.* **1999**, *578*, 31-42. (b) Herbert, D. E.; Mayer, U. F. J.; Manners, I. *Angew. Chem., Int. Ed.* **2007**, *46*, 5060-5081. (c) Tamm, M. *Chem. Commun.* **2008**, 3089-3100. (d) Braunschweig, H.; Kupfer, T. *Acc. Chem. Res.* **2010**, *43*, 455-465. (e) Braunschweig, H.; Kupfer, T. *Eur. J. Inorg. Chem.* **2012**, 1319-1332. (f) Musgrave, R. A.; Russell, A. D.; Manners, I. *Organometallics* **2013**, *32*, 5654-5667. (g) Russell, A. D.; Musgrave, R. A.; Stoll, L. K.; Choi, P.; Qiu, H.; Manners, I. *J. Organomet. Chem.* **2015**, *784*, 24-30. (h) Bhattacharjee, H.; Müller, J. *Coord. Chem. Rev.* **2016**, *314*, 114-133.

(5) (a) Rausch, M. D.; Ciappenelli, D. J. *J. Organomet. Chem.* **1967**, *10*, 127-136. (b) Butler, I. R.; Cullen, W. R.; Ni, J.; Rettig, S. J. *Organometallics* **1985**, *4*, 2196-2201.

(6) (a) Rulkens, R.; Lough, A. J.; Manners, I. *Angew. Chem., Int. Ed.* **1996**, *35*, 1805-1807. (b) Bagh, B.; Gilroy, J. B.; Staubitz, A.; Müller, J. *J. Am. Chem. Soc.* **2010**, *132*, 1794-1795. (c) Bagh, B.; Schatte, G.; Green, J. C.; Müller, J. *J. Am. Chem. Soc.* **2012**, *134*, 7924-7936.

(7) (a) Braunschweig, H.; Dirk, R.; Müller, M.; Nguyen, P.; Resendes, R.; Gates, D. P.; Manners, I. *Angew. Chem., Int. Ed.* **1997**, *36*, 2338-2340. (b) Berenbaum, A.; Braunschweig, H.; Dirk, R.; Englert, U.; Green, J. C.; Jäkle, F.; Lough, A. J.; Manners, I. *J. Am. Chem. Soc.* **2000**, *122*, 5765-5774. (c) Sadeh, S.; Schatte, G.; Müller, J. *Chem.-Eur. J.* **2013**, *19*, 13408-13417. (d) Sadeh, S.; Bhattacharjee, H.; Khozeimeh Sarbisheh, E.; Quail, J. W.; Müller, J. *Chem.-Eur. J.* **2014**, *20*, 16320-16330.

(8) (a) Marquarding, D.; Klusacek, H.; Gokel, G.; Hoffmann, P.; Ugi, I. *J. Am. Chem. Soc.* **1970**, *92*, 5389-5393. (b) Schwink, L.; Knochel, P. *Chem.-Eur. J.* **1998**, *4*, 950-968.

(9) Bailey, W. F.; Luderer, M. R.; Jordan, K. P. *J. Org. Chem.* **2006**, *71*, 2825-2828.

(10) Goerigk, L.; Grimme, S. *Phys. Chem. Chem. Phys.* **2011**, *13*, 6670-6688.

(11) (a) Irigoras, A.; Mercero, J. M.; Silanes, I.; Ugalde, J. M. *J. Am. Chem. Soc.* **2001**, *123*, 5040-5043. (b) Scheibitz, M.; Winter, R. F.; Bolte, M.; Lerner, H.-W.; Wagner, M. *Angew. Chem., Int. Ed.* **2003**, *42*, 924-927.

(12) Gerrard, W.; Hudson, H. R.; Mooney, E. F. *J. Chem. Soc.* **1960**, 5168-5172.

(13) Kang, J.; Lee, J. H.; Im, K. S. *J. Mol. Catal. A: Chem.* **2003**, *196*, 55-63.

(14) Bruker *APEX2*; 2014.3–0 ed.; Bruker AXS Inc., 2014.

(15) Bruker *SAINT and SADABS*; v8.34a ed.; Bruker AXS Inc., 2013.

(16) (a) Sheldrick, G. M. *SHELXL, Program for the Solution of Crystal Structures*; University of Göttingen, Germany. (b) Sheldrick, G. M. *Acta Crystallogr., Sec A: Found. Crystallogr.* **2008**, *64*, 112-122.

(17) Farrugia, L. J. *J. Appl. Crystallogr.* **1997**, *30*, 565.

(18) Spek, A. L. *PLATON, A Multipurpose Crystallographic Tool*; University of Utrecht: The Netherlands, 2011.

(19) Frisch, M. J.; Trucks, G. W.; Schlegel, H. B.; Scuseria, G. E.; Robb, M. A.; Cheeseman, J. R.; Scalmani, G.; Barone, V.; Mennucci, B.; Petersson, G. A.; Nakatsuji, H.; Caricato, M.; Li, X.; Hratchian, H. P.; Izmaylov, A. F.; Bloino, J.; Zheng, G.; Sonnenberg, J. L.; Ha-da, M.; Ehara, M.; Toyota, K.; Fukuda, R.; Hasegawa, J.; Ishida, M.; Nakajima, T.; Honda, Y.; Kitao, O.; Nakai, H.; Vreven, T.; J. A. Montgomery, J.; Peralta, J. E.; Ogliaro, F.; Bearpark, M.; Heyd, J. J.; Brothers, E.; Kudin, K. N.; Staroverov, V. N.; Keith, T.; Kobayashi, R.; Normand, J.; Raghavachari, K.;

Rendell, A.; Burant, J. C.; Iyengar, S. S.; Tomasi, J.; Cossi, M.; Rega, N.; Millam, J. M.; Klene, M.; Knox, J. E.; Cross, J. B.; Bakken, V.; Adamo, C.; Jaramillo, J.; Gomperts, R.; Stratmann, R. E.; Yazyev, O.; Austin, A. J.; Cammi, R.; Pomelli, C.; Ochterski, J. W.; Martin, R. L.; Morokuma, K.; Zakrzewski, V. G.; Voth, G. A.; Salvador, P.; Dannenberg, J. J.; Dapprich, S.; Daniels, A. D.; Farkas, O.; Foresman, J. B.; Ortiz, J. V.; Cioslowski, J.; Fox, D. J. *Gaussian 09*, Revision E.01; Gaussian, Inc.: Wallingford, CT, 2013.

(20) (a) Becke, A. D. *J. Chem. Phys.* **1993**, *98*, 5648-5652. (b) Lee, C.; Yang, W.; Parr, R. G. *Phys. Rev. B: Condens. Matter Matter. Phys.* **1988**, *37*, 785-789.

(21) (a) Perdew, J. P. *In Electronic Structure of Solids '91*; Ziesche, P., Eschrig, H., Eds.; Akademie Verlag: Berlin, 1991, p 11-20. (b) Perdew, J. P.; Chevary, J. A.; Vosko, S. H.; Jackson, K. A.; Pederson, M. R.; Singh, D. J.; Fiolhais, C. *Phys. Rev. B: Condens. Matter Mater. Phys.* **1992**, *46*, 6671-6687. (c) Perdew, J. P.; Chevary, J. A.; Vosko, S. H.; Jackson, K. A.; Pederson, M. R.; Singh, D. J.; Fiolhais, C. *Phys. Rev. B: Condens. Matter Mater. Phys.* **1993**, *48*, 4978-4978. (d) Perdew, J. P.; Burke, K.; Wang, Y. *Phys. Rev. B: Condens. Matter Mater. Phys.* **1996**, *54*, 16533-16539. (e) Burke, K.; Perdew, J. P.; Wang, Y. In *Electronic Density Functional Theory: Recent Progress and New Directions*; Dobson, J. F., G. Vignale, Das, M. P., Eds.; Plenum, 1998; p 81-111.

(22) Grimme, S.; Antony, J.; Ehrlich, S.; Krieg, H. *J. Chem. Phys.* **2010**, *132*, 154104.

(23) Grimme, S.; Ehrlich, S.; Goerigk, L. *J. Comput. Chem.* **2011**, *32*, 1456-1465.

(24) Legault, C. Y. CYLview. http://www.cylview.org, 2009.

(25) *The Cambridge Crystallographic Data Centre*. http://www.ccdc.cam.ac.uk/mercury, Mercury.

4 Strained Azabora[2]ferrocenophanes

4.1 Author Contribution and Relation to the Research Objectives

This work was done in collaboration with Dr. Subhayan Dey, Dr. Jianfeng Zhu, Dr. Wei Sun, and Prof. Jens Müller. Dr. Dey synthesized and partially characterized 2-di(isopropyl)amino-1-trimethylsilyl-1,2-azabora[2]ferrocenophane (**30a)**. All single-crystal X-ray analyses were performed by Drs. Jianfeng Zhu and Wei Sun. All DFT calculations were performed by Prof. Müller. I synthesized (neopentylamino)bromoferrocene (**29b**), dichloro(diisopropylamino)borane, dichloro[tris(trimethylsilyl)methyl]borane, 2-di(isopropyl)amino-1-neopentyl-1,2-azabora-[2]ferrocenophane (**30b**), and 1-trisyl-2-neopentyl-1,2-azabora[2]ferrocenophane (**30c**). I performed complete characterizations of the two azabora[2]ferrocenophanes that I synthesized and further characterization for the other azabora[2]ferrocenophane synthesized by Dr. Dey. I prepared the first draft of the manuscript, which was further edited by Prof. Müller. Moreover, I compiled the entire experimental section and supporting information of this manuscript and contributed on referencing and editing of the manuscript.

In this work, we reported the first examples of [2]FCPs with nitrogen and boron in the bridging positions, which are essentially structural isomers of so far published amino-substituted bora[1]ferrocenphanes. All three [2]FCPs are equipped with unsaturated B=N moieties which are isoelectronic with C=C moieties in known dicarba[2]ferrocenophanes. DFT calculations revealed these species to be as strained as the well-known Me_2Si-bridged [1]FCP ($\Delta H° \approx -70$ kJ mol^{-1}).

We intended to synthesize the first examples of azabora[2]ferrocenophanes as new examples of a rather rare class of unsaturated *ansa*-bridged strained FCPs. Moreover, polar *ansa* B=N bridges are expected to be more reactive compared to the non-polar C=C bridges in dicarba[2]ferrocenophanes. Overall, we anticipated that these highly strained monomers can result

in BN-bridged polyferrocenes. Molecular structures of all three species obtained from X-ray crystallography showed high α angles (23–24°). However, none of these strained compounds did ring open under thermal conditions. DSC analyses of all three [2]FCPs were performed and, in every case, no exothermic peak indicative of ROP was observed even after heating samples to 300 °C. With the help of DFT calculations it was concluded that these [2]FCPs are sterically overprotected and, therefore, unsuitable for ROP.

The following is a verbatim copy[h,i] of the published article Bhattacharjee, H.; Dey, S.; Zhu, J.; Sun, W.; Müller, J. *Chem. Commun.* **2018**, *54*, 5562-5565.

4.2 Abstract

Three [2]ferrocenophanes equipped with unsaturated BN moieties at bridging positions were synthesized and structurally characterized. As revealed by DFT calculations, these first examples of azabora[2]-ferrocenophanes are similarly strained to the well-known Me_2Si-bridged [1]ferrocenophane.

4.3 Introduction

Since the first reports describing the successful application of ferrocenophanes (FCPs) as monomers for ring-opening polymerization (ROP) appeared (**G^{Me}** and **J**; Chart 4-1),[1] this methodology has been developed into a flexible approach towards new metal-containing materials.[2] The most widely applied monomers are silicon-bridged [1]FCPs, in particular, species **G^{Me}**.[3] The exploration of

[h] Reproduced from Bhattacharjee, H.; Dey, S.; Zhu, J.; Sun, W.; Müller, J. *Chem. Commun.* **2018**, *54*, 5562-5565 with permission from the Royal Society of Chemistry.
[i] Compound numbers and some chemical drawings were changed; subheadings and an Experimental Section were added to the main text to maintain a uniform style in the thesis.

FCPs already began a few years after the discovery of ferrocene,[4] with the first published derivative being a carbon-bridged [3]FCP.[5] To date, many different *ansa*-sandwich compounds are known,[6] but only a few types of strained sandwich compounds allow ROP with control over molecular weight and molecular weight distribution. In order to fully utilize ROP of FCPs, existing monomers need to be improved or new monomers need to be synthesized. In this context, we were inspired by the known dicarba[2]ferrocenophanes $\mathbf{M^{H}}$ and $\mathbf{M^{tBu}}$ (Chart 4-1).[7] Strained FCPs with unsaturated *ansa* bridges are rather rare and the most recent example is the carbene-stabilized compound **N** with an unusual bonding pattern.[8] We intended to prepare the first azabora[2]ferrocenophanes with the hope that the highly strained monomers would be converted into BN-bridged polyferrocenes. Such materials might be of interest in the light of recent successes in the preparation of new polymers with BN moieties in the backbone.[9] Our targeted FCPs can be derived from dicarba[2]ferrocenophanes by substitution of the C=C by an isoelectronic B=N moiety. This concept of isosterism has been providing guidance to main-group chemists for many decades; still, to date, surprising results can be obtained as illustrated in a very recent perspective article.[10] In contrast to the non-polar C=C moiety, one would expect that the polar B=N bridge in the targeted compounds allows polar reagents to act as initiators for ROP. Motivated by these thoughts, we targeted azabora[2]ferrocenophanes and synthesized compounds **30a-c** by using four different groups at nitrogen and boron (Scheme 4-1).[11]

Chart 4-1. Examples of Known Ferrocenophanes

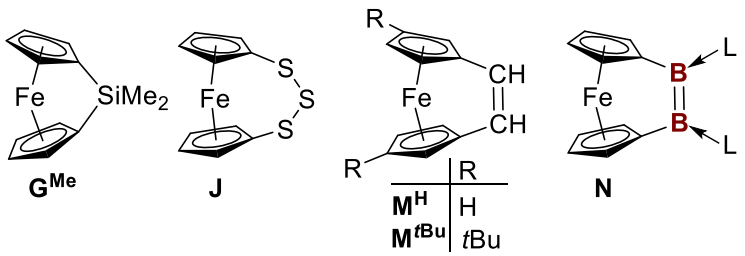

4.4 Results and Discussion

Recently, we reported a modular approach to nitrogen-bridged [2]FCPs with silicon, tin, or phosphorus as the second bridging element.[12] In light of this new methodology, the 1-amino-1′-bromoferrocene derivatives **29a** or **1b**[12] were *in situ* lithiated and reacted with either *i*Pr_2NBCl_2 or $(Me_3Si)_3CBCl_2$ at 0 °C. We had chosen these bulky substituents, as increased sterics often facilitates the formation of the targeted strained FCPs. The salt-metathesis reactions gave almost quantitative conversions towards the targeted strained compounds; this is illustrated using the ^{1}H NMR spectrum of the reaction mixture of azabora[2]ferrocenophane **30b** (Figure 4-1). The new [2]FCPs were purified either by crystallization from hexanes (**30b**, **30c**) or by vacuum sublimation (60 °C; **30a**) and obtained as crystalline red solids in yields of 55–70%. The ^{1}H NMR spectra of all three compounds showed the presence of a set of four equally intense pseudo triplets for the cyclopentadienyl (Cp) protons; similarly, their ^{13}C NMR spectra showed four signals for the proton substituted Cp carbons. These signal patterns indicate the presence of a two-fold symmetry element, i.e., the compounds are C_s symmetric. The *i*Pr groups in **30a** and **30b**, however, resonate as only one set of a doublet and a septet (see Figure 4-1 for **30b** at δ = 1.20 and 3.53 ppm). As already depicted in Scheme 4-1, one would expect that the acceptor and donor p orbitals of the BN moiety are lined up for a π interaction to give two inequivalent *i*Pr groups. The fact that this expectation is not reflected in the NMR data reveals that the N*i*Pr_2 group rotates fast about the BN bond on the NMR timescale. Species **30a** and **30b** show ^{11}B NMR spectra with chemical shifts of 34.2 and 33.3 ppm, respectively, which match the expected range for this type of substitution at boron.[13] The ^{11}B nucleus in **30c** with δ = 49.0 ppm is expectedly more deshielded; again, species with comparable substitution patterns are known with similar chemical shifts.[13] The molecular structures of all three [2]FCPs were determined by single-crystal X-ray crystallography (Figure

4-3). Table 4-1 shows the determined sets of angles that are commonly used to describe distortions in FCPs (see Figure 4-2 for definitions).

Scheme 4-1. Syntheses of Azabora[2]ferrocenophanes

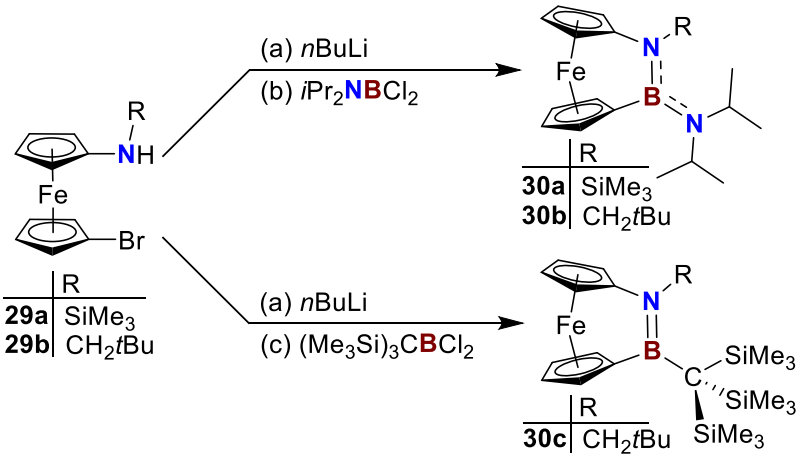

(a) hexanes/thf (9/1), 2.1 equiv *n*BuLi, −78 °C → 0 °C; (b) iPr$_2$NBCl$_2$ in hexanes; (c) (Me$_3$Si)$_3$CBCl$_2$ in hexanes

As expected, the structures of [2]FCPs **30a-c** are very similar, revealing only subtle differences. For example, the bridging B1–N1 bond length shortens on going from **30a** to **30c** [1.472(2) (**30a**), 1.453(4) (**30b**), 1.436(2) Å (**30c**)]. The external B1–N2 bonds of the iPr$_2$N-substituted compounds are only slightly different (1.419(2) (**30a**), 1.4137(19) Å (**30b**)). The latter values are close to 1.41 Å, which is the suggested value for a typical BN double bond length of non-cyclic aminoboranes.[14] One would expect that the trend in the bridging B1–N1 bond lengths has an impact on thea angle in the [2]FCPs. In fact, the α angle of **30c** is indeed the highest (24.2(1)°; Table 4-1) of these three species; nonetheless, those of **30a** and **30b** are identical (both 22.9(1)°; Table 4-1). In addition to the measured distortion angles of **30a-c**, values obtained from optimized geometries are shown in Table 4-1 for comparison. We applied the B3PW91/6-311+G(d,p) level of theory as this DFT method not only provides realistic geometries for [1]FCPs, but also allows quantification of their intrinsic strain.[15] All deviations between the calculated and

measured distortion angles for **30a-c** are below 1°, with the exception of τ of **30a** (Δ = 2.9°) and for β and τ of 30b (Δ = 2.4, 3.6°). Of course, one should take into consideration that forces in the crystal lattice could contribute to deviations. Overall, the predicted structures match the measured structures very well. Table 4-1 also shows that the experimental distortion angles of the known HCCH-bridged [2]FCP $\mathbf{M^H}$ match with the calculated values. Hence, it is reasonable to assume that the predicted structure of the unknown parent HBNH-bridged [2]FCP **30d** is also very realistic. Compared to its carbon analogue $\mathbf{M^H}$, species **30d** exhibits less Cp ring tilt as is evident by a smaller α and a larger δ angle (Table 4-1). This can be traced back to the difference in bond lengths of the bridging elements. While the calculated C–C bond length is 1.340 Å ($\mathbf{M^H}$), the B–N bond length is 1.405 Å (**30d**); no other bond length shows a comparably large difference.[j] That means, the weaker B–N bond tilts the Cp rings less than a C–C bond; hence, the HCCH-bridged [2]FCP $\mathbf{M^H}$ should be more strained than **30d**.

[j] Calculated values in Å: Fe–$Cp^{centroid}$ = 1.635/1.639 (**30d**), 1.637 ($\mathbf{M^H}$); E–Cp^{ipso} = 1.435/1.588 (Ø = 1.512; **30d**), 1.496 ($\mathbf{M^H}$).

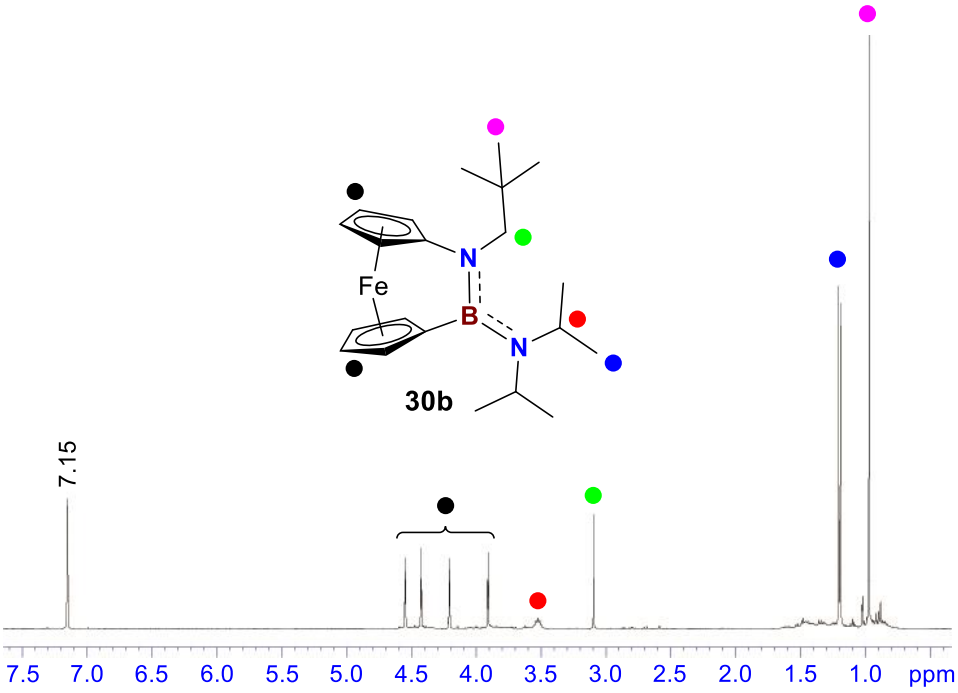

Figure 4-1. ^{1}H NMR (500 MHz; C_6D_6) spectrum of **30b**, taken from an aliquot of the reaction mixture 1 h after addition of *i*Pr_2NBCl_2.

Differential scanning calorimetry (DSC) analyses of all three [2]FCPs were performed; however, in every case an exothermic peak indicative of ROP was not observed even after heating samples to 300 °C (see Supporting Information). Are these FCPs indeed strained as indicated by their structures? We addressed this question using DFT calculations and applied the two different homodesmotic reactions[16] as shown in Scheme 4-2. For both reactions, standard reaction enthalpies were calculated for a set of five [2]FCPs (**30a-d**, $\mathbf{M^H}$; Table 4-2).

Recently, we have demonstrated that the homodesmotic reaction between $FeCp_2$ and [1]FCPs provides reaction enthalpies that compare well to measured enthalpies of polymerization (ΔH_{ROP}).[15] For example, for the most widely applied [1] FCP, the Me_2Si-bridged species $\mathbf{G^{Me}}$ (Chart 4-1), a ΔH_{ROP} of −72(±2) kJ mol^{-1} was determined by DSC analysis while an enthalpy of −75 kJ mol^{-1} was calculated.[15]

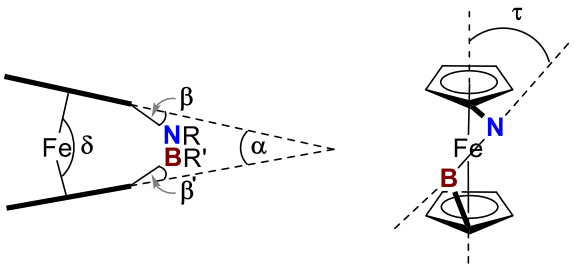

Figure 4-2. Common angles to characterize distortions in azabora[2]ferrocenophanes (α = angle between the least-squares planes of Cp rings; β = 180° − ($Cp^{centroid}$–C^{ipso}–E); δ = $Cp^{centroid}$–Fe–$Cp^{centroid}$; τ is the angle between the least-squares plane $Cp^{centroid}$–Fe–$Cp^{centroid}$ and the N−B bridging bond vector).

Table 4-1. Calculated [a] and Experimental Distortion Angles [deg] in [2]FCPs (**30a-d** and $\mathbf{M^H}$)

	α	β [b]	β' [b]	δ	τ
30a	22.9(1)	6.9(2)	15.0(2)	163.23(2)	0.6(1)
	[23.5]	[6.7]	[15.0]	[163.8]	[3.5]
30b [c]	22.9(1)	11.4(2) [d]	15.8(1)	163.36(2)	11.2(2) [d]
	[22.6]	[9.0] [d]	[16.3]	[164.3]	[7.6] [d]
30c	24.2(1)	8.1(1)	14.4(2)	162.78(2)	0.7(1)
	[24.0]	[8.3]	[14.2]	[163.6]	[1.1]
30d [e]	[21.3]	[13.0]	[18.2]	[165.2]	[0.0]
$\mathbf{M^H}$ [f]	23.7	15.7	15.9	162.5	4.7
	[23.0]	[15.4]	[15.4]	[164.0]	[0.0]

[a] Calculated B3PW91/6-311+G(d,p) values in square brackets. [b] For BN-bridged compounds: β at N and β' at B (see Figure 4-2); $\beta = \beta'$ for C_{2v} symmetric HCCH-bridged [2]FCP $\mathbf{M^H}$. [c] Measured values are for the main occupied sides in the disordered structure. [d] The disorder of nitrogen in the crystal lattice might have contributed to the larger than expected differences between calculated and measured angles. [e] The unknown HBNH-bridged [2]FCP. [f] Values obtained from the deposited CIF file CCDC 1249478 with *Mercury 3.9* and *Platon*. This structure had been published in reference 7a where α = 22.6° was given. The same compound was published in reference 7b with α = 23°.

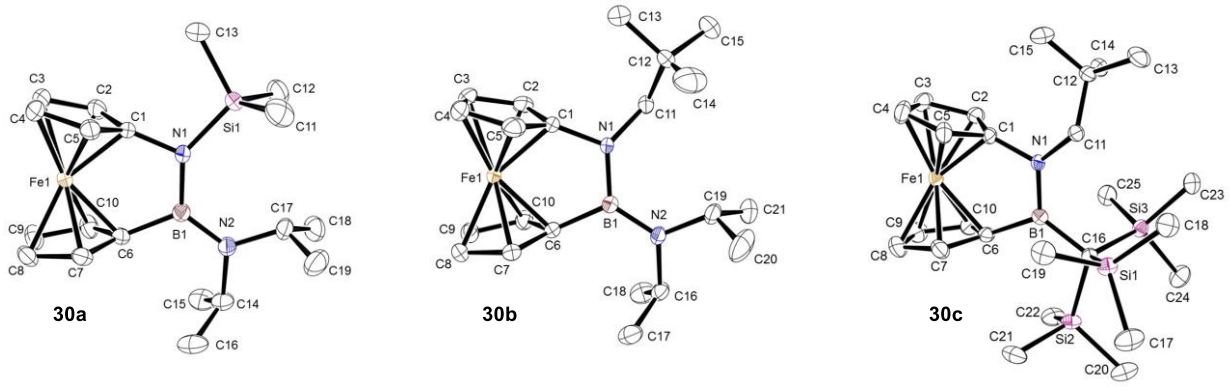

Figure 4-3. Molecular structures of **30a-c** with thermal ellipsoids at a probability level of 50%. Hydrogen atoms are omitted for clarity. For bond lengths [Å] and angles [deg], see Tables S2–S4 (Supporting Information); for crystal and structural refinement data, see Table S1 (Supporting Information).

As apparent from the thermodynamic data in Table 4-2, the carbon-bridged [2]FCP MH is the most strained compound among the investigated species, and very similar reaction enthalpies, −85.8 and −84.9 kJ mol^{-1}, were obtained for both reactions. The parent azabora[2]ferrocenophane **30d** is around 13 kJ mol^{-1} less strained than its carbon counterpart $\mathbf{M^H}$; again, both homodesmotic reactions gave very similar values (−72.6 and −71.7 kJ mol^{-1}). In contrast, this is different for the synthesized [2]FCPs **30a-c**. While reaction (2) is expectedly exothermic, reaction (1) is rather endothermic (Scheme 4-2). The endothermic nature of reaction (1) can be rationalized by reviewing the structures of the formed products of type **31** (Scheme 4-2). While the HBNH-bridged compound as well as its carbon analogue do not show any structural signs of steric interactions, species **31** equipped with bulky groups like Me_3Si, *t*$BuCH_2$, *i*Pr_2N, and $(Me_3Si)_3C$ are severely distorted (see Supporting Information). The most extreme case is that of **31c** resulting from **30c** ($\Delta H°$ = +91.9 kJ mol^{-1}; Table 4-2). As illustrated with the optimized geometry of **31c** in Figure 4-4, steric congestion does not allow for the formation of a BN double bond, as the donor orbital at nitrogen is forced to be almost perpendicular to the acceptor orbital at boron. Furthermore, in

Scheme 4-2. Homodesmotic Reactions to Evaluate Strain in **30a-d** and $\mathbf{M^H}$ (Table 4-2)

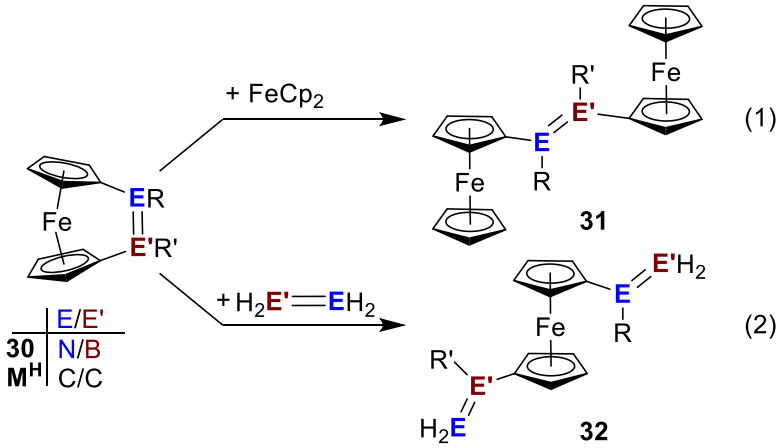

Table 4-2. Calculated $\Delta H°$ Values for Reaction Equations 1 and 2 (Scheme 4-2) [a]

	30a [b]	**30b** [b]	**30c** [b]	**30d** [c]	$\mathbf{M^H}$ [d]
Eqn 1	+8.9	+34.4	+91.9	–72.6	–85.8
Eqn 2	–70.6	–68.7	–102.8	–71.7	–84.9

[a] B3PW91/6-311+G(d,p) values in kJ mol^{-1}; [b] See Scheme 1; [c] The unknown HBNH-bridged [2]FCP; [d] The known HCCH-bridged [2]FCP (see Chart 4-1).

both ferrocenyl moieties, the Cp rings deviate from co-planarity with the intercepting angles between Cp planes being 10.5 and 10.9°, respectively. However, in the (hetero)olefin metathesis reaction (2) (Scheme 4-2), possible steric interactions in product **32** are minimized as the bulky groups at nitrogen and boron get spatially separated in this approach. Consequently, the predicted enthalpies should be similar to that of the parent species **30d** (Table 4-2). While this is the case for **30a** and **30b** with −70.6 and −68.7 kJ mol^{-1}, respectively, **30c** surprisingly resulted in a significantly larger release of heat ($\Delta H°$ = −102.8 kJ mol^{-1}). The latter result cannot be explained by the small differences in the Cp ring tilt of **30c** compared to that of **30a** and **30b**, or any other distortion angle as discussed before (Table 4-1). The unusually large heat release is probably due

to additional strain in **30c** caused by additional steric interactions. For example, the tetrahedral geometry around the central carbon atom of the $(Me_3Si)_3C$ group is distorted. While the calculated Si–C–Si angles in **30c** are 105.6, 106.2, and 118.2°, those of the product **32c** are 109.2, 109.6, and 110.1° with almost ideal tetrahedral angles.

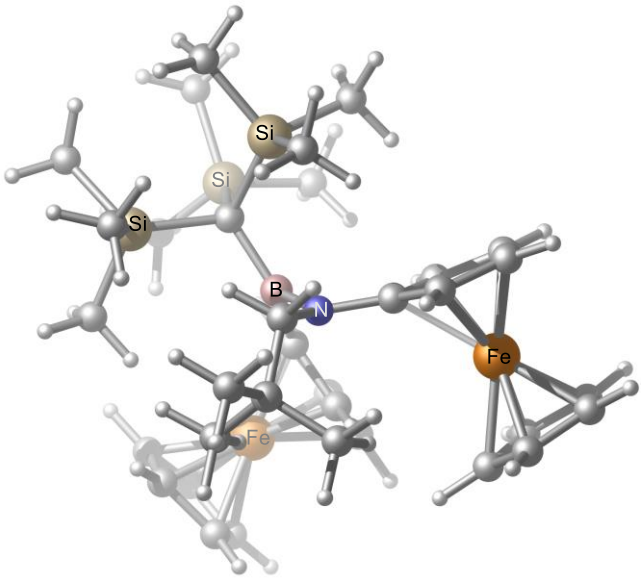

Figure 4-4. B3PW91/6-311+G(d,p) geometry of product **31c** (see Scheme 4-2 and Table 4-2).

4.5 Conclusions

In conclusion, the new [2]FCPs **30a-c** are similarly strained as the well-known sila[1]ferrocenophane $\mathbf{G^{Me}}$, which is widely used to prepare metallopolymers.[3] However, these new [2]FCPs are sterically overprotected and, therefore, unsuitable for ROP. Hence, we are planning to apply our methodology to prepare azabora[2]ferrocenophanes with smaller groups attached to bridging elements.

4.6 Experimental Section

General Methods. If not mentioned otherwise, all syntheses were carried out using standard Schlenk and glovebox techniques. Solvents were dried using an MBraun Solvent Purification System and stored under nitrogen over 3 Å molecular sieves. C_6D_6 for NMR spectroscopy was degassed by freeze-pump-thaw cycles and stored under nitrogen over 3 Å molecular sieves. Unless otherwise noted, temperatures refer to that of the bath (e.g., dry ice/acetone bath for −78 °C).

Characterization Methods. ^{1}H, ^{11}B, and ^{13}C NMR spectra were recorded on 500 MHz Bruker Avance, 500 MHz Bruker Avance III HD, and 600 MHz Bruker Avance III HD NMR spectrometers at 25 °C in C_6D_6. ^{1}H chemical shifts are referenced to the residual protons of the deuterated solvent C_6D_6 at δ = 7.15 ppm; ^{13}C chemical shifts are referenced to the C_6D_6 signal at δ = 128.00 ppm. ^{11}B NMR spectra were calibrated using $F_3B{\cdot}OEt_2$ (0.0 ppm) as external reference. The following abbreviations are used to described NMR signals: s (singlet), d (doublet), pst (pseudo triplet), sept (septet), br (broad). Some Cp protons appear as slightly broadened singlets, while others appear as pseudo triplets. Coupling constants obtained from ^{1}H NMR spectra are associated with an error and reported to the first decimal point (the digital resolution in ^{1}H NMR spectra is 0.2 Hz). Assignments for newly synthesized compounds were supported by additional NMR experiments (COSY, HMQC, HMBC, and DEPT). High resolution mass data were obtained with a JEOL AccuTOF GCv 4G instrument using field desorption ionization (FDI). For the isotopic pattern, only the mass peak of the isotopoloque or isotope with the highest natural abundance is listed. Elemental analyses were performed on a Perkin Elmer 2400 CHN Elemental Analyzer. Differential Scanning Calorimetry (DSC) analyses were performed on a TA Instrument Q20 at a heating rate of 10 °C min^{-1}. Samples, sealed in hermetic aluminum pans, were tared using a balance with a repeatability of 0.1 mg (AB204-S Mettle Toledo). For each run, around 3 mg of

a sample was measured. The known melting enthalpy of a sample of indium was used to check on the calibration of the DSC instrument. DSC data was analyzed with TA Instruments Universal Analysis 2000 software. After each DSC run, the content of the pan was dissolved in organic solvent under inert atmosphere and a ^{1}H NMR spectrum of the solution showed mainly unaltered starting material, which revealed that thermal ROP did not occur.

Reagents. Dichloro(diisopropylamino)borane,[17] dichloro[tris(trimethylsilyl)methyl]borane,[18] 1-bromo-1′-(trimethylsilylamino)ferrocene (**29a**),[12a] and 1-bromo-1′-(neopentylamino)ferrocene (**29b**)[12b] were synthesized as reported. For **29a** and **29b** please note that small amounts the impurity $CpFeC_5H_4NHR$ are present (see reference 12 for details). However, molar amounts were calculated as if these starting materials were absolutely pure. The reagent *n*BuLi (2.5 M in hexanes) was purchased from Sigma Aldrich.

Synthesis of azabora[2]ferrocenophane 30a. *n*BuLi (2.5 M in hexanes, 0.41 mL, 1.0 mmol) was added dropwise to a −78 °C cooled solution of 1-bromo-1′-(trimethylsilylamino)ferrocene **29a** (0.171 g, 0.486 mmol) in a solvent mixture of hexanes and thf (10 mL; hexanes/thf; 9/1), resulting in a colour change from pale yellow to bright orange. After the reaction mixture was stirred for 40 min at −78 °C, the dry ice bath was replaced by an ice bath, followed by stirring of the reaction mixture at 0 °C for 1 h. A solution of iPr$_2$NBCl$_2$ (0.090 g, 0.49 mmol) in hexanes (6.0 mL) was added dropwise over 2 min. The reaction mixture was warmed to ambient temperature and stirred for 1 h. After all volatiles were removed under high vacuum, the product was dissolved in hexanes (15 mL) and LiCl was removed by Schlenk filtration and the white residue was washed with more hexanes (2 × 2.0 mL). From this red filtrate, residual solvents were removed under high vacuum, resulting in a red sticky solid. Product **30a** was obtained by vacuum sublimation (60 °C; p ≈ 10^{-2} mbar) in form of red crystals (0.103 g, 55%). ^{1}H NMR (C_6D_6, 500.1 MHz): δ 0.26 (s, 9H,

$Si(CH_3)_3$), 1.20 (d, J_{HH} = 6.8 Hz, 12H, $N[CH(C\underline{H}_3)_2]_2$), 3.72 (sept, J_{HH} = 6.7 Hz, 2H, $N[C\underline{H}(CH_3)_2]_2$), 3.91 (pst, 2H, α-H of Cp^N), 4.21 (pst, 2H, α-H of Cp^B), 4.27 (pst, 2H, β-H of Cp^N), 4.53 (pst, 2H, β-H of Cp^B). $^{13}C\{^1H\}$ NMR (C_6D_6, 125.8 MHz): δ 2.4 ($Si(CH_3)_3$), 25.0 ($N[CH(\underline{C}H_3)_2]_2$), 47.8 ($N[\underline{C}H(CH_3)_2]_2$), 67.6 ($\alpha$-C of Cp^N), 70.6 (α-C of Cp^B), 72.8 (β-C of Cp^N), 76.3 (β-C of Cp^B), 86.4 (*ipso*-C of Cp^B), 98.4 (*ipso*-C of Cp^N). ^{11}B NMR (C_6D_6, 160.5 MHz): δ 34.2 ppm. HRMS (FDI): *m*/*z* calcd for $C_{19}H_{31}BFeN_2Si$, 382.1699; found 382.1707. Elemental anal. calcd (%) for $C_{19}H_{31}BFeN_2Si$ (382.211): C, 59.71; H, 8.18; N, 7.33. Found: C, 59.61; H, 8.33; N, 7.23.

Synthesis of azabora[2]ferrocenophane 30b. *n*BuLi (2.4 M in hexanes, 0.72 mL, 1.7 mmol) was added dropwise to a −78 °C cooled solution of 1-bromo-1′-(neopentylamino)ferrocene (**29b**) (0.287 g, 0.820 mmol) in a solvent mixture of hexanes and thf (15 mL; hexanes/thf; 9/1), resulting in a colour change from pale yellow to bright orange. After the reaction mixture was stirred for 40 min at −78 °C, the dry ice bath was replaced by an ice bath, followed by stirring of the reaction mixture at 0 °C for 1 h. A solution of iPr_2NBCl_2 (0.165 g, 0.907 mmol) in hexanes (7.5 mL) was added dropwise over 2 min. The reaction mixture was warmed to ambient temperature and stirred for 1 h. After all volatiles were removed under high vacuum, the product was dissolved in hexanes (20 mL) and LiCl was removed by a Schlenk filtration and the white residue was washed with more hexanes (2 × 2.0 mL). From this red filtrate, residual solvents were removed under high vacuum, resulting in a red sticky solid. Product **30b** was obtained by crystallization in hexanes at −80 °C in form of red crystals (0.217 g, 70%). ^1H NMR (C_6D_6, 500.3 MHz): δ 0.97 (s, 9H, $C(CH_3)_3$), 1.20 (d, J_{HH} = 6.6 Hz, 12H, $N[CH(C\underline{H}_3)_2]_2$), 3.10 [s, 2H, NCH_2], 3.53 (sept, J_{HH} = 6.7 Hz, 2H, $N[C\underline{H}(CH_3)_2]_2$), 3.90 (pst, 2H, α-H of Cp^N), 4.20 (pst, 2H, α-H of Cp^B), 4.42 (pst, 2H, β-H of Cp^N), 4.54 (pst, 2H, β-H of Cp^B). $^{13}C\{^1H\}$ NMR (C_6D_6, 125.8 MHz): δ 24.4 ($C(\underline{C}H_3)_3$), 29.4

(N[CH(CH$_3$)$_2$]$_2$), 32.9 (CH$_2$C(CH$_3$)$_3$), 46.2 (N[CH(CH$_3$)$_2$]$_2$), 62.5 (NCH$_2$), 67.4 (α-C of Cp^N), 70.4 (α-C of Cp^B), 71.4 (β-C of Cp^N), 76.1 (β-C of Cp^B), 83.0 (*ipso*-C of Cp^B), 104.0 (*ipso*-C of Cp^N). ^{11}B NMR (C$_6$D$_6$, 160.5 MHz): δ 33.3 ppm. HRMS (FDI): *m/z* calcd for C$_{21}$H$_{33}$BFeN$_2$, 380.2086; found 380.2072. Elemental anal. calcd (%) for C$_{21}$H$_{33}$BFeN$_2$ (380.164): C, 66.35; H, 8.75; N, 7.37; found: C, 66.52; H, 8.96; N, 6.94.

Synthesis of azabora[2]ferrocenophane 30c. *n*BuLi (2.4 M in hexanes, 0.41 mL, 0.98 mmol) was added dropwise to a −78 °C cooled solution of 1-bromo-1′-(neopentylamino)ferrocene (**29b**) (0.161 g, 0.460 mmol) in a solvent mixture of hexanes and thf (10 mL; hexanes/thf; 9/1), resulting in a colour change from pale yellow to bright orange. After the reaction mixture was stirred for 40 min at −78 °C, the dry ice bath was replaced by an ice bath, followed by stirring of the reaction mixture at 0 °C for 1 h. A solution of [(Me$_3$Si)$_3$C]BCl$_2$ (0.156 g, 0.498 mmol) in hexanes (5.0 mL) was added dropwise over 2 min. The reaction mixture was warmed to ambient temperature and stirred for 1 h. After all volatiles were removed under high vacuum, the product was dissolved in hexanes (15 mL), LiCl was removed by a Schlenk filtration, and the white residue was washed with more hexanes (2 × 2.0 mL). From this red filtrate, residual solvents were removed under high vacuum, resulting in a red oil. Product **30c** was obtained by crystallization in hexanes at −80 °C in form of red crystals (0.160 g, 68%). ^{1}H NMR (C$_6$D$_6$, 600.2 MHz): δ 0.39 (s, 27H, C[Si(CH$_3$)$_3$]$_3$), 0.94 (s, 9H, C(CH$_3$)$_3$), 3.41 (s, 2H, NCH$_2$), 3.81 (s, br, 2H, α-H of Cp^N), 4.06 (s, br, 2H, α-H of Cp^B), 4.34 (s, br, 2H, β-H of Cp^N), 4.39 (s, br, 2H, β-H of Cp^B). ^{13}C{^{1}H} NMR (C$_6$D$_6$, 150.9 MHz): δ 7.9 (C[Si(CH$_3$)$_3$]$_3$), 14.1 (C[Si(CH$_3$)$_3$]$_3$), 29.7 (C(CH$_3$)$_3$), 32.8 (C(CH$_3$)$_3$), 63.7 (NCH$_2$), 67.4 (α-C of Cp^N), 69.9 (α-C of Cp^B), 71.4 (β-C of Cp^N), 75.4 (β-C of Cp^B), 82.9 (*ipso*-C of Cp^B), 103.8 (*ipso*-C of Cp^N). ^{11}B NMR (C$_6$D$_6$, 192.6 MHz): δ 49.0 ppm. HRMS (FDI): *m/z* calcd for

$C_{25}H_{46}BFeNSi_3$, 511.2381; found 511.2401. Elemental anal. calcd (%) for $C_{25}H_{46}BFeNSi_3$ (511.560): C, 58.70; H, 9.06; N, 2.74; found: C, 58.62; H, 9.36; N, 2.73.

Attempted Thermal ROP of 30b. Compound **30b** (0.023 g, 0.061 mmol) was taken in a vacuum-sealed NMR tube and heated at 200 °C and 250 °C for 1 h each and then at 300 °C for 4 h. ^{1}H NMR spectroscopy (see Figure S14) of the resulting solid showed mainly the presence of the unaltered starting material **30b**. New signals at δ 0.95, 2.77, and 4.23 ppm were present, possibly indicating the generation of new species caused by heat. The experiment was then repeated as following. Compound **30b** (0.018 g, 0.047 mmol) was taken in a vacuum-sealed NMR tube and heated at 300 °C for an extended period of 22 h. A ^{1}H NMR spectrum of the reaction displayed similar signals to those previously observed (see Figure S15). The new signals did not show any increase in their relative intensities. This may indicate that the new unknown compound(s) is(are) probably forming due to the residual moisture left in the NMR tube and not due to any thermal reactivity.

Crystal Structure Determination of 30a-c. Single crystals were coated with Paratone-N oil, mounted using a micromount (MiTeGen—Microtechnologies for Structural Genomics), and frozen in the cold stream of an Oxford Cryojet attached to the diffractometer. Crystal data were collected on a Bruker APEX II diffractometer at −100 °C using monochromated Mo Kα radiation (λ = 0.71073 Å). An initial orientation matrix and cell was determined by ω scans, and the X-ray data were measured using ϕ and ω scans.[19] Frames were integrated with the Bruker SAINT software package[20] and data reduction was performed with the APEX2 software package.[19] A multi-scan absorption correction (SADABS) was applied.[20] The structures were solved by the Intrinsic Phasing method implemented with SHELXT and refined using the Bruker SHELXTL software package.[21] Non-hydrogen atoms were refined with independent anisotropic displacement parameters. Hydrogen atoms were placed at geometrically idealized positions (riding model) and

their displacement parameters were fixed to be 20 or 50% larger than those of the attached non-hydrogen atoms. Crystallographic data are summarized in Table S1, while bond lengths and bond angles are shown in Table S2–S4. Crystallographic data were submitted to the Cambridge Crystallographic Data Centre (**30a-c**: CCDC 1825153–1825155). The ellipsoid plots were prepared using ORTEP-3 for Windows.[22] The common set of distortion angles was calculated using the program PLATON.[23] The esds of all distortion angles that involve centroids of Cp rings (β, δ, τ) might be somewhat smaller than they should be, as esds on centroids were not included in the calculation.

DFT Calculations. All calculations were done employing the software package GAUSSIAN 09.[24] Geometries were optimized at the B3PW91/6-311+G(d,p) level.[25] The B3PW91 functional had been chosen based on the benchmark investigation of Grimme et al.,[26] as well as our recent application to [1]FCPs.[6g,15,27] Frequency calculations were used to confirm minima. An ultrafine grid (int = ultrafine) and tight requirements for geometry optimizations (opt = tight) were used for all calculations. Structural parameters from the calculated coordinates were extracted with the help of Mercury (version 3.9)[28] and CYLview (version 1b).[29]

For products of type **32** (see eq 2; Scheme 4-2) different isomers of very similar enthalpies were optimized and only the one resulting in the largest heat release were taken into consideration. The difference between isomers is due to different conformations of the amino and/or boryl groups with respect to the ferrocene moiety. However, differences for the different isomers in each series were very small (in kJ mol^{-1}; **32a**: −69.3 to −70.6; **32b**: −67.6 to −68.7; **32c**: −102.0 to −102.8; **32d**: −71.4 to −71.7; **32e** (CC case): −84.7 to −84.9). Please note that different isomers with respect to rotation about the Fe–$Cp^{centroid}$ bonds were not considered. For all isomers of type **32** the relative

positions of amino to boryl groups were the same. See the attached file for calculated Cartesian coordinates of the considered isomers.

4.7 Associated Content

Supporting Information

The Supporting Information is available on rsc.li/chemcomm at DOI: 10.1039/c8cc02965b.

Acknowledgements

We thank the Natural Sciences and Engineering Research Council of Canada (Discovery Grant, JM) for support and the Canada Foundation for Innovation and the Government of Saskatchewan for funding of the X-ray and NMR facilities at the Saskatchewan Structural Sciences Centre. We thank Dr V. MacKenzie (DSC) and K. Thoms (MS and CHN) for help and support. For DFT calculations, we are grateful to WestGrid (www.westgrid.ca) and Compute Canada (www.computecanada.ca) for support.

4.8 References

(1) (a) Brandt, P. F.; Rauchfuss, T. B. *J. Am. Chem. Soc.* **1992**, *114*, 1926-1927. (b) Foucher, D. A.; Tang, B.-Z.; Manners, I. *J. Am. Chem. Soc.* **1992**, *114*, 6246-6248.

(2) (a) Manners, I. *Synthetic Metal-Containing Polymers*; Wiley-VCH: Weinheim, 2004. (b) Bellas, V.; Rehahn, M. *Angew. Chem., Int. Ed.* **2007**, *46*, 5082-5104.

(3) Hailes, R. L. N.; Oliver, A. M.; Gwyther, J.; Whittell, G. R.; Manners, I. *Chem. Soc. Rev.* **2016**, *45*, 5358-5407.

(4) (a) Kealy, T. J.; Pauson, P. L. *Nature* **1951**, *168*, 1039-1040. (b) Miller, S. A.; Tebboth, J. A.; Tremaine, J. F. *J. Chem. Soc.* **1952**, 632-635.

(5) Rinehart, K. L.; Curby, R. J. *J. Am. Chem. Soc.* **1957**, *79*, 3290-3291.

(6) (a) Braunschweig, H.; Breitling, F. M.; Gullo, E.; Kraft, M. *J. Organomet. Chem.* **2003**, *680*, 31-42. (b) Herbert, D. E.; Mayer, U. F. J.; Manners, I. *Angew. Chem., Int. Ed.* **2007**, *46*, 5060-5081. (c) Tamm, M. *Chem. Commun.* **2008**, 3089-3100. (d) Braunschweig, H.; Kupfer, T. *Eur. J. Inorg. Chem.* **2012**, 1319-1332. (e) Musgrave, R. A.; Russell, A. D.; Manners, I. *Organometallics* **2013**, *32*, 5654-5667. (f) Russell, A. D.; Musgrave, R. A.; Stoll, L. K.; Choi, P.; Qiu, H.; Manners, I. *J. Organomet. Chem.* **2015**, *784*, 24-30. (g) Bhattacharjee, H.; Müller, J. *Coord. Chem. Rev.* **2016**, *314*, 114-133.

(7) (a) Aggarwal, V. K.; Jones, D.; Turner, M. L.; Adams, H. *J. Organomet. Chem.* **1996**, *524*, 263-266. (b) Buretea, M. A.; Tilley, T. D. *Organometallics* **1997**, *16*, 1507-1510. (c) Masson, G.; Lough, A. J.; Manners, I. *Macromolecules* **2008**, *41*, 539-547.

(8) Braunschweig, H.; Krummenacher, I.; Lichtenberg, C.; Mattock, J. D.; Schäfer, M.; Schmidt, U.; Schneider, C.; Steffenhagen, T.; Ullrich, S.; Vargas, A. *Angew. Chem., Int. Ed.* **2017**, *56*, 889-892.

(9) (a) Staubitz, A.; Robertson, A. P. M.; Sloan, M. E.; Manners, I. *Chem. Rev.* **2010**, *110*, 4023-4078. (b) Baggett, A. W.; Guo, F.; Li, B.; Liu, S.-Y.; Jäkle, F. *Angew. Chem., Int. Ed.* **2015**, *54*, 11191-11195. (c) Lorenz, T.; Lik, A.; Plamper, F. A.; Helten, H. *Angew. Chem., Int. Ed.* **2016**, *55*, 7236-7241. (d) Ayhan, O.; Eckert, T.; Plamper, F. A.; Helten, H. *Angew. Chem., Int. Ed.* **2016**, *55*, 13321-13325. (e) Helten, H. *Chem.-Eur. J.* **2016**, *22*, 12972-12982. (f) Lorenz, T.; Crumbach, M.; Eckert, T.; Lik, A.; Helten, H. *Angew. Chem., Int. Ed.* **2017**, *56*, 2780-2784.

(10) Giustra, Z. X.; Liu, S.-Y. *J. Am. Chem. Soc.* **2018**, *140*, 1184-1194.

(11) For related NBN- and PBP-bridged FCPs see: (a) Wrackmeyer, B.; Klimkina, E. V.; Millus, W.; Tok, O. L.; Herberhold, M. *Inorg. Chim. Acta* **2005**, *358*, 1420-1428. (b) Lik, A.; Kargin, D.; Isenberg, S.; Kelemen, Z.; Pietschnig, R.; Helten, H. *Chem. Commun.* **2018**, *54*, 2471-2474.

(12) (a) Dey, S.; Quail, J. W.; Müller, J. *Organometallics* **2015**, *34*, 3039-3046. (b) Dey, S.; Sun, W.; Müller, J. *Inorg. Chem.* **2016**, *55*, 3630-3639.

(13) Nöth, H.; Wrackmeyer, B. Nuclear Magnetic Resonance Spectroscopy of Boron Compounds. In *NMR: Basic Principles and Progress*, Diehl, P.; Fluck, E.; Kosfeld, R., Eds.; Spinger: Berlin Heidelberg New York, 1978; Vol. 14.

(14) Paetzold, P. I. *Adv. Inorg. Chem.* **1987**, *31*, 123-170.

(15) Khozeimeh Sarbisheh, E.; Bhattacharjee, H.; Cao, M. P. T.; Zhu, J.; Müller, J. *Organometallics* **2017**, *36*, 614-621.

(16) Poli, R.; Cacelli, I. *Eur. J. Inorg. Chem.* **2005**, 2324-2331.

(17) Gerrard, W.; Hudson, H. R.; Mooney, E. F. *J. Chem. Soc.* **1960**, 5168-5172.

(18) (a) Aljuaid, S. S.; Eaborn, C.; Elkheli, M. N. A.; Hitchcock, P. B.; Lickiss, P. D.; Molla, M. E.; Smith, J. D.; Zora, J. A. *J. Chem. Soc., Dalton Trans.* **1989**, 447-452. (b) Tapper, A., Dissertation, 1988, RWTH Aachen.

(19) Bruker *APEX2*, 2014.3–0 ed.; Bruker AXS Inc., 2014.

(20) Bruker *SAINT and SADABS*; v8.34a ed.; Bruker AXS Inc., 2013.

(21) (a) Sheldrick, G. M. *SHELXL, Program for the Solution of Crystal Structures*; University of Göttingen: Germany. (b) Sheldrick, G. M. *Acta Crystallogr. Sect. A: Found. Crustallogr.* **2008**, *64*, 112-122.

(22) Farrugia, L. J. *J. Appl. Crystallogr.* **1997**, *30*, 565.

(23) Spek, A. L. *PLATON, A Multipurpose Crystallographic Tool*; University of Utrecht: The Netherlands, 2011.

(24) Frisch, M. J.; Trucks, G. W.; Schlegel, H. B.; Scuseria, G. E.; Robb, M. A.; Cheeseman, J. R.; Scalmani, G.; Barone, V.; Mennucci, B.; Petersson, G. A.; Nakatsuji, H.; Caricato, M.; Li, X.; Hratchian, H. P.; Izmaylov, A. F.; Bloino, J.; Zheng, G.; Sonnenberg, J. L.; Hada, M.; Ehara, M.; Toyota, K.; Fukuda, R.; Hasegawa, J.; Ishida, M.; Nakajima, T.; Honda, Y.; Kitao, O.; Nakai, H.; Vreven, T.; J. A. Montgomery, J.; Peralta, J. E.; Ogliaro, F.; Bearpark, M.; Heyd, J. J.; Brothers, E.; Kudin, K. N.; Staroverov, V. N.; Keith, T.; Kobayashi, R.; Normand, J.; Raghavachari, K.; Rendell, A.; Burant, J. C.; Iyengar, S. S.; Tomasi, J.; Cossi, M.; Rega, N.; Millam, J. M.; Klene, M.; Knox, J. E.; Cross, J. B.; Bakken, V.; Adamo, C.; Jaramillo, J.; Gomperts, R.; Stratmann, R. E.; Yazyev, O.; Austin, A. J.; Cammi, R.; Pomelli, C.; Ochterski, J. W.; Martin, R. L.; Morokuma, K.; Zakrzewski, V. G.; Voth, G. A.; Salvador, P.; Dannenberg, J. J.; Dapprich, S.; Daniels, A. D.; Farkas, O.; Foresman, J. B.; Ortiz, J. V.; Cioslowski, J.; Fox, D. J. *Gaussian 09*; Revision E.01; Gaussian, Inc.: Wallingford, CT, 2013.

(25) (a) Perdew, J. P. In *Electronic Structure of Solids '91*; Ziesche, P., Eschrig, H., Eds.; Akademie Verlag: Berlin, 1991; p 11-20. (b) Perdew, J. P.; Chevary, J. A.; Vosko, S. H.; Jackson, K. A.; Pederson, M. R.; Singh, D. J.; Fiolhais, C. *Phys. Rev. B: Condens. Matter Mater. Phys.*

1992, *46*, 6671-6687. (c) Perdew, J. P.; Chevary, J. A.; Vosko, S. H.; Jackson, K. A.; Pederson, M. R.; Singh, D. J.; Fiolhais, C. *Phys. Rev. B: Condens. Matter Mater. Phys.* **1993**, *48*, 4978-4978. (d) Becke, A. D. *J. Chem. Phys.* **1993**, *98*, 5648-5652. (e) Perdew, J. P.; Burke, K.; Wang, Y. *Phys. Rev. B: Condens. Matter Mater. Phys.* **1996**, *54*, 16533-16539. (f) Burke, K.; Perdew, J. P.; Wang, Y. In *Electronic Density Functional Theory: Recent Progress and New Directions*; Dobson, J. F., G. Vignale, Das, M. P., Eds.; Plenum, 1998; p 81-111.

(26) Goerigk, L.; Grimme, S. *Phys. Chem. Chem. Phys.* **2011**, *13*, 6670-6688.

(27) (a) Khozeimeh Sarbisheh, E.; Esteban Flores, J.; Zhu, J.; Müller, J. *Chem.-Eur. J.* **2016**, *22*, 16838-16849. (b) Khozeimeh Sarbisheh, E.; Esteban Flores, J.; Anderson, B. J.; Zhu, J.; Müller, J. *Organometallics* **2017**, *36*, 2182-2189.

(28) *The Cambridge Crystallographic Data Centre.* http://www.ccdc.cam.ac.uk/mercury, Mercury.

(29) Legault, C. Y. *CYLview.* http://www.cylview.org, 2009.

5 Sterically Protected Bora[1]ferrocenophanes

5.1 Author Contribution and Relation to the Research Objectives

This work was done in collaboration with Dr. Jianfeng Zhu and Prof. Jens Müller. The single crystal X-ray analysis of **27b^{MeEt}** was performed by Dr. Zhu. All DFT calculations were performed by Prof. Müller. I wrote the manuscript and performed all syntheses, characterizations, and reactivity studies of a new class of bora[1]ferrocenophanes (**27d-f^{MeMe}**) that are described here.

Our previous investigation on ROP of bora[1]ferrocenophanes (**27a-c^{R1R2}**; see Chapters 2 and 3) with electronically stabilized boron did not provide high molecular weight polymers. Moreover, elemental analysis proved the obtained polymers to be impure. The high thermal stability of previously mentioned bora[1]ferrocenophane monomers required high temperatures for ROP which leads to extrusion of iron and lower ΔH_{ROP} (obtained from DSC) than calculated values. One can speculate that amino groups at the bridging boron contributes significantly to the stability of the [1]FCPs. This speculation is also supported by the thermal stability of azabora[2]ferrocenophanes (**30a-c**) that are described in Chapter 4. Hence, getting access to bora[1]ferrocenophanes that are aryl or alkyl substituted at boron might be key for the preparation of new boron-containing polymers in a controlled way. Moreover, a sterically stabilized boron is expectedly more electrophilic in nature compared to an electronically stabilized boron (such as BNR′R″ bridging moieties in previously reported bora[1]ferrocenophanes). Therefore, such [1]FCPs will be more reactive towards anionic ROP. Indeed, sterically protected bora[1]ferrocenophane **27d^{MeMe}** showed reactivity towards thermal ROP only at 120 °C and resulted a chiral poly(ferrocenylborane).

The following is a copy of the manuscript that is currently under preparation (Bhattacharjee, H.; Zhu, J.; Müller, J. manuscript under preparation).

5.2 Abstract

The first examples of sterically stabilized bora[1]ferrocenophanes [**27d-f**$^{\mathbf{MeMe}}$; RBfc$^{i\mathrm{Pr}}$; fc$^{i\mathrm{Pr}}$ = [(*i*Pr)H_3C_5]$_2$Fe; R = Mes (**27d**$^{\mathbf{MeMe}}$), Tip (**27e**$^{\mathbf{MeMe}}$), Tsi (**27f**$^{\mathbf{MeMe}}$)] were synthesized via the common salt-metathesis approach. Compounds **27d**$^{\mathbf{MeMe}}$ (MesBfc$^{i\mathrm{Pr}}$) and **27e**$^{\mathbf{MeMe}}$ (TipBfc$^{i\mathrm{Pr}}$), in particular, show exceptional bathochromic shifts in UV-Vis spectroscopy and their optimized geometries at B3PW91/6-311+G(d,p) level of theory portray them as the new record holders with respect to tilting of Cp rings ($\alpha \approx 34°$). Moreover, thermal ring-opening polymerization of **27d**$^{\mathbf{MeMe}}$ provided a poly(ferrocenylborane).

5.3 Introduction

There has been significant improvement in the field of organometallic polymers in last few years.[1] Out of many methodologies to prepare metallopolymers, ring-opening polymerization (ROP) of strained ferrocenophanes (FCPs) has been of paramount interest in the scientific community.[2] Unambiguously, sila[1]ferrocenophanes (**G**$^{\mathbf{R}}$, Chart 5-1) are the most intensively studied strained compounds amongst the plethora of [*n*]FCPs reported since the discovery of the first FCP, a carbon-bridged [3]FCP, in 1957.[3] Various ROP methods have been developed ever since and applied particularly on silicon-bridged [1]FCPs to obtain poly(ferrocenylsilane)s (**PFS**s, Chart 5-1), a versatile class of metallopolymers.[2c] Amongst a multitude of applications of PFS materials the most notable discovery is their ability to form block copolymers that can produce micelles with rod-like core-shell structures in selective solvents that further undergo "crystallization driven self-assembly" (CDSA) to form materials with well-defined 1D or 2D structures.[2c,4]

Chart 5-1. Some Known Ferrocene Derivatives

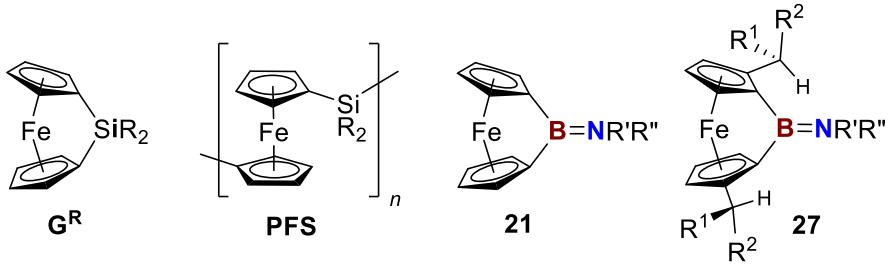

However, other FCPs with different bridging elements are far less explored, maybe due to a difficulty of their synthesis, a lack of polymerizability, or an insolubility of obtained polymers. One can envision poly(ferrocene)s with three-coordinate boron spacers as of special interest due to possible conjugative interactions of empty p orbitals of boron with the cyclopentadienyl π-system. ROP of boron-bridged [1]FCPs has the potential to produce such polymers. Thermal ROP of the first examples of boron-bridged [1]FCPs (**21**, Chart 5-1), however, led to materials with low solubility in organic solvents preventing their full characterization.[5] A new synthetic strategy was adopted by the research groups of Jäkle and Wagner where fc(BBr_2)$_2$ (fc = Fe(C_5H_4)$_2$) was applied for a polycondensation to obtain poly(ferrocenylborane)s with BBr spacers.[6] Post-polymerization modifications of these materials gave the corresponding BMes and B[$O(CH_2)_4Br$] polymers. However, this method only gave polymers of M_w up to ca. 7 kDa.[6a] The only other report on poly(ferrocenylborane)s came from our laboratory and was based on a new family of boron-bridged [1]FCPs (**27**, Chart 5-1) equipped with alkyl groups on Cp moieties.[7] These alkyl groups increased the solubility of the resulting polymers. However, monomers **27** are thermally robust up to ca. 240 °C and only produced polymers through thermal ROP about that threshold ($M_w \approx 10$ kDa).

Chart 5-2. Sterically Stabilized Bora[1]ferrocenophanes

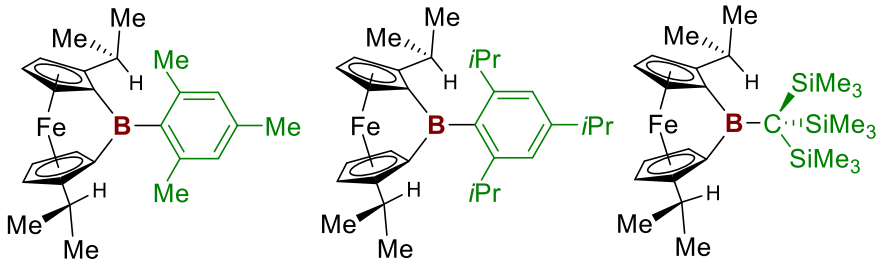

27d$^{\mathbf{MeMe}}$ **27e**$^{\mathbf{MeMe}}$ **27f**$^{\mathbf{MeMe}}$

One can speculate that amino groups at the bridging boron atom contribute significantly to the stability of these [1]FCPs. In order to test this hypothesis, we targeted bora[1]ferrocenophanes with aryl or alkyl substituents at boron. It was expected, these targeted FCPs compared to the known compounds **21** and **27** will exhibit an increased electrophilicity at boron that should increase their reactivity, in particular, with respect to ROPs. In this work, we report the first examples of boron-bridged [1]FCPs with aryl and alkyl substituted three-coordinated boron centers (Chart 5-2). It will be shown that they are the new record holders in terms of the tilt angle α (see Figure 5-1 for definitions of different geometric parameters of [1]FCPs).

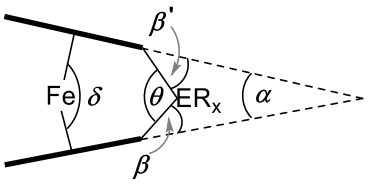

Figure 5-1. Common angles to characterize distortions in [1]FCPs [definition of angles: α = angle between the least-squares planes of Cp rings; β = 180° − (Cp^{centroid}–C^{ipso}–E); δ = Cp^{centroid}–Fe–Cp^{centroid}; θ = C^{ipso}–E–C^{ipso}].

5.4 Results and Discussion

In our recent report on the new family of bora[1]ferrocenophanes we thoroughly investigated the outcome and mechanism of the salt-metathesis reactions that were used for their preparation.[7-8] We discovered that the 1,1′-bis(boryl)ferrocene species **15**$^{\mathbf{R1R2}}$ (Scheme 5-1) is the main side product in the synthesis of the strained [1]FCPs **27b**$^{\mathbf{R1R2}}$. We were also able to improve reaction conditions in order to increase the conversion towards the targeted strained compounds **27b**$^{\mathbf{R1R2}}$.

Scheme 5-1. Recently Investigated Preparation of Boron-Bridged [1]FCPs

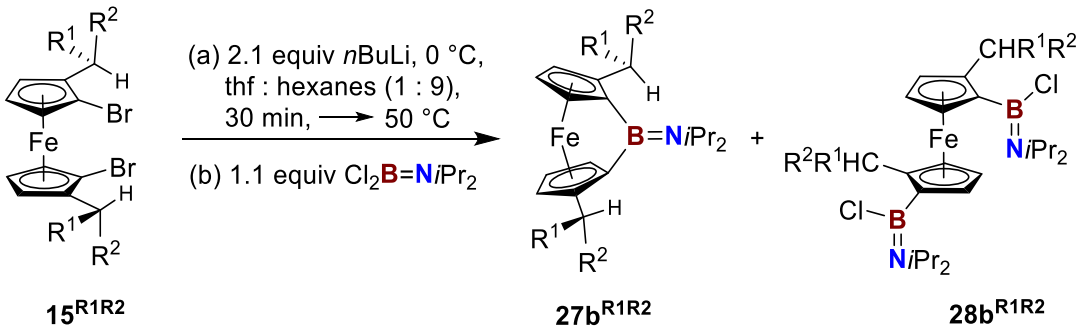

To synthesize the new targeted bora[1]ferrocenophanes **27d-f**$^{\mathbf{MeMe}}$ (Chart 5-2), the improved conditions of the recent study of **27b**$^{\mathbf{R1R2}}$ were applied (Scheme 5-1).[7-8] Therefore, the dibromoferrocene derivative **15**$^{\mathbf{MeMe}}$ was first lithiated (thf/hexanes, 1/9; 0 °C; Scheme 5-1), after 30 minutes the cold bath was replaced by a preheated oil bath of 50 °C, and after 10 minutes the respective $RBCl_2$ solution (0.1 M in hexanes) was added dropwise. However, the obtained results were different for each of the three boron dichlorides $RBCl_2$. ^{1}H NMR spectroscopy from aliquots of reaction mixtures did not reveal that that **27d**$^{\mathbf{MeMe}}$ was formed, whereas under the same conditions clearly the targeted FCP **27e**$^{\mathbf{MeMe}}$ was produced. On the other hand, the salt-metathesis reaction with $TsiBCl_2$ [Tsi = tris(trimethylsilyl)methyl] resulted in the formation of **27f**$^{\mathbf{MeMe}}$ along with its 1,1′-bis(boryl)ferrocene (**28f**$^{\mathbf{MeMe}}$) counterpart. When the same reaction was carried out at a lower temperature (0 °C), **28f**$^{\mathbf{MeMe}}$ was obtained almost exclusively. The latter result was

expected as it matched with our previously investigated salt-metathesis reactions mentioned above (Scheme 5-1). In contrast, when $TipBCl_2$ [Tip = 2,4,6-tri(isopropyl)phenyl] was applied, lowering temperature from 50 to 0 °C *increased* the conversion towards the targeted [1]FCP **27e**$^{\mathbf{MeMe}}$; surprisingly, no significant change was observed using the same temperature change in the attempted synthesis of the Mes-substituted species **27d**$^{\mathbf{MeMe}}$ [Mes = 2,4,6-trimethylphenyl].

Scheme 5-2. Synthesis of New Bora[1]ferrocenophanes

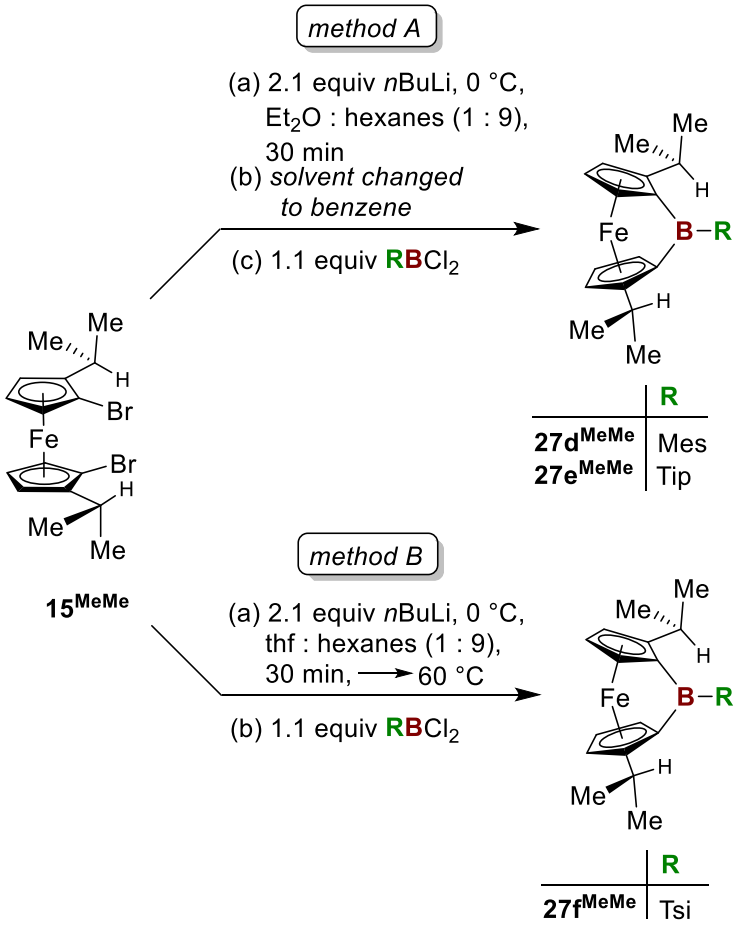

The latter results clearly indicate that the formation of compound **27e**$^{\mathbf{MeMe}}$ is more favoured under slower kinetics. Moreover, to our surprise, over the course of 1–2 days the amount of **27e**$^{\mathbf{MeMe}}$ in an NMR sample that was taken from an aliquot of a reaction mixture increased. This must have resulted from slow reaction between the leftover starting materials in the NMR solvent

C_6D_6. This triggered our motivation to pursue a different reaction condition in the preparation of **27e**$^{\mathbf{MeMe}}$. After the lithiation of **15**$^{\mathbf{MeMe}}$ in a solvent mixture of Et_2O/hexanes (1/9) was completed, the solvent was replaced by benzene resulting in an orange suspension (*method A*, Scheme 5-2). After the addition of a benzene solution of $TipBCl_2$ and stirring over a period of 24 h, the colour of the reaction mixture changed from orange to red brown to dark purple. As shown in Figure 5-2, the ^{1}H NMR spectrum of the reaction mixture revealed an almost quantitative conversion towards the targeted bora[1]ferrocenophane **27e**$^{\mathbf{MeMe}}$. Interestingly, the same method applied to $MesBCl_2$ gave a similarly clean reaction mixture with **27d**$^{\mathbf{MeMe}}$ as the main product. In this case, the dark purple colour developed much faster than in the case of the Tip-substituted [1]FCP **27e**$^{\mathbf{MeMe}}$ and the reaction was already completed after 1 h. Applying the same conditions (*method A*) for $TsiBCl_2$ did not result in a high conversion to the strained FCP **27f**$^{\mathbf{MeMe}}$. Instead, even after 48 h significant amounts of unreacted $TsiBCl_2$ were present. Given the fact that **27f**$^{\mathbf{MeMe}}$ could be synthesized more successfully using the reaction conditions developed for amino-substituted bora[1]ferrocenophanes **27b**$^{\mathbf{R1R2}}$ (Scheme 5-1), we further tweaked the conditions by increasing the reaction temperature (50 to 60 °C) and reducing the speed of addition of $TsiBCl_2$ (10 to 20 min; *method B*, in Scheme 5-2). A ^{1}H NMR spectrum measured from the reaction mixture showed a significant improvement in the conversion towards the targeted strained compound **27f**$^{\mathbf{MeMe}}$.

Compounds **27e**$^{\mathbf{MeMe}}$ and **27f**$^{\mathbf{MeMe}}$ sublime under vacuum at 110 °C as a dark purple sticky solid and a dark red oily solid, respectively (in yields of 69 and 28%). However, repeated sublimation attempts for **27d**$^{\mathbf{MeMe}}$ led only to minute amounts of sublimed product that were significantly contaminated with other unknown species. Under these conditions most of **27d**$^{\mathbf{MeMe}}$ polymerized to a dark purple material which will be discussed later in this section.

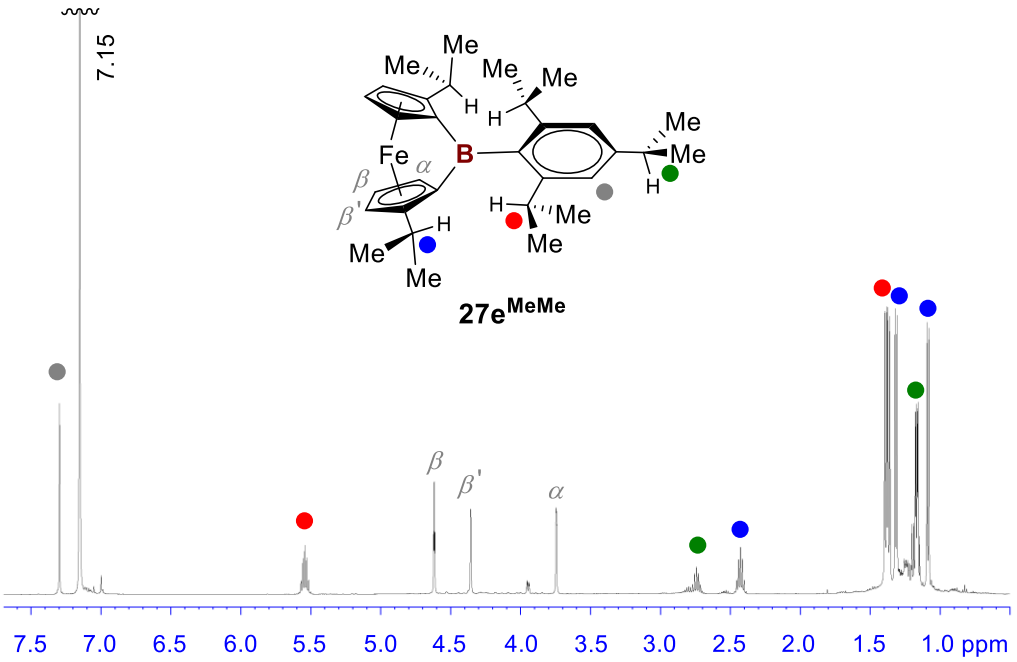

Figure 5-2. ^{1}H NMR spectrum of **27e^{MeMe}** in the reaction mixture (*method A*, Scheme 5-2).

As expected, all three new bora[1]ferrocenophanes are C_2 symmetric in solution. For instance, the ^{1}H NMR spectrum of the Tip-substituted species **27e^{MeMe}** (Figure 5-2) shows the Cp protons as three equally intense *pseudo*-triplets with a large difference of 0.74 ppm[9] in chemical shifts between α- and β-H signals, which matches with previously reported boron-bridged [1]FCPs (**27**, Chart 5-1).[7-8] The presence of three inequivalent *i*Pr groups is revealed by a set of three septets and six doublets, which are marked with red, green, and blue dots in Figure 5-2. While all doublets and two of the three septets appear within the expected chemical-shift range, the third septet stands out with an unusually high chemical shift of δ = 5.53 ppm. Clearly, this signal is caused by the methine protons of the *ortho*-*i*Pr groups and indicates that these CH protons are situated in the low-field area caused by the ring current of the Cp moieties. A similar, but less pronounced effect is notable in compound **27d^{MeMe}** where the *ortho*-Me groups of the Mes substituent is significantly more deshielded (δ = 3.04 ppm) compared to the *para*-Me protons (δ = 2.05 ppm).

Table 5-1. Calculated [a] and Measured [b] Distortion Angles (deg)

	α	δ	β / β'	θ
$(Me_3Si)_2NBfc$ [c]	32.0	156.6	33.8 / 34.3	100.9
	[32.4(2)]	[155.2(2)]	[33.7(2) / 34.0(2)]	[100.1]
27b^{MeEt}	30.7	157.6	35.7 / 36.1	103.2
	[31.4(2)]	[156.11(3)]	[35.7(2) / 35.2(2)]	[103.0(2)]
27d^{MeMe} [d]	32.8	155.7	33.4 / 33.4	100.4
27e^{MeMe} [d]	33.3	155.4	32.6 / 32.6	99.2
27f^{MeMe}	32.0	156.7	33.4 / 34.7	99.3

[a] Calculated at the B3PW91/6-311+G(d,p) level of theory. [b] Measured values are given in brackets. [c] Measured and calculated data were taken from references 5a and 10. [d] The optimized geometry (C_1 point-group symmetry) deviates only slightly from the expected C_2 symmetry.

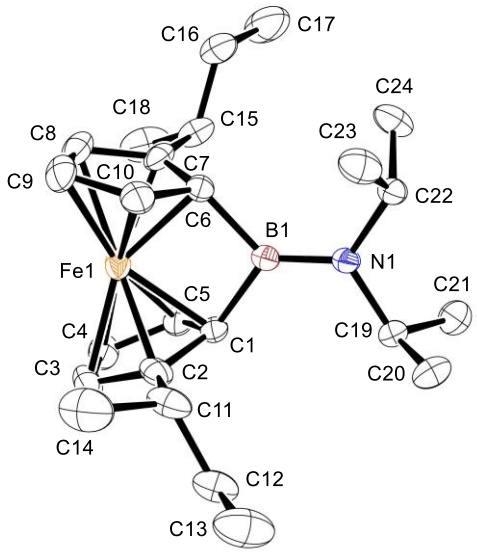

Figure 5-3. Molecular structure of **27b^{MeEt}** with thermal ellipsoids at 50% probability level. Hydrogen atoms are omitted for clarity. For bond lengths [Å] and angles [deg], see Table A2 (Appendix); for crystal and structural refinement data, see Table A1 (Appendix).

As crystals of the new [1]FCPs could not be obtained, their geometries were investigated by DFT calculations. With any calculated geometry the question arises how realistic the so-obtained molecular structures are. We addressed this question by including a comparison between calculated and measured geometries of two known bora[1]ferrocenophanes. Table 5-1 provides an overview of measured and calculated distortion angles (see Figure 5-1) of the known [1]FCPs $(Me_3Si)_2NBfc$ [5a] (fc = $(C_5H_4)_2Fe$) and **27b^{MeEt}**.

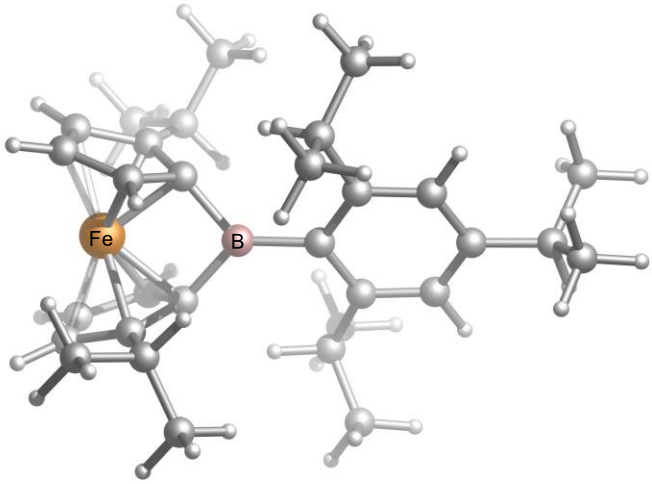

Figure 5-4. Optimized geometry of **27e^{MeMe}** at B3PW91/6-311+G(d,p) level of theory.

Single crystals of the known compound **27b^{MeEt}** [8] were obtained by crystallization from hexanes at −80 °C; the result of its single-crystal X-ray analysis is illustrated in Figure 5-3. We applied the B3PW91/6-311+G(d,p) level of theory as this method gives realistic geometries and also can be used to predict thermodynamic data for ROP.[10] The comparison of distortion angles of $(Me_3Si)_2NBfc$ and **27b^{MeEt}**, respectively, shows that measured and calculated values match very well. While the α angle is slightly underestimated by theory the related δ angle is slightly overestimated. The known $(Me_3Si)_2NBfc$ is included in this study as this [1]FCP is the record holder among all known [*n*]FCPs with respect to the degree of Cp ring tilting (α = 32.4(2)°). From the new group of bora[1]ferrocenophanes **27d-f^{MeMe}**, the Tip-substituted compound **27e^{MeMe}**

shows with α = 33.3° the largest calculated tilt angle. That means the α angle of this species will be approximately 34° if one takes the common mismatch between calculated and measured values into account. Even though this tilt angle is not vastly different from that of $(Me_3Si)_2NBfc$, there is no doubt that the TipB-bridged compound **27e^{MeMe}** (Figure 5-4) is the new record holder among all isolated [*n*]FCPs. Further evidence that this is indeed the case comes from UV-Vis spectroscopy, which will be discussed in the following paragraph.

Table 5-2. Comparison of UV-Vis Data and Tilt Angles (α)

Compound		λ_{max} (nm)	ε (M^{-1} cm^{-1})	α (°)
	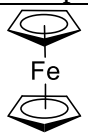	440	96	0
27b^{MeEt}	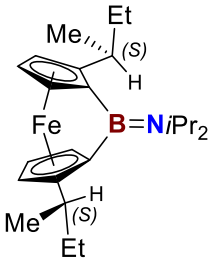	495	550	31.4(2)
I	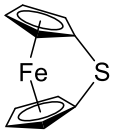	504	540	31.0(1)
27e^{MeMe}	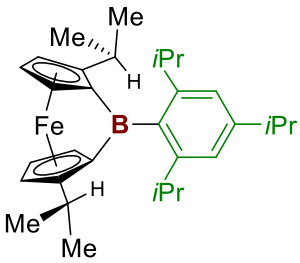	516	992	33.3[a]

[a] Calculated α angle [B3PW91/6-311+G(d,p)].

Previous studies have elucidated a correlation between molecular orbital energies and the tilt angle α in strained ferrocenophanes.[11] For instance, a steady change in colour is observed on going from ferrocene to sila[1]ferrocenophane to phospha[1]ferrocenophane (λ_{max} = 440, 478, and 498 nm, respectively) as the size of the bridging element decreases and the α angle gradually

increases.[12] The dark purple colour of our new bora[1]ferrocenophane **27e^{MeMe}** shows with λ_{max} = 516 nm a further bathochromic shift, which is higher than both of the known bora[1]ferrocenophane **27b^{MeEt}** [8] and the sulfur-bridged [1]FCP **I**[11b] (Table 5-2). To the best of our knowledge, the Tip-substituted [1]FCP **27e^{MeMe}** shows the lowest energy absorption maximum of any strained FCP reported till date. This clearly supports the evaluation of the calculated geometry of **27e^{MeMe}** (Table 5-1 and Figure 5-4): a record high α angle gives a record low energy absorption maximum. Moreover, the colour of **27e^{MeMe}** is exceptionally intense compared to other [1]FCPs, which is also reflected from its high molar absorptivity (Table 5-2).

As mentioned before, an attempted sublimation of the Mes-substituted bora[1]ferrocenophane **27d^{MeMe}** resulted polymerization of this monomer at an oil bath temperature of 120 °C. The so-obtained polymer **(27d^{MeMe})$_n$** was purified by precipitation into methanol from thf solution and analyzed by gel permeation chromatography (GPC). This material, which is readily soluble in organic solvents, such as hexanes, thf, and CH_2Cl_2, showed a trimodal molecular-weight distribution in the GPC trace; unfortunately, individual peaks could not be resolved. Integration of the structured peak gave an estimated M_w of 6.6 kDa relative to polystyrene as a standard ($Đ$ = 2.9).

5.5 Conclusions

A series of new bora[1]ferrocenophanes are reported, and to the best of our knowledge, these are the first examples of boron-bridged [1]FCPs with sterically protected boron in the bridging moiety. In the salt-metathesis reactions to prepare **27d-e^{MeMe}**, we applied the strategy of using the dilithio derivative of **15^{MeMe}** as a suspension in benzene which gave clean conversion towards the targeted products. Both **27d^{MeMe}** and **27e^{MeMe}** show exceptional bathochromic shifts in the UV-Vis spectroscopy which is also reflected in their optimized geometries calculated at the B3PW91/6-311+G(d,p) level of theory. The optimized geometry of **27e^{MeMe}** also shows the Cp ring tilting α = 33.3°; keeping common mismatch between calculated and measured values of α angle into account, one can assume that the tilt angle α for **27e^{MeMe}** will be approximately 34° which makes this compound the new record holder of all isolated [*n*]FCPs till date. Moreover, species **27d^{MeMe}** ring opens thermally to produce a poly(ferrocenylborane) **(27d^{MeMe})$_n$**. Currently, DFT studies are ongoing to better understand the UV-Vis spectroscopy of **27e^{MeMe}** and the question whether the aryl substituent has an influence towards this intense purple colour will be addressed. Furthermore, the isolated polymer **(27d^{MeMe})$_n$** might show an interesting secondary structure. As the monomer **27d^{MeMe}** is enantiopure, its resulting polymer might exhibit a chiral secondary structure. Initial measurements by UV-Vis circular dichroism (CD) spectroscopy indicated that the polymer has a helical structure in solution. However, further studies are needed and we hope to report on the outcomes in the near future.

5.6 Experimental Section

General Methods. If not mentioned otherwise, all syntheses were carried out using standard Schlenk and glovebox techniques. Solvents were dried using an MBraun Solvent Purification

System and stored under nitrogen over 3 Å molecular sieves. C_6D_6 for NMR spectroscopy was degassed by freeze-pump-thaw cycles and stored under nitrogen over 3 Å molecular sieves. Unless otherwise noted, temperatures refer to that of the bath (e.g., dry ice/acetone bath for –78 °C).

Characterization Methods. ^{1}H, ^{11}B, and ^{13}C NMR spectra were recorded on 500 MHz Bruker Avance, 500 MHz Bruker Avance III HD, and 600 MHz Bruker Avance III HD NMR spectrometers at 25 °C in C_6D_6. ^{1}H chemical shifts are referenced to the residual protons of the deuterated solvent C_6D_6 at $\delta = 7.15$ ppm; ^{13}C chemical shifts are referenced to the C_6D_6 signal at $\delta = 128.00$ ppm. ^{11}B NMR spectra were calibrated using $F_3B{\cdot}OEt_2$ (0.0 ppm) as external reference. The following abbreviations are used to described NMR signals: s (singlet), d (doublet), pst (pseudo triplet), sept (septet), br (broad). Some Cp protons appear as slightly broadened singlets, while others appear as pseudo triplets. Coupling constants obtained from ^{1}H NMR spectra are associated with an error and reported to the first decimal point (the digital resolution in ^{1}H NMR spectra is 0.2 Hz). Assignments for newly synthesized compounds were supported by additional NMR experiments (COSY, NOESY, DEPTq, HSQC, and HMBC); for example, *ipso*-carbons of compounds **27d^{MeMe}**, **27e^{MeMe}**, and dichloro[2,4,6-tri(isopropyl)phenyl]borane (**TipBCl$_2$**), that do not appear in $^{13}C\{^{1}H\}$ NMR spectra, are assigned from HMBC experiments. Elemental analyses were performed on a Perkin Elmer 2400 CHN Elemental Analyzer. UV/Vis spectra were measured at ambient temperature with dry, degassed solvents, using a Varian Cary 50 Bio UV-Visible spectrophotometer. GPC chromatograms were recorded on a Viscotek 350 HT-GPC system (Malvern) that was used at low temperature (column temperature of 37.5 °C; thf; flowrate = 1.0 mL min^{-1}; calibrated for polystyrene standards). The instrument was equipped with the following Viscotek components: autosampler (Model 430 Vortex), degasser (model 7510), two pumps (model 1122), 7° and 90° light scattering detectors, refractometer, and viscometer. GPC columns

cover the range of M_w of 500 to 10,000,000 g mol^{-1} (three main columns: Plgel 10 µM MIXED-B LS 300 × 7.5 mm; one guard column: 10 µM GUARD 50 × 7.5 mm; Agilent Technologies). Samples were dissolved in thf and filtered through 0.2 µm syringe PTFE filters before GPC analysis. 'Cannula transfer' of a solution was performed by applying a small N_2 pressure difference between two Schlenk flasks that were connected through a fluoropolymer tubing by inserting both ends into septa. For controlled addition of solutions of boron dihalides a syringe pump has been used (Sage Instruments, model 355).

Reagents. Dichloro[2,4,6-tri(methyl)phenyl]borane (MesBCl$_2$),[13] dichloro[tris(trimethylsily)-methyl]borane (TsiBCl$_2$),[14-15] (S_p,S_p)-1,1′-dibromo-2,2′-di(isopropyl)ferrocene (**15**$^{\mathbf{MeMe}}$),[16] and bora[1]ferrocenophane **27b**$^{\mathbf{MeEt}}$ [8] were synthesized as reported. Copper(I) bromide (98%), 2,4,6-triisopropylphenylbromide (TipBr; 95%), BCl$_3$ (1.0 M in heptane), *t*BuLi (1.7 M in pentane), and *n*BuLi (2.5 M in hexanes) were purchased from Sigma Aldrich.

Synthesis of 2,4,6-tri(isopropyl)phenylcopper (TipCu).[17] This synthesis is adapted and modified from ref. 14. *t*BuLi (1.32 M in pentane, 30.8 mL, 40.7 mmol) was added drop wise over 10 min to a cold solution (−78 °C) of TipBr (5.765 g, 20.35 mmol) in diethylether (40.0 mL). The solution was slowly warmed to r.t. and stirred for 2 h. An orange-brown coloured clear solution was obtained. This solution of TipLi was transferred via cannula over 20 min to a cold (–78 °C) suspension of CuBr (3.083 g, 21.49 mmol) in diethylether (40.0 mL). It was then warmed up to r.t. and stirred for 2 h. All volatiles were removed under vacuum and to the resulting grey solid hexanes (80.0 mL) was added and warmed using a 40 °C water bath. Filtration was done very slowly with occasional heating of the solution with a heat gun (in order to prevent the formation of crystals of TipCu near the filter frit, which causes hindrance towards the filtration process). Residue of LiBr was then washed with hexanes (2 × 10.0 mL). All volatiles were removed from

the filtrate giving an off-white solid to which hexanes was added (25.0 mL) and the slurry was stirred at −78 °C for 30 min. The suspension was then filtered in cold and washed with cold (−78 °C) hexanes (2 × 5.00 mL), giving a white solid (3.869 g, 71%). ^{1}H NMR (C_6D_6, 500.3 MHz): δ 1.20 (d, 6H, *para*-[CH(C$\underline{H}_3$)$_2$]), 1.32 (d, 12H, *ortho*-[CH(C$\underline{H}_3$)$_2$]), 2.76 (sept, 1H, *para*-[C$\underline{H}$(CH$_3$)$_2$]), 3.94 (sept, 2H, *ortho*-[C$\underline{H}$(CH$_3$)$_2$]), 7.06 (s, 2H, *meta*-aromatic) ppm.

Synthesis of dichloro[2,4,6-tri(isopropyl)phenyl]borane (TipBCl$_2$). BCl_3 (1.00 M in heptane, 5.1 mL, 5.1 mmol) was added drop wise via syringe over 2 min to a cold solution (–78 °C) of TipCu (1.303 g, 4.880 mmol) in toluene (25 mL). The resulting solution was stirred for 90 min at that temperature. The colour of the solution turned pale red during that course. It was then slowly warmed up to r.t. On warming up the red colour of the solution gradually faded and bluish white precipitate of CuCl started forming. The reaction mixture was stirred overnight. CuCl was removed by filtration and washed with toluene (2 × 5.0 mL). All volatiles were removed from the filtrate under vacuum, and the product was sublimed (50 °C oil bath temperature; p ≈ 10^{-2} mbar) to give white crystals of $TipBCl_2$ (1.078 g, 77%). ^{1}H NMR (C_6D_6, 600.2 MHz): δ 1.16 (d, 6H, *para*-[CH(C$\underline{H}_3$)$_2$]), 1.19 (d, 12H, *ortho*-[CH(C$\underline{H}_3$)$_2$]), 2.71 (sept, 1H, *para*-[C$\underline{H}$(CH$_3$)$_2$]), 2.79 (sept, 2H, *ortho*-[C$\underline{H}$(CH$_3$)$_2$]), 7.00 (s, 2H, *meta*-aromatic). ^{13}C{^{1}H} NMR (C_6D_6, 125.8 MHz): δ 24.1 (*para*-[CH(C$\underline{H}_3$)$_2$]), 24.3 (*ortho*-[CH(C$\underline{H}_3$)$_2$]), 34.8 (*para*-[C$\underline{H}$(CH$_3$)$_2$]), 36.3 (*ortho*-[C$\underline{H}$(CH$_3$)$_2$]), 121.0 (*meta*-aromatic), 134.8 (*ipso*-aromatic), 149.1 (*ortho*-aromatic), 151.5 (*para*-aromatic). ^{11}B NMR (C_6D_6, 192.6 MHz): δ 62 ppm. Elemental anal. calcd (%) for $C_{15}H_{23}BCl_2$ (285.0590): C, 63.20; H, 8.13. Found: C, 63.45; H, 8.08.

Synthesis of bora[1]ferrocenophane 27d$^{\mathbf{MeMe}}$. *n*BuLi (2.5 M in hexanes, 2.50 mL, 6.3 mmol) was added dropwise to a cold (0 °C) solution of **15$^{\mathbf{MeMe}}$** (1.286 g, 3.005 mmol) in a mixture of Et_2O (3.0 mL) and hexanes (27 mL). The reaction mixture was stirred at 0 °C for 30 min, resulting

in an orange solution. Removal of all volatiles from the solution resulted in pyrophoric orange powder which was then suspended in 30 mL benzene. A solution of $MesBCl_2$ (0.730 g, 3.63 mmol) in benzene (30 mL) was dropwise added within 30 min applying a syringe pump at r.t. The reaction mixture was further stirred at r.t. for 1 h while it gradually changed colour to dark purple. After that, a ^{1}H NMR spectrum was measured from an aliquot of the reaction mixture which showed a clean conversion towards the targeted [1]FCP **27d^{MeMe}**. Additional NMR experiments of the same sample provided enough details to assign all signals of the targeted compound and listed below. ^{1}H NMR (C_6D_6, 500.3 MHz): δ 1.07 (d, 6H, Cp-[CH(C$\underline{H}_3$)$_2$]), 1.24 (d, 6H, Cp-[CH(C$\underline{H}_3$)$_2$]), 2.05 (s, 3H, *para*-C$\underline{H}_3$), 2.29 (sept, 2H, Cp-[C$\underline{H}$(CH$_3$)$_2$]), 3.04 (s, 6H, *ortho*-C$\underline{H}_3$), 3.57 (br, 2H, α-H of Cp), 4.34 (br, 2H, β'-H of Cp), 4.61 (pst, 2H, β-H of Cp), 6.78 (s, 2H, *meta*-aromatic). ^{13}C{^{1}H} NMR (C_6D_6, 125.8 MHz): δ 21.6 (*para*-$\underline{C}$H$_3$), 22.5 (Cp-[CH($\underline{C}$H$_3$)$_2$]), 25.1 (*ortho*-$\underline{C}$H$_3$), 26.7 (Cp-[CH($\underline{C}$H$_3$)$_2$]), 30.7 (Cp-[$\underline{C}$H(CH$_3$)$_2$]), 44.2 (br, *ipso*-C of Cp, B), 72.8 (β'-C of Cp), 77.45 (α-C of Cp), 77.52 (β-C of Cp), 99.8 (*ipso*-C of Cp, *i*Pr), 130.5 (*meta*-aromatic), 135.6 (*ipso*-aromatic), 145.6 (*para*-aromatic), 150.5 (*ortho*-aromatic). ^{11}B NMR (C_6D_6, 160.5 MHz): δ 74 ppm.

An attempt to isolate **27d^{MeMe}** via sublimation at under reduced pressure (ca. 10^{-2} mbar) at 120 °C, only a minor amount of the strained compound sublimed along with significant amounts of unknown species. Moreover, it resulted rest of the monomer to polymerize to a dark purple glassy material which was then purified without any inert gas protection as follows.

Purification of the MesB-Polymer ***(27d^{MeMe})$_n$***. The glassy material (1.642 g) was dissolved in 30 mL hexanes, filtered, and dried under reduced pressure obtaining sparkling red flakes (0.909 g, 76%). It was then dissolved in 20 mL thf and added dropwise to vigorously stirred methanol (300 mL). An immediate formation of red-purple fluffy material was observed which was filtered through a glass frit and washed with more methanol until colourless filtrate obtained. The residue

was then dried under reduced pressure obtaining a red-purple powder **(27d^{MeMe})$_n$** (0.422 g, 35%). ^{1}H NMR (C_6D_6, 500.3 MHz): δ 0.60-1.70 (br, 12H, Cp-[CH(C<u>H</u>$_3$)$_2$]), 1.90-3.00 (br, 9H, *ortho*- and *para*-C<u>H</u>$_3$), 3.20-3.73 (br, 2H, Cp-[C<u>H</u>(CH$_3$)$_2$]), 4.02-5.16 (br, 6H, Cp-H), 6.68-6.97 (br, 2H, *meta*-aromatic). UV/Vis (hexanes): λ_{max} (ε) = 517 nm (945 M^{-1}cm^{-1}).

Synthesis of bora[1]ferrocenophane 27e^{MeMe}. *n*BuLi (2.5 M in hexanes, 2.50 mL, 6.3 mmol) was added dropwise to a cold (0 °C) solution of **15^{MeMe}** (1.257 g, 2.937 mmol) in a mixture of Et_2O (3.0 mL) and hexanes (27 mL). The reaction mixture was stirred at 0 °C for 30 min, resulting in an orange solution. Removal of all volatiles from the solution resulted in pyrophoric orange powder which was then suspended in 30 mL benzene. A solution of TipBCl$_2$ (0.877 g, 3.08 mmol) in benzene (30 mL) was dropwise added within 10 min applying a syringe pump at r.t. The reaction mixture was further stirred at r.t. for 24 h while it gradually changed colour from orange to dark red-brown to dark purple. After that, a ^{1}H NMR spectrum was measured from an aliquot of the reaction mixture which showed a clean conversion towards the targeted [1]FCP **27e^{MeMe}**. All volatiles were removed from the reaction mixture under vacuum followed by a flask-to-flask condensation (120 °C oil bath temperature; $p \approx 10^{-2}$ mbar) to yield **27e^{MeMe}** as a dark purple sticky oil (0.972 g, 69%). ^{1}H NMR (C_6D_6, 600.2 MHz): δ 1.08 (d, 6H, Cp-[CH(C<u>H</u>$_3$)$_2$]), 1.16 (d, 3H, *para*-[CH(C<u>H</u>$_3$)$_2$]), 1.17 (d, 3H, *para*-[CH(C<u>H</u>$_3$)$_2$]), 1.31 (d, 6H, Cp-[CH(C<u>H</u>$_3$)$_2$]), 1.36 (d, 6H, *ortho*-[CH(C<u>H</u>$_3$)$_2$]), 1.39 (d, 6H, *ortho*-[CH(C<u>H</u>$_3$)$_2$]), 2.43 (sept, 2H, Cp-[C<u>H</u>(CH$_3$)$_2$]), 2.74 (sept, 1H, *para*-[C<u>H</u>(CH$_3$)$_2$]), 3.74 (pst, 2H, α-H of Cp), 4.35 (pst, 2H, β'-H of Cp), 4.61 (pst, 2H, β-H of Cp), 5.53 (sept, 2H, *ortho*-[C<u>H</u>(CH$_3$)$_2$]), 7.29 (s, 2H, *meta*-aromatic). ^{13}C{^{1}H} NMR (C_6D_6, 150.9 MHz): δ 22.2 (Cp-[CH(<u>C</u>H$_3$)$_2$]), 23.59 (*para*-[CH(<u>C</u>H$_3$)$_2$]), 23.69 (*para*-[CH(<u>C</u>H$_3$)$_2$]), 23.72 (*ortho*-[CH(<u>C</u>H$_3$)$_2$]), 27.0 (Cp-[CH(<u>C</u>H$_3$)$_2$]), 27.6 (*ortho*-[CH(<u>C</u>H$_3$)$_2$]), 30.7 (*ortho*-[<u>C</u>H(CH$_3$)$_2$]), 31.0 (Cp-[<u>C</u>H(CH$_3$)$_2$]), 35.1 (*para*-[<u>C</u>H(CH$_3$)$_2$]), 43.3 (br, *ipso*-C of Cp, B), 72.8 (β'-C of Cp), 77.3

(β-C of Cp), 77.5 (α-C of Cp), 99.8 (*ipso*-C of Cp, *i*Pr), 121.9 (*meta*-aromatic), 134.1 (*ipso*-aromatic), 156.1 (*para*-aromatic), 161.5 (*ortho*-aromatic). ^{11}B NMR (C_6D_6, 192.6 MHz): δ 74 ppm. UV/Vis (hexanes): λ_{max} (ε) = 516 nm (992 $M^{-1}cm^{-1}$). Elemental Anal. Calcd for $C_{31}H_{43}BFe$ (482.34): C, 77.19; H, 8.99. Found: C, 76.94; H, 9.13.

Synthesis of bora[1]ferrocenophane 27f^{MeMe}. *n*BuLi (2.5 M in hexanes, 2.20 mL, 5.5 mmol) was added dropwise to a cold (0 °C) solution of **15^{MeMe}** (1.123 g, 2.624 mmol) in a mixture of thf (2.6 mL) and hexanes (23.4 mL). The reaction mixture was stirred at 0 °C for 30 min, resulting in an orange solution. The cold bath was removed and replaced with a preheated oil bath (60 °C), followed by stirring of the solution for 10 min. A solution of $TsiCl_2$ (0.901 g, 2.88 mmol) in hexanes (25 mL) was added dropwise within 25 min applying a syringe pump at 60 °C followed by stirring at that temperature for 20 min. After that, the oil bath was removed and the reaction mixture was slowly cooled to ambient temperature by continuous stirring at r.t. for 20 min. The reaction colour changed from orange to dark-red along with formation of a white precipitate. A ^{1}H NMR spectrum was measured from an aliquot of the reaction mixture which showed two sets of Cp protons: a) δ 3.56, 4.23, 4.55 ppm and b) δ 4.41, 4.56, 4.63 ppm. Set "a" matches with the typical chemical shifts for Cp protons in boron-bridged [1]FCPs and set "b" corresponds to the 1,1′-bis(boryl)ferrocene **28f^{MeMe}**. The ratio between the compounds **27f^{MeMe}** and **28f^{MeMe}** was determined based on the integrations of the Cp signals (δ 3.55 and 4.63 ppm) as 1.0:0.47. All volatiles were removed from the reaction mixture under vacuum followed by a flask-to-flask condensation (110 °C oil bath temperature; $p \approx 10^{-2}$ mbar) to yield **27f^{MeMe}** as a red oily solid (0.376 g, 28%) which was contaminated with unknown impurities.^{1}H NMR (C_6D_6, 500.1 MHz): δ0.46 (s, 27H, [Si(CH_3)]$_3$), 1.22 (d, 6H, Cp-[CH($C\underline{H}_3$)$_2$]), 1.43 (d, 6H, Cp-[CH($C\underline{H}_3$)$_2$]), 2.52 (sept, 2H, Cp-[$C\underline{H}$(CH_3)$_2$]), 3.56 (br, 2H, α-H of Cp), 4.23 (br, 2H, β'-H of Cp), 4.55 (pst, 2H, β-H of

Cp). $^{13}C\{^{1}H\}$ NMR (C_6D_6, 125.8 MHz): δ 7.0 ([Si($\underline{C}H_3$)]$_3$), 24.4 (Cp-[CH($\underline{C}H_3$)$_2$]), 27.9 (Cp-[CH($\underline{C}H_3$)$_2$]), 29.2 (Cp-[$\underline{C}$H(CH$_3$)$_2$]), 72.8 (β'-C of Cp), 75.7 (β-C of Cp), 79.6 (α-C of Cp), 99.0 (*ipso*-C of Cp, *i*Pr). ^{11}B NMR (C_6D_6, 160.5 MHz): δ 80 ppm.

Salt-metathesis reaction between compounds 15^{MeMe} and TsiBCl$_2$ at 0 °C. *n*BuLi (2.4 M in hexanes, 0.44 mL, 1.1 mmol) was added dropwise to a cold (0 °C) solution of **3^{MeMe}** (0.213 g, 0.498 mmol) in a mixture of thf (0.5 mL) and hexanes (4.5 mL). The reaction mixture was stirred at 0 °C for 30 min, resulting in an orange solution. A solution of TsiBCl$_2$ (0.171 g, 0.546 mmol) in hexanes (5.0 mL) was added dropwise within 10 min applying a syringe pump at 0 °C. The reaction mixture was further stirred at 0 °C for 10 min and at r.t. for 10 min. The reaction colour changed gradually to red along with formation of a white precipitate. After that, a ^{1}H NMR spectrum was measured from an aliquot of the reaction mixture which showed mainly the presence of **28f^{MeMe}** along with minute amount of **27f^{MeMe}**. All volatiles were removed from the reaction mixture and the resulting dark red residue was dissolved in hexanes (10 mL). LiCl was removed by filtration and washed with hexanes (2.0 mL). The resulting solution was concentrated to around 3.0 mL and left at -80 °C 48 h. Orange crystals of **28f^{MeMe}** were obtained (0.073 g, 32%). ^{1}H NMR (C_6D_6, 600.2 MHz): δ 0.38 (s, 54 H, [(Si(C$\underline{H}_3$)$_3$]), 1.04 (d, 6H, Cp-[CH(C$\underline{H}_3$)$_2$]), 1.41 (d, 6H, Cp-[CH(C$\underline{H}_3$)$_2$]), 3.09 (sept, 2H, Cp-[C$\underline{H}$(CH$_3$)$_2$]), 4.41 (br, 2H, Cp-H), 4.56 (br, 2H, Cp-H), 4.63 (br, 2H, Cp-H) ppm.

Crystal Structure Determination of 27b^{MeEt}. Single crystals were coated with Paratone-N oil, mounted using a micromount (MiTeGen - Microtechnologies for Structural Genomics), and frozen in the cold stream of an Oxford Cryojet attached to the diffractometer. Crystal data were collected on a Bruker APEX II diffractometer at –100 °C using monochromated Mo Kα radiation (λ = 0.71073 Å). An initial orientation matrix and cell was determined by ω scans, and the X-ray data

were measured using ϕ and ω scans.[18] Frames were integrated with the Bruker SAINT software package[19] and data reduction was performed with the *APEX2* software package.[18] A multi-scan absorption correction (SADABS) was applied.[19] The structures were solved by the Intrinsic Phasing method implemented with SHELXT and refined using the Bruker SHELXTL software package.[20] Non-hydrogen atoms were refined with independent anisotropic displacement parameters. Hydrogen atoms were placed at geometrically idealized positions (riding model) and their displacement parameters were fixed to be 20 or 50% larger than those of the attached non-hydrogen atoms. Crystallographic data are summarized in Table A1, while bond lengths and bond angles are shown in Table A2 (see Appendix). The ellipsoid plots were prepared using ORTEP-3 for Windows.[21] The common set of distortion angles was calculated using the program PLATON.[22] The esds of all distortion angles that involve centroids of Cp rings (β, δ) might be somewhat smaller than they should be, as esds on centroids were not included in the calculation.

DFT Calculations. All calculations were done employing the software package GAUSSIAN 09.[23] Geometries were optimized at the B3PW91/6-311+G(d,p) level.[24] The B3PW91 functional had been chosen based on the benchmark investigation of Grimme *et al.*,[25] as well as our recent application to [1]FCPs.[26] Frequency calculations were used to confirm minima. An ultrafine grid (int = ultrafine) and tight requirements for geometry optimizations (opt = tight) were used for all calculations. Structural parameters from the calculated coordinates were extracted with the help of Mercury (version 3.9)[27] and CYLview (version 1b)[28].

5.7 Associated Content

Supporting Information

Crystallographic data (Table A1) and bond lengths and bond angles (Table A2) of **27b^{MeEt}** are summarized in the Appendix.

Acknowledgements

We thank the Natural Sciences and Engineering Research Council of Canada (Discovery Grant, JM) for support and the Canada Foundation for Innovation and the Government of Saskatchewan for funding of the X-ray and NMR facilities at the Saskatchewan Structural Sciences Centre. We thank Dr V. MacKenzie (DSC) and K. Thoms (CHN) for help and support. For DFT calculations, we are grateful to WestGrid (www.westgrid.ca) and Compute Canada (www.computecanada.ca) for support.

5.8 References

(1) (a) Manners, I. *Science* **2001**, *294*, 1664-1666. (b) Manners, I. *Synthetic Metal-Containing Polymers*; Wiley-VCH: Weinheim, 2004. (c) Wang, L.; Cole, M.; Li, J.; Zheng, Y.; Chen, Y. P.; Miller, K. P.; Decho, A. W.; Benicewicz, B. C. *Polym. Chem.* **2015**, *6*, 248-255. (d) Li, Y.; Krentz, T. M.; Wang, L.; Benicewicz, B. C.; Schadler, L. S. *ACS Appl. Mater. Interfaces* **2014**, *6*, 6005-6021. (e) Whittell, G. R.; Manners, I. *Adv. Mater.* **2007**, *19*, 3439-3468.

(2) (a) Kulbaba, K.; Manners, I. *Macromol. Rapid Commun.* **2001**, *22*, 711-724. (b) Bellas, V.; Rehahn, M. *Angew. Chem., Int. Ed.* **2007**, *46*, 5082-5104. (c) Hailes, R. L. N.; Oliver, A. M.; Gwyther, J.; Whittell, G. R.; Manners, I. *Chem. Soc. Rev.* **2016**, *45*, 5358-5407.

(3) Rinehart, K. L.; Curby, R. J. *J. Am. Chem. Soc.* **1957**, *79*, 3290-3291.

(4) (a) Qiu, H.; Gao, Y.; Du, V. A.; Harniman, R.; Winnik, M. A.; Manners, I. *J. Am. Chem. Soc.* **2015**, *137*, 2375-2385. (b) Qiu, H.; Cambridge, G.; Winnik, M. A.; Manners, I. *J. Am. Chem. Soc.* **2013**, *135*, 12180-12183. (c) Hudson, Z. M.; Boott, C. E.; Robinson, M. E.; Rupar, P. A.; Winnik, M. A.; Manners, I. *Nat. Chem.* **2014**, *6*, 893-898. (d) Hudson, Z. M.; Lunn, D. J.; Winnik, M. A.; Manners, I. *Nat. Commun.* **2014**, *5*, 3372.

(5) (a) Braunschweig, H.; Dirk, R.; Müller, M.; Nguyen, P.; Resendes, R.; Gates, D. P.; Manners, I. *Angew. Chem., Int. Ed.* **1997**, *36*, 2338-2340. (b) Berenbaum, A.; Braunschweig, H.; Dirk, R.; Englert, U.; Green, J. C.; Jäkle, F.; Lough, A. J.; Manners, I. *J. Am. Chem. Soc.* **2000**, *122*, 5765-5774.

(6) (a) Heilmann, J. B.; Qin, Y.; Jäkle, F.; Lerner, H.-W.; Wagner, M. *Inorg. Chim. Acta* **2006**, *359*, 4802-4806. (b) Heilmann, J. B.; Scheibitz, M.; Qin, Y.; Sundararaman, A.; Jäkle, F.; Kretz, T.; Bolte, M.; Lerner, H. W.; Holthausen, M. C.; Wagner, M. *Angew. Chem., Int. Ed.* **2006**, *45*, 920-925.

(7) Sadeh, S.; Bhattacharjee, H.; Khozeimeh Sarbisheh, E.; Quail, J. W.; Müller, J. *Chem.-Eur. J.* **2014**, *20*, 16320-16330.

(8) Bhattacharjee, H.; Martell, J. D.; Khozeimeh Sarbisheh, E.; Sadeh, S.; Quail, J. W.; Müller, J. *Organometallics* **2016**, *35*, 2156-2164.

(9) Difference in chemical shifts of α- and β-H signals, $\Delta = [(\beta + \beta')/2] - \alpha$

(10) Khozeimeh Sarbisheh, E.; Bhattacharjee, H.; Cao, M. P. T.; Zhu, J.; Müller, J. *Organometallics* **2017**, *36*, 614-621.

(11) (a) Green, J. C. *Chem. Soc. Rev.* **1998**, *27*, 263-271. (b) Rulkens, R.; Gates, D. P.; Balaishis, D.; Pudelski, J. K.; McIntosh, D. F.; Lough, A. J.; Manners, I. *J. Am. Chem. Soc.* **1997**, *119*, 10976-10986.

(12) Herbert, D. E.; Mayer, U. F. J.; Manners, I. *Angew. Chem., Int. Ed.* **2007**, *46*, 5060-5081.

(13) (a) Eriksson, H.; Håkansson, M. *Organometallics* **1997**, *16*, 4243-4244. (b) Sundararaman, A.; Jäkle, F. *J. Organomet. Chem.* **2003**, *681*, 134-142.

(14) Aljuaid, S. S.; Eaborn, C.; Elkheli, M. N. A.; Hitchcock, P. B.; Lickiss, P. D.; Molla, M. E.; Smith, J. D.; Zora, J. A. *J. Chem. Soc., Dalton Trans.* **1989**, 447-452.

(15) Tapper, A., Dissertation, 1988, RWTH Aachen.

(16) Sadeh, S.; Schatte, G.; Müller, J. *Chem.-Eur. J.* **2013**, *19*, 13408-13417.

(17) Procedure was obtained from Juan Araneda, Warren Piers group, University of Calgary.

(18) Bruker *APEX2*; 2014.3-0 ed.; Bruker AXS Inc.: 2014.

(19) Bruker *SAINT and SADABS*; v8.34a ed.; Bruker AXS Inc.: 2013.

(20) (a) Sheldrick, G. M. *SHELXL, Program for the Solution of Crystal Structures*; University of Göttingen, Germany. (b) Sheldrick, G. M. *Acta Crystallogr., Sect. A: Found. Crystallogr.* **2008**, *64*, 112-122.

(21) Farrugia, L. J. *J. Appl. Crystallogr.* **1997**, *30*, 565.

(22) Spek, A. L. *PLATON, A Multipurpose Crystallographic Tool*; University of Utrecht, The Netherlands: 2011.

(23) Frisch, M. J.; Trucks, G. W.; Schlegel, H. B.; Scuseria, G. E.; Robb, M. A.; Cheeseman, J. R.; Scalmani, G.; Barone, V.; Mennucci, B.; Petersson, G. A.; Nakatsuji, H.; Caricato, M.; Li, X.; Hratchian, H. P.; Izmaylov, A. F.; Bloino, J.; Zheng, G.; Sonnenberg, J. L.; Hada, M.; Ehara, M.; Toyota, K.; Fukuda, R.; Hasegawa, J.; Ishida, M.; Nakajima, T.; Honda, Y.; Kitao, O.; Nakai, H.; Vreven, T.; J. A. Montgomery, J.; Peralta, J. E.; Ogliaro, F.; Bearpark, M.; Heyd, J. J.; Brothers, E.; Kudin, K. N.; Staroverov, V. N.; Keith, T.; Kobayashi, R.; Normand, J.; Raghavachari, K.; Rendell, A.; Burant, J. C.; Iyengar, S. S.; Tomasi, J.; Cossi, M.; Rega, N.; Millam, J. M.; Klene,

M.; Knox, J. E.; Cross, J. B.; Bakken, V.; Adamo, C.; Jaramillo, J.; Gomperts, R.; Stratmann, R. E.; Yazyev, O.; Austin, A. J.; Cammi, R.; Pomelli, C.; Ochterski, J. W.; Martin, R. L.; Morokuma, K.; Zakrzewski, V. G.; Voth, G. A.; Salvador, P.; Dannenberg, J. J.; Dapprich, S.; Daniels, A. D.; Farkas, O.; Foresman, J. B.; Ortiz, J. V.; Cioslowski, J.; Fox, D. J. *Gaussian 09*; Revision E.01 ed.; Gaussian, Inc.: 2013.

(24) (a) Perdew, J. P. In *Electronic Structure of Solids '91*; Ziesche, P., Eschrig, H., Eds.; Akademie Verlag: Berlin, 1991, p 11-20. (b) Perdew, J. P.; Chevary, J. A.; Vosko, S. H.; Jackson, K. A.; Pederson, M. R.; Singh, D. J.; Fiolhais, C. *Phys. Rev. B: Condens. Matter Mater. Phys.* **1992**, *46*, 6671-6687. (c) Perdew, J. P.; Chevary, J. A.; Vosko, S. H.; Jackson, K. A.; Pederson, M. R.; Singh, D. J.; Fiolhais, C. *Phys. Rev. B: Condens. Matter Mater. Phys.* **1993**, *48*, 4978-4978. (d) Becke, A. D. *J. Chem. Phys.* **1993**, *98*, 5648-5652. (e) Perdew, J. P.; Burke, K.; Wang, Y. *Phys. Rev. B: Condens. Matter Mater. Phys.* **1996**, *54*, 16533-16539. (f) Burke, K.; Perdew, J. P.; Wang, Y. In *Electronic Density Functional Theory: Recent Progress and New Directions*; Dobson, J. F., G. Vignale, Das, M. P., Eds.; Plenum: 1998, p 81-111.

(25) Goerigk, L.; Grimme, S. *Phys. Chem. Chem. Phys.* **2011**, *13*, 6670-6688.

(26) (a) Bhattacharjee, H.; Müller, J. *Coord. Chem. Rev.* **2016**, *314*, 114-133. (b) Khozeimeh Sarbisheh, E.; Esteban Flores, J.; Zhu, J.; Müller, J. *Chem.-Eur. J.* **2016**, *22*, 16838-16849. (c) Khozeimeh Sarbisheh, E.; Bhattacharjee, H.; Cao, M. P. T.; Zhu, J.; Müller, J. *Organometallics* **2017**, *36*, 614-621. (d) Khozeimeh Sarbisheh, E.; Esteban Flores, J.; Anderson, B. J.; Zhu, J.; Müller, J. *Organometallics* **2017**, *36*, 2182-2189.

(27) Mercury; 3.9 ed.; http://www.ccdc.cam.ac.uk/mercury.

(28) Legault, C. Y. *CYLview*; http://www.cylview.org: 2009.

6 Summary and Conclusions

A dormant chemistry[1] of bora[1]ferrocenophanes was rejuvenated by employing a new series of C_2-symmetric dilithioferrocene derivatives (**16**$^{\mathbf{R1R2}}$, Chart 6-1). A set of new boron-bridged [1]FCPs (**27a-c**$^{\mathbf{R1R2}}$, Scheme 6-1) was synthesized via salt-metathesis reactions between species **16**$^{\mathbf{MeMe}}$ and **16**$^{\mathbf{EtEt}}$, and the three amino(dichloro)boranes Et_2NBCl_2, *i*Pr_2NBCl_2, and *t*Bu(SiMe$_3$)$NBCl_2$. Single crystal X-ray analysis of these new bora[1]ferrocenophanes showed tilt angles α of approximately 32°, which match results obtained for the first reported boron-bridged [1]FCPs.[1] Thermal ROP of species **27a**$^{\mathbf{EtEt}}$ and **27b**$^{\mathbf{EtEt}}$ resulted in soluble poly(ferrocenylborane)s with a molecular weight of ca. 10 kDa (see Chapter 2).[2]

Chart 6-1. Chiral Dibromoferrocenes (**15**$^{\mathbf{R1R2}}$), Dilithioferrocenes (**16**$^{\mathbf{R1R2}}$), and Preferred Conformation of CHR^1R^2 Moieties

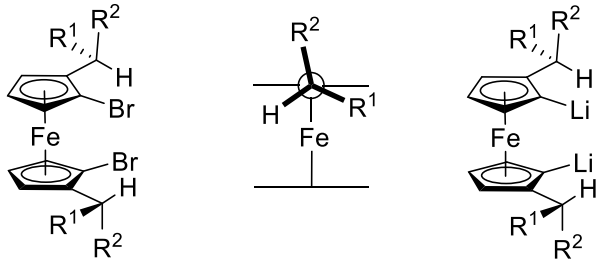

15$^{\mathbf{R1R2}}$ **16**$^{\mathbf{R1R2}}$

Furthermore, inspection of the ^{1}H NMR spectra of the reaction mixtures revealed that significant amounts of 1,1′-bis(boryl)ferrocene species **28**$^{\mathbf{R1R2}}$ (Scheme 6-1) formed as side products. Rigorous attempts of optimization of reaction conditions showed that the following factors have an impact on the product ratios:

a) *Reaction temperature*: a higher reaction temperature yields higher conversion towards the targeted [1]FCPs.

b) *Rate of addition of the amino(dichloro)borane*: a slower rate of addition yields higher conversion towards the targeted [1]FCPs.

c) *Bulkiness of the groups attached to Cp moieties (CHR^1R^2)*: dilithioferrocene derivative **16^{EtEt}** always forms more [1]FCPs compared to **16^{MeMe}**.

Scheme 6-1. Synthesis of Boron-Bridged [1]FCPs (**27a-c^{R1R2}**) with Amino Substituents at Boron

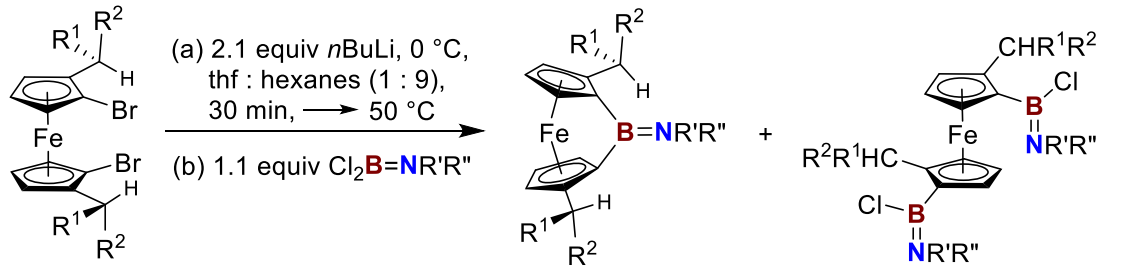

15^{R1R2}

	NR'R"
27a^{R1R2}	NEt_2
27b^{R1R2}	$NiPr_2$
27c^{R1R2}	$N(tBu)SiMe_3$

	NR'R"
28a^{R1R2}	NEt_2
28b^{R1R2}	$NiPr_2$
28c^{R1R2}	$N(tBu)SiMe_3$

Modified reaction conditions with an addition of the amino(dichloro)borane solution (0.1 M) during 10 min at 50 °C resulted in significant improvement of the product ratios (**27^{R1R2}**:**28^{R1R2}**). We rationalized such experimental observations by proposing a mechanism shown in Scheme 6-2. The intermediate **I$^{27\text{-}28}$**, formed after the first step, can either react *intermolecularly* with a second molecule of amino(dichloro)borane to form the byproduct **28**, or an *intramolecular* ring-closure can yield the targeted strained species **27**. A higher activation barrier is expected in the formation of the [1]FCP **27**, as one can assume that some of the strain of the product is already established in the transition state of this ring-closure reaction. This explains the requirement of higher reaction temperature to increase the conversion towards the targeted strained [1]FCPs. On the other hand, a slower addition of the boron dihalide reagent simply slows the formation of the unwanted byproduct **28** down and, therefore, favours the first-order kinetics of the formation of the [1]FCP **27**. Moreover, molecular structures of [1]FCPs (**27^{R1R2}**) and dibromoferrocene derivatives (**15^{MeMe}** and **15^{EtEt}**, Chart 6-1) revealed that one of the alkyl arms

(R^1) is approximately in the same plane as a Cp ring and the other arm (R^2) is pointing away from iron and almost perpendicular to a Cp ring (see Chart 6-1 for the preferred conformation of the CHR^1R^2 moiety). We proposed a hypothesis that group R^2 (and not R^1) has an impact on the ratio of the two products by reducing the rate of formation of the byproduct **28** as R^2 points approximately in the direction of the incoming amino(dichloro)borane (rate constants k_1 and k_3 in Scheme 6-2).

Scheme 6-2. Proposed Mechanism of the Salt-Metathesis Reactions

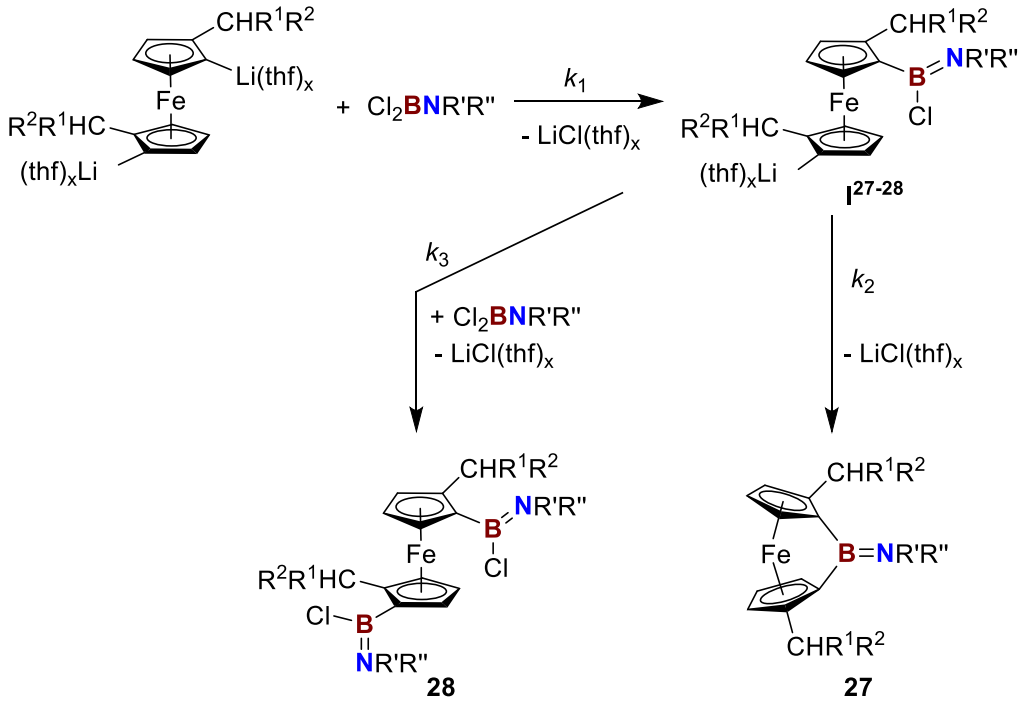

To further test this hypothesis, two more C_2-symmetric dibromoferrocene derivatives (**15**$^{\mathbf{MeEt}}$ and **15**$^{\mathbf{EtMe}}$, Chart 6-2) were prepared and used along with the previously mentioned ferrocene dibromides **15**$^{\mathbf{MeMe}}$ and **15**$^{\mathbf{EtEt}}$. A set of salt-metathesis reactions were performed by following the modified reaction conditions as mentioned before (Scheme 6-1). To collect meaningful data, reaction conditions were controlled as precise as possible. Therefore, all experiments were done on the same scale, using the same conditions and the same

amino(dichloro)borane (iPr$_2$NBCl$_2$); each experiment was repeated multiple times to assure reproducibility of the data. Product ratios of **27^{R1R2}**:**28^{R1R2}** obtained from the ^{1}H NMR spectra of the reaction mixtures indeed showed that R^2 = Et [1.0:0.30 (CHMeEt), 1.0:0.27 (CHEt$_2$)] reduces the rate formation of the byproduct more efficiently than R^2 = Me [1.0:0.51 (CHMe$_2$), 1.0:0.49 (CHEtMe)].[3] These results supported our hypothesis that the alkyl group that is oriented approximately perpendicular to the Cp ring (R^2, and not R^1) affects the outcome of the salt-metathesis reactions. Furthermore, these experimental results were supported by DFT calculations (see Chapter 3 for more details).[3]

Along with this successful synthesis of a new family of bora[1]ferrocenophanes and a better understanding of the mechanism of such salt-metathesis reactions it was realized that the presence of a nitrogen donor to electronically stabilize the boron center is apparently essential to prepare isolable boron-bridged [1]FCPs. We extended our research along this direction and prepared the first examples of azabora[2]ferrocenophanes (**30a-c**, Scheme 6-3) in anticipation that the highly strained monomers would be excellent candidates for the preparation of new polymers with BN moieties in the backbone.[4] These [2]FCPs were synthesized from previously reported amino(bromo)ferrocene derivatives[5] **29a-b** and isolated as crystalline solids. Molecular structures of these species showed tilt angles α of ca. 24°, however, unfortunately all three of them were proven to be thermally robust and did not ring open even up to 300 °C. DFT calculations were applied to evaluate strain in these molecules which revealed that these azabora[2]ferrocenophanes (**30a-c**, Scheme 6-3) are similarly strained as the well-known Me$_2$Si-bridged sila[1]ferrocenophane.[6] Moreover, DFT calculations also suggested that these monomers are sterically overprotected and are not suitable for ROP (see Chapter 4).[4]

Scheme 6-3. Preparation of Azabora[2]ferrocenophanes **30**

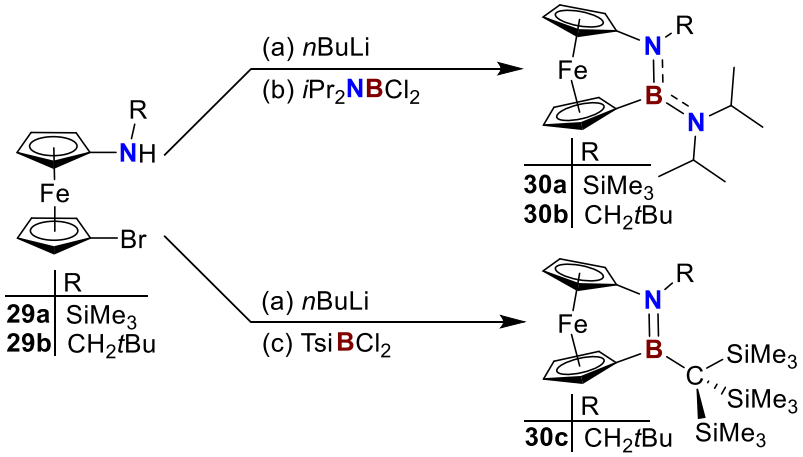

Similar thermal stability were shown by the [1]FCPs (**27**$^{\mathbf{R1R2}}$) discussed before (Scheme 6-1). The thermal ROP of these species required a threshold temperature as high as 240 °C, which could be due to the stabilization from the amino group attached to the boron atom. In order to test this hypothesis, a new family of boron-bridged [1]FCPs with alkyl or aryl substituents at boron were targeted (**27d-f**$^{\mathbf{MeMe}}$; Scheme 6-4).

Initial attempts of their synthesis following the previously established modified reaction conditions were unsuccessful for **27d-e**$^{\mathbf{MeMe}}$ (see Scheme 6-1). Over the course of finding the right reaction conditions it was noticed that the formation of these two species are favoured under slower kinetics. Therefore, we applied a new strategy of using the dilithioferrocene derivative **16**$^{\mathbf{MeMe}}$ as a suspension in benzene so that the salt-metathesis reaction can take place slowly at the surface of the undissolved particles of **16**$^{\mathbf{MeMe}}$ (see Chapter 5 for details). This strategy indeed resulted in clean conversion to the targeted [1]FCPs **27d-e**$^{\mathbf{MeMe}}$ (*method A*, Scheme 6-4). However, this reaction condition did not yield any of **27f**$^{\mathbf{MeMe}}$, rather the reaction conditions previously discussed (Scheme 6-1) were used with some further modifications. An increase in the reaction temperature

Scheme 6-4. Synthesis of Boron-Bridged [1]FCPs (**27d-f^{MeMe}**) with Alkyl or Aryl Substituents at Boron

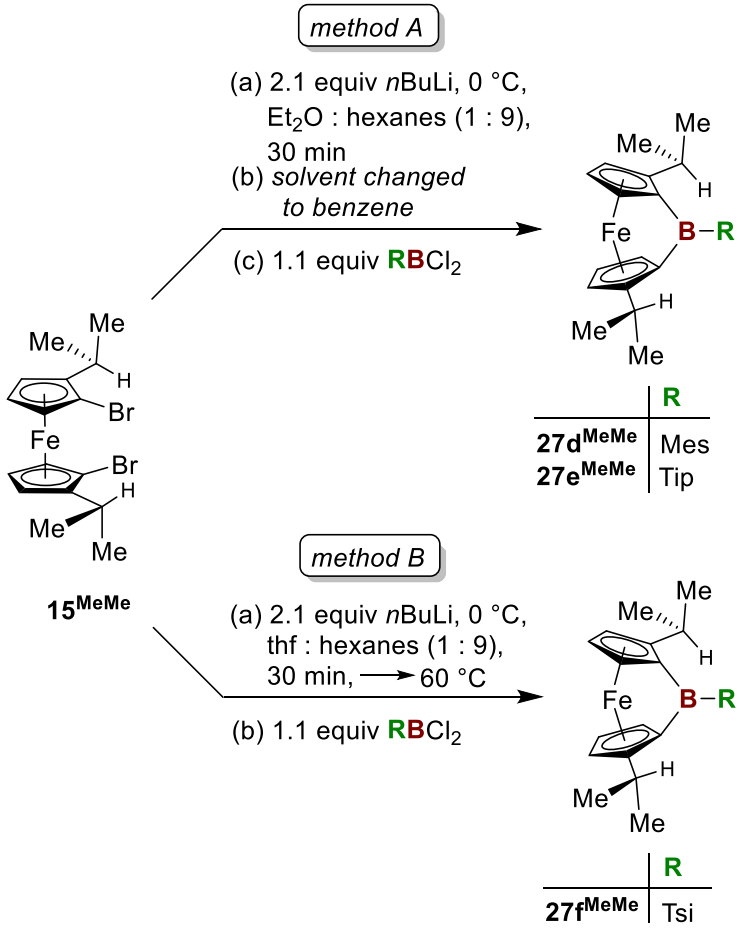

to 60 °C and reduction in the speed of addition of the boron dihalide reagent to 20 min (*method B*, Scheme 6-4) resulted in the targeted strained compound along with 1,1′-bis(boryl) byproduct **28f^{MeMe}** in a ratio of 1.0:0.47. Both **27e^{MeMe}** and **27f^{MeMe}** were isolated via vacuum sublimation at 110 °C, whereas attempted isolation of species **27d^{MeMe}** under the similar conditions resulted in poly(ferrocenylborane) **(27d^{MeMe})$_n$**. Reaction mixtures of both **27d^{MeMe}** and **27e^{MeMe}** are dark purple in colour and the isolated species **27e^{MeMe}** showed an exceptional bathochromic shift and a record low energy absorption maximum (λ_{max} = 516 nm) with a high molar absorptivity (ε = 992 M^{-1} cm^{-1}). Moreover, the optimized geometry [B3PW91/6-311+G(d,p)] of the same compound showed an α angle of 33.3° (see Chapter 5). It was shown before that the B3PW91/6-311+G(d,p)

level of theory gives realistic geometries, however, often slightly underestimates the α angle.[6b] Keeping this common mismatch in mind, one can assume that the α angle of species **27e^{MeMe}** will be approximately 34°, which means that **27e^{MeMe}** is the new record holder among all isolated [*n*]FCPs. This high tilt angle is also reflected by the large bathochromic shift in UV-Vis spectroscopy as discussed above.[7] However, the fact that species **27d^{MeMe}** and **27e^{MeMe}** are dark purple in colour but **27f^{MeMe}** is dark red triggered a question if the aryl substituents (Mes and Tip) on the boron atom has any influence towards the resulting colours. Further DFT studies are needed to better understand these results.

The poly(ferrocenylborane) **(27d^{MeMe})$_n$** is highly soluble in common organic solvents (such as thf, hexanes, CH_2Cl_2) and stable under ambient conditions. GPC analyses of the polymer showed a trimodal molecular-weight distribution and the integration of the structured peak gave an estimated M_w of 6.6 kDa relative to polystyrene as a standard (see Chapter 5). Furthermore, initial results from UV-Vis CD spectroscopy indicated that the polymer has a helical structure in solution. However, more information is needed to determine the chiral nature of the secondary structure of the isolated polymer.

6.1 References

(1) (a) Braunschweig, H.; Dirk, R.; Müller, M.; Nguyen, P.; Resendes, R.; Gates, D. P.; Manners, I. *Angew. Chem., Int. Ed.* **1997**, *36*, 2338-2340. (b) Berenbaum, A.; Braunschweig, H.; Dirk, R.; Englert, U.; Green, J. C.; Jäkle, F.; Lough, A. J.; Manners, I. *J. Am. Chem. Soc.* **2000**, *122*, 5765-5774.

(2) Sadeh, S.; Bhattacharjee, H.; Khozeimeh Sarbisheh, E.; Quail, J. W.; Müller, J. *Chem.-Eur. J.* **2014**, *20*, 16320-16330.

(3) Bhattacharjee, H.; Martell, J. D.; Khozeimeh Sarbisheh, E.; Sadeh, S.; Quail, J. W.; Müller, J. *Organometallics* **2016**, *35*, 2156-2164.

(4) Bhattacharjee, H.; Dey, S.; Zhu, J.; Sun, W.; Müller, J. *Chem. Commun.* **2018**, *54*, 5562-5565.

(5) (a) Dey, S.; Sun, W.; Müller, J. *Inorg. Chem.* **2016**, *55*, 3630-3639. (b) Dey, S.; Quail, J. W.; Müller, J. *Organometallics* **2015**, *34*, 3039-3046.

(6) (a) Foucher, D. A.; Tang, B.-Z.; Manners, I. *J. Am. Chem. Soc.* **1992**, *114*, 6246-6248. (b) Khozeimeh Sarbisheh, E.; Bhattacharjee, H.; Cao, M. P. T.; Zhu, J.; Müller, J. *Organometallics* **2017**, *36*, 614-621.

(7) Rulkens, R.; Gates, D. P.; Balaishis, D.; Pudelski, J. K.; McIntosh, D. F.; Lough, A. J.; Manners, I. *J. Am. Chem. Soc.* **1997**, *119*, 10976-10986.

APPENDIX

Table A1. Crystal and Structural Refinement Data for Compound **27b^{MeEt}** (see Chapter 5)

Compound name	**27b^{MeEt}**
empirical formula	$C_{24}H_{38}BFeN$
Fw / g mol^{-1}	407.21
cryst. size / mm^3	0.500 × 0.190 × 0.070
cryst. system	hexagonal
space group	$P6_1$
Z	4
a / Å	14.4131(7)
b / Å	14.4131(7)
c / Å	18.9848(8)
α / °	90
β / °	90
γ / °	120
volume / Å^3	3415.5(4)
ρ_{calc} / g cm^{-3}	1.188
temperature / K	173(2)
μ_{calc}./ mm^{-1}	0.670
θ range / °	1.953 to 27.515
completeness / %	99.9
collected reflections	66283
independent reflections	5212 [R(int) = 0.0549]
absorption correction	multi-scan
data / restraints / params	5212 / 1 / 252
goodness-of-fit	1.041
R_1 [I > 2 σ(I)] [a]	0.0296
wR_2 (all data) [a]	0.0687
largest diff. peak and hole, $\Delta\rho_{elect}$ / e Å^{-3}	0.175 and –0.331

[a] $R_1 = [\Sigma||F_o|-|F_c||]/[\Sigma|F_o|]$ for $[F_o^2 > 2\sigma(F_o^2)]$, $wR_2 = \{[\Sigma w(F_o^2-F_c^2)^2]/[\Sigma w(F_o^2)^2]\}^{1/2}$ [all data].

Table A2. Bond Lengths (Å) and Bond Angles (deg) for Compound **27b^{MeEt}** (see Chapter 5)

Fe(1)-C(1)	1.985(2)	C(19)-C(21)	1.527(4)	C(10)-Fe(1)-C(8)	67.64(11)
Fe(1)-C(6)	1.991(2)	C(22)-C(24)	1.509(4)	C(7)-Fe(1)-C(8)	40.58(10)
Fe(1)-C(5)	2.021(3)	C(22)-C(23)	1.519(4)	C(2)-Fe(1)-C(8)	163.56(11)
Fe(1)-C(10)	2.025(3)			C(4)-Fe(1)-C(8)	126.98(11)
Fe(1)-C(7)	2.031(3)	C(1)-Fe(1)-C(6)	78.79(10)	C(3)-Fe(1)-C(8)	145.70(12)
Fe(1)-C(2)	2.040(3)	C(1)-Fe(1)-C(5)	42.39(10)	C(1)-Fe(1)-C(9)	142.14(10)
Fe(1)-C(4)	2.091(3)	C(6)-Fe(1)-C(5)	101.35(10)	C(6)-Fe(1)-C(9)	70.32(10)
Fe(1)-C(3)	2.092(3)	C(1)-Fe(1)-C(10)	101.68(10)	C(5)-Fe(1)-C(9)	164.24(11)
Fe(1)-C(8)	2.094(3)	C(6)-Fe(1)-C(10)	42.49(10)	C(10)-Fe(1)-C(9)	40.46(10)
Fe(1)-C(9)	2.096(3)	C(5)-Fe(1)-C(10)	139.24(11)	C(7)-Fe(1)-C(9)	68.27(11)
Fe(1)-B(1)	2.540(3)	C(1)-Fe(1)-C(7)	102.60(10)	C(2)-Fe(1)-C(9)	124.65(12)
N(1)-B(1)	1.381(4)	C(6)-Fe(1)-C(7)	42.31(10)	C(4)-Fe(1)-C(9)	146.20(11)
N(1)-C(19)	1.481(3)	C(5)-Fe(1)-C(7)	96.45(11)	C(3)-Fe(1)-C(9)	126.77(12)
N(1)-C(22)	1.489(3)	C(10)-Fe(1)-C(7)	69.45(11)	C(8)-Fe(1)-C(9)	39.48(12)
B(1)-C(6)	1.613(4)	C(1)-Fe(1)-C(2)	42.33(10)	C(1)-Fe(1)-B(1)	39.41(9)
B(1)-C(1)	1.613(4)	C(6)-Fe(1)-C(2)	102.68(10)	C(6)-Fe(1)-B(1)	39.40(9)
C(1)-C(5)	1.449(4)	C(5)-Fe(1)-C(2)	69.54(11)	C(5)-Fe(1)-B(1)	70.20(9)
C(1)-C(2)	1.454(4)	C(10)-Fe(1)-C(2)	96.84(11)	C(10)-Fe(1)-B(1)	69.05(10)
C(2)-C(3)	1.428(4)	C(7)-Fe(1)-C(2)	140.64(11)	C(7)-Fe(1)-B(1)	70.97(9)
C(2)-C(11)	1.511(4)	C(1)-Fe(1)-C(4)	70.05(10)	C(2)-Fe(1)-B(1)	69.67(9)
C(3)-C(4)	1.415(4)	C(6)-Fe(1)-C(4)	141.91(11)	C(4)-Fe(1)-B(1)	107.20(10)
C(4)-C(5)	1.427(4)	C(5)-Fe(1)-C(4)	40.57(10)	C(3)-Fe(1)-B(1)	106.73(10)
C(6)-C(7)	1.452(4)	C(10)-Fe(1)-C(4)	164.38(12)	C(8)-Fe(1)-B(1)	107.56(10)
C(6)-C(10)	1.456(4)	C(7)-Fe(1)-C(4)	124.58(12)	C(9)-Fe(1)-B(1)	106.60(9)
C(7)-C(8)	1.432(4)	C(2)-Fe(1)-C(4)	68.01(11)	B(1)-N(1)-C(19)	120.5(2)
C(7)-C(15)	1.508(4)	C(1)-Fe(1)-C(3)	69.88(10)	B(1)-N(1)-C(22)	123.8(2)
C(8)-C(9)	1.415(4)	C(6)-Fe(1)-C(3)	143.02(11)	C(19)-N(1)-C(22)	115.7(2)
C(9)-C(10)	1.427(4)	C(5)-Fe(1)-C(3)	67.97(11)	N(1)-B(1)-C(6)	130.7(2)
C(11)-C(14)	1.524(4)	C(10)-Fe(1)-C(3)	125.72(13)	N(1)-B(1)-C(1)	126.1(2)
C(11)-C(12)	1.532(4)	C(7)-Fe(1)-C(3)	163.55(11)	C(6)-B(1)-C(1)	103.0(2)
C(12)-C(13)	1.531(4)	C(2)-Fe(1)-C(3)	40.40(11)	N(1)-B(1)-Fe(1)	173.6(2)
C(15)-C(18)	1.529(4)	C(4)-Fe(1)-C(3)	39.55(12)	C(6)-B(1)-Fe(1)	51.61(12)
C(15)-C(16)	1.540(4)	C(1)-Fe(1)-C(8)	143.11(10)	C(1)-B(1)-Fe(1)	51.39(12)
C(16)-C(17)	1.519(4)	C(6)-Fe(1)-C(8)	69.93(10)	C(5)-C(1)-C(2)	105.8(2)
C(19)-C(20)	1.527(4)	C(5)-Fe(1)-C(8)	125.63(12)	C(5)-C(1)-B(1)	120.3(2)

C(2)-C(1)-B(1)	119.3(2)	C(1)-C(5)-Fe(1)	67.48(14)	C(10)-C(9)-Fe(1)	67.11(15)
C(5)-C(1)-Fe(1)	70.12(13)	C(7)-C(6)-C(10)	105.2(2)	C(9)-C(10)-C(6)	109.6(3)
C(2)-C(1)-Fe(1)	70.84(14)	C(7)-C(6)-B(1)	122.3(2)	C(9)-C(10)-Fe(1)	72.43(16)
B(1)-C(1)-Fe(1)	89.20(15)	C(10)-C(6)-B(1)	117.3(2)	C(6)-C(10)-Fe(1)	67.50(13)
C(3)-C(2)-C(1)	108.4(2)	C(7)-C(6)-Fe(1)	70.31(14)	C(2)-C(11)-C(14)	112.7(3)
C(3)-C(2)-C(11)	126.4(3)	C(10)-C(6)-Fe(1)	70.00(14)	C(2)-C(11)-C(12)	108.9(2)
C(1)-C(2)-C(11)	125.2(2)	B(1)-C(6)-Fe(1)	88.99(15)	C(14)-C(11)-C(12)	111.8(2)
C(3)-C(2)-Fe(1)	71.79(18)	C(8)-C(7)-C(6)	108.6(2)	C(13)-C(12)-C(11)	114.8(2)
C(1)-C(2)-Fe(1)	66.83(14)	C(8)-C(7)-C(15)	125.2(2)	C(7)-C(15)-C(18)	112.3(3)
C(11)-C(2)-Fe(1)	128.97(18)	C(6)-C(7)-C(15)	125.9(2)	C(7)-C(15)-C(16)	109.1(2)
C(4)-C(3)-C(2)	108.7(2)	C(8)-C(7)-Fe(1)	72.05(17)	C(18)-C(15)-C(16)	110.6(2)
C(4)-C(3)-Fe(1)	70.16(16)	C(6)-C(7)-Fe(1)	67.38(15)	C(17)-C(16)-C(15)	114.4(3)
C(2)-C(3)-Fe(1)	67.81(16)	C(15)-C(7)-Fe(1)	130.31(18)	N(1)-C(19)-C(20)	111.6(2)
C(3)-C(4)-C(5)	108.1(2)	C(9)-C(8)-C(7)	108.9(2)	N(1)-C(19)-C(21)	111.9(2)
C(3)-C(4)-Fe(1)	70.29(15)	C(9)-C(8)-Fe(1)	70.35(16)	C(20)-C(19)-C(21)	111.4(2)
C(5)-C(4)-Fe(1)	67.09(15)	C(7)-C(8)-Fe(1)	67.37(15)	N(1)-C(22)-C(24)	112.2(2)
C(4)-C(5)-C(1)	109.0(2)	C(8)-C(9)-C(10)	107.6(2)	N(1)-C(22)-C(23)	111.5(2)
C(4)-C(5)-Fe(1)	72.35(16)	C(8)-C(9)-Fe(1)	70.16(15)	C(24)-C(22)-C(23)	111.2(3)